DENSE PARTICLE CONCENTRATION USING THIN CHANNEL FLOW WITH RIFFLES

by

Danny George

B.A.Sc., The University of British Columbia, 2019

A THESIS SUBMITTED IN PARTIAL FULFILLMENT OF

THE REQUIREMENTS FOR THE DEGREE OF

MASTER OF APPLIED SCIENCE

in

THE FACULTY OF GRADUATE AND POSTDOCTORAL STUDIES

(Mining Engineering)

THE UNIVERSITY OF BRITISH COLUMBIA

(Vancouver)

April 2021

The following individuals certify that they have read, and recommend to the Faculty of Graduate and Postdoctoral Studies for acceptance, the thesis entitled:

Dense Particle Concentration Using Thin Channel Flow with Riffles

submitted by   Danny George   in partial fulfillment of the requirements for

the degree of   Master of Applied Science

in   Mining Engineering

Examining Committee:

Dr. Sanja Miskovic, Mining Engineering, UBC
Supervisor

Dr. Marek Pawlik, Mining Engineering, UBC
Supervisory Committee Member

Dr. Bern Klein, Mining Engineering, UBC
Supervisory Committee Member

Abstract

As supplies of valuable minerals become scarcer and demand increases, the mining industry must develop more efficient and effective methods to recover these minerals from ore. Various gravity separation methods are extensively used in the industry for concentration of gold, platinum group metals (PGMs), mineral sands, chromite, tin, tantalum, tungsten, iron ore, cobalt and many other metals and minerals with sufficient differences in density. The Falcon enhanced gravity separator is one example of a semi-batch enhanced gravity separation device that uses centrifugal force to enable liberated precious metal recovery within grinding circuits and from placer deposits. During run cycle, concentrator accepts feed continuously, heavy particles are retained in the riffled section of the unit's bowl, and concentrate is produced during periodic rinse cycles by water jets. Limited research has attempted to understand particle behaviour in the riffled section of the Falcon enhanced gravity separator, and little is known about the effect of design and operating parameters on the unit's concentration efficiency. This thesis focuses on studying particle behaviour in the riffled section of the Falcon gravity separator's bowl to recover the highest fraction of heavy particles. An open thin channel setup was built to emulate a cross-section of Falcon gravity separator's riffled section. Testing was conducted on the effects of riffle designs, inclination angles, and flow rates on particle behaviour. This study shows the need and value of improving the gravity separators' bowl geometry, which would significantly benefit heavy retention capabilities of this equipment.

Two experimental setups using a centrifugal pump and a peristaltic pump were developed to test 9 riffle designs over 4 flow rates and 3 inclination angles resulting in 99 distinct experimental cases. Semi-elliptical designs coupled with lower inclination angles and flow rates lead to higher heavy particle retention in riffles. This considerably improved particle recovery rates of the system possibly due to its ability to expel light particles from the riffles while pushing the heavy particles downward.

Observations of particle behaviour in this study can serve as a foundation for study on Falcon enhanced gravity separator and any gravity separation devices using engineered riffles.

Lay Summary

Falcon enhanced gravity separators are used to separate fine particles of heavy minerals from waste particles based on the density differences between heavy minerals and unwanted material.

This study focuses on developing a lab-scale model that enables a deeper understanding of particle behaviour in the riffled sections of the enhanced gravity separator and aims to provide suggestions on enhancing riffle design.

The study analyzes results from various riffle designs, inclination angles, and flow rates, providing recommendations on these parameters that are effective at retaining the highest heavy-to-light fraction in the riffles.

Preface

This thesis is the original contribution of the writer, Danny George.

This thesis is a product of collaborative research between the University of British Columbia (UBC) and Sepro Mineral Systems Corporation, under the supervision of Dr. Sanja Miskovic in the Norman B. Keevil Department of Mining Engineering department at UBC. It is part of an ongoing research project to optimize the Falcon enhanced gravity separator.

The author of this thesis designed and developed the experimental setups for this study as well as conducted experimental trials. Experimental trials were conducted at the Process Intensification in Minerals Engineering (PIME) lab at the Coal and Mineral Processing (CMP) facility at UBC.

Table of Contents

List of Tables

List of Figures

List of Graphs

List of Symbols

A	Empirical value obtained by Jiménez and Madsen
B	Empirical value obtained by Jiménez and Madsen
C_D	Drag coefficient
cm	Centimeter
D_{CF}	Depth of the flow (characteristic distance of the fluid)
D_p	Diameter of the particle
F	Froude number
F_c	Centrifugal force experienced by mass m
F_g	Gravitational force experienced by mass m
g	Gram
g_c	Factor of proportionality
g_G	Acceleration due to gravity
G	Gravitational force field
G_{CG}	Relative centrifugal force
Hz	Hertz
kg	Kilogram
L	Liter
L_{FD}	Length of flow developing zone
m	Meter
μm	Micrometer
mm	Millimeter
min	minute
m	Mass of a particle
ω	Angular velocity of mass m
r	Radius of the circular motion of mass m
Re	Reynolds number
Re_p	Reynolds number of the particle
ρ_f	Density of the fluid

ρ_p	Density of the particle
T	Dimensionless variable for time
μ	Local viscosity of the suspending medium
ν	Sedimentation velocity under a centrifugal force field
ν_g	Sedimentation velocity under a gravitational force field
γ	Inclination angle of the thin channel setup

List of Abbreviations

BEP   Best efficiency point

C-clamp   Type of clamp used to hold two parts together

CC   Concentration criterion

CSF   Corey shape factor

DOE   Design of experiment

G-force   Gravitational force

MGS   Multigravity separator

PGMs   Platinum group metals

Re   Reynolds number

RPM   Rotations per minute

SG   Specific gravity

VFD   Variable-frequency drive

Acknowledgements

I would not have been able to conjure the strength nor courage to make this work a reality if not for the help of many who were involved directly or indirectly in this work.

I am deeply grateful for the continued support and guidance of my supervisor Dr. Sanja Miskovic. Her unwavering leadership and expertise have been a great asset for me in successfully completing this work. I would also like to acknowledge her willingness and nurturing skills that allowed me to shine and hone the expertise to develop and execute innovations that help society.

I would like to thank my research sponsor, Sepro Mineral Systems Corporation, for their enormous contributions. I appreciate their willingness to go above and beyond in lending support from technical assistance to troubleshooting various aspects of the project. Their support and funding were crucial in making this thesis a reality.

I would like to thank all the members of my research group and my friends who have lent their help whenever they could to provide me with assistance. I am forever grateful to the team for assisting me through various hurdles of my research journey. I would like to give special thanks to Mr. Marwan Kenawi, Mr. Guilherme Lindner, Mr. Ikechukwu Joel, and my project partner, Mr. Utkan Caliskan, for helping me conduct the experiments. I would also like to thank Mr. Aaron Hope and Mr. Libin Tong for their continued help and support in conducting this experiment.

I am confident that without my family's unwavering support, especially my parents, I would not have been able to start such an enormous endeavor, let alone complete it. I would also like to thank my partner for all her support and help.

Special thanks to anyone I may have forgotten to mention who helped make this project a success.

Dedication

To my mom, Rani George, and my dad, George T. J., who have always believed in me and encouraged me to take on new challenges.

To my closest ally and companion, Lauren Brown, whose help and support has been invaluable for me.

Chapter 1: Introduction

Gravity concentration has been employed for millennia to capitalize on the varying density and hydraulic properties of minerals in viscous media [1]–[3]. Gravity separation and gravity concentration are interchangeable terms in the literature. There are several types of gravity separators intended for different conditions. Heavy media separation, jigging, multi-gravity separators (MGS), and flowing water streams on horizontal or inclined planes are commonly used gravity separation methods. Gravity separation using flowing streams of water on horizontal or inclined planes employ specific methods such as panning, pinched sluices and cones, shaking tables, spiral concentrators, and enhanced gravity separators such as the Falcon enhanced gravity separator of Sepro Mineral Systems Corporation. Enhanced gravity separators are the focus of this thesis.

Falcon enhanced gravity separators rely on centrifugal phenomena to separate valuable minerals from gangue. Therefore, it is important to understand these mechanics to optimize these gravity separators. In theory, solutions to simultaneously coupled partial differential equations of motion in a steady rotational field for slurry coupled with appropriate flux in the centrifugal force field and appropriate boundary conditions should be sufficient to describe all the centrifugal phenomena in an enhanced gravity separator. However, in reality, these solutions cannot be obtained even in ideal conditions, thus necessitating experimental work to supplement the analysis of centrifugal phenomena [4].

1.1   Research Motivation

To date, very little research has attempted to understand the bidensity particle laden flow in a riffled thin channel, let alone within an enhanced gravity separator. Various gravity separators have used different riffled surface designs for heavy recovery. There is little known experimental work that has analyzed the potential to maximize the performance of the riffled section of gravity separation devices by manipulating their designs and operating conditions. Specifically, the riffle shapes and the inclination angle of the edges of the gravity separator bowl have the potential for further improvements.

A lab-scale open thin channel setup allows for easier modification of riffle geometry and better control of flow rate, inclination angle, and turbulence within the system. It also enables easier recovery of heavy particles and the ability to visually gauge heavy recovery. Hence, the open thin channel setup is intended to represent a portion of the full-scale enhanced gravity separator at 1G, using a mathematical correlation established in Section 2.2. As mentioned, theory alone is insufficient to understand particle behaviour in a riffled section of an enhanced gravity separator. Therefore, this research will provide further experimental data to support theoretical conclusions.

This thesis focuses on studying potential new improvements in the riffle designs, flow rates, and inclination angles of an open thin channel setup and how this affects heavy mineral recovery. For experimental purposes, heavy minerals such as gold are substituted with steel shots due to accessibility and ease of separation from gangue materials using a magnet. The gangue is represented by glass beads. Despite the difference in density between steel shots and gold particles, the relative density differences between steel shots versus glass beads and gold particles versus its gangue are comparable, allowing experimental results to be extrapolated. This study also acts as a platform for future work on improving the functionality of enhanced gravity separators and thin channel setups (sluices) using experimental work or computation simulations.

1.2   Objectives

The purpose of this thesis is to study the flow behaviour and separation efficiency of heavy particles at the riffled section of an enhanced gravity separator using the thin channel experimental setup. This will be achieved by varying riffle designs, inclination angles, and flow rates in the experiments. The specific sub-objectives of this thesis are:

a. Investigate the effect of riffle design on separation efficiency of heavy particles in open thin channel with riffles

b. Investigate the effect of slurry flow rate and inclination angle on separation efficiency of heavy particles in open thin channel with riffles

c. Understand how separation behaviour at different flow rates, inclination angles, and riffle shapes affects heavy particle retention in the riffled section

This thesis will evaluate the rationale and development of the experimental thin channel setup, experimental matrix, results, and recommendations for the future work.

1.3   Thesis Structure

Chapter 1 presents a general introduction to the thesis, the motivation, and objectives.

Chapter 2 reviews the relevant literature on gravity separation, the analytical correlation of 1G to 200G centrifugal force, granular segregation, hydraulic transport, bidensity particle laden flow and the science behind the thin channel setup.

Chapter 3 presents the experimental methodology; the thin channel segment; the manipulated variables such as flow rate, inclination angle, and riffle design; design of experiments; performance indices; and an assessment of experimental errors.

Chapter 4 presents experimental results with analysis of grade recovery, mass yield, enrichment factor, separation efficiency, and the impact of manipulated variables on heavy particle retention.

Chapter 5 summarizes and concludes the thesis.

Chapter 6 discusses future recommendations for research and the industry.

Chapter 2: Background

One of the most important applications of enhanced gravity separators is within the process of concentration of gold, PGMs, mineral sands, chromite, tin, tantalum, tungsten, iron ore, cobalt as well as many other metals and minerals with sufficient differences in density. Various extraction methods have been employed to extract gold from their ores, and selection of the processing approach is based on the quantity and quality of the gold particle within the deposit [5]. For instance, in open-pit mines, the ores are excavated from hard rocks using dynamite and processed further using chemicals like cyanide to recover gold [6]. It has been shown that gravity recovery of coarse gold before any chemical processing helps in maximizing overall gold recovery [7]. Enhanced gravity separators can recover fine gold particles, increasing their importance in the gold production industry. As the demand for gold increases, the need to further understand and improve the design of conventional enhanced gravity separator devices, like the Falcon enhanced gravity concentrator, increases [8], [9]. Improvements in enhanced gravity separators would lead to increased efficiency by means of lower water and energy consumption and higher valuables recovery.

There are several types of gravity separators intended for different applications and conditions. Commonly used gravity separators are jigs, shaking tables, spiral concentrators, and enhanced gravity separators to name a few [2]. In jigging, the jig screen is constantly pulsating, separating minerals based on the difference in their density. In this setup, the heavier particles penetrate down through the jig screen while lighter particles exit as tailings due to particle density and size. Jigging is not suitable for separating finer particles [10]. Another commonly used gravity separation technique is shaking tables, where a motor driven table with an engineered riffled sloped deck surface shakes at a slow forward stoke followed by a rapid return along the riffle pattern. The riffles convey heavy minerals parallel to the oscillation motion. The intermediate section on the sloped deck allows recovery of middlings. Shaking tables are not a viable separator for minerals that are ultra-fine or flat-shaped [1], [11]. Similarly, a spiral concentrator is a low-cost gravity separator that has a high-capacity system for the concentration of low-grade mineral ore in slurry form. Separation in this system is achieved through stratification of minerals due to centrifugal force, differential settling, and heavy particle migration as the minerals in slurry form travel

through helical sluices wrapped around a central collection column [1], [11]. Spiral concentrators are not ideal for recovering minerals below 150 µm though they are effective for separation of larger particles. Compared to previous gravity separation techniques, enhanced gravity separators are a relatively new technology in flowing film concentration that utilizes the effects of centrifugal force [1]. This technology is better in recovering particles of size up to 1µm in diameter, which would otherwise flow into the tailings [1].

One of the earliest enhanced gravity separators was developed by Benjamin Virgil Knelson, who started working on industry scale gravity separators in the mid-1970s. Later, Falcon developed their enhanced gravity separators in the 1980s [12]–[14]. There are several types of gravity separators intended for separation based on mass pull, bowl geometries, particle size, modes of operation, and concentrate collection and retention areas. Enhanced gravity separators utilize an elevated gravitational force field of a spinning bowl with fluidized riffles along the walls. The minerals enter the bowl at the center in slurry form and are pushed up along the riffled edges of the bowl, where the heavier minerals are retained in the riffles. The lighter particles are carried out of the bowl as tailings [12]. As seen in Figure 2.1, the Falcon enhanced gravity separators have specialized riffles along the top edge of the spinning bowl meant for the recovery of heavy particles [4], [15], [16].
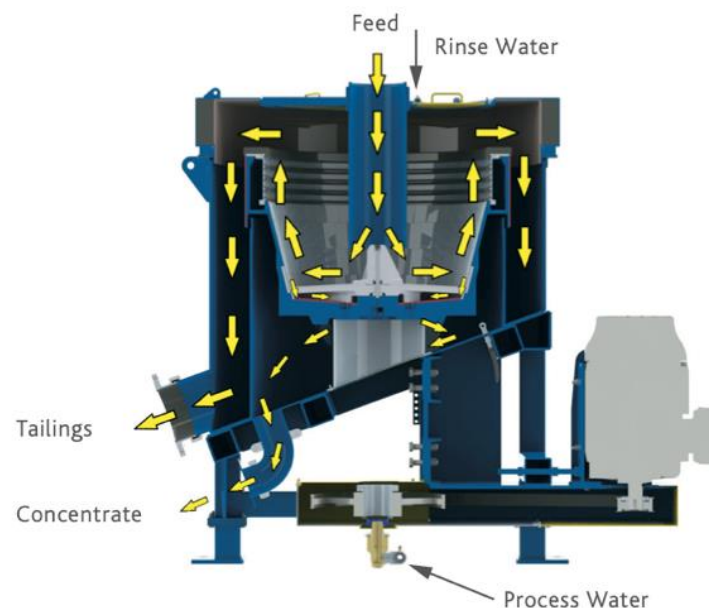
Figure 2.1: Falcon enhanced gravity separator. Reprinted from [16]

Ancia et al. [15] compared the Knelson and Falcon enhanced gravity separators' mineral recovery in lab-scale models. They found that at lower flow rates, fine heavy minerals particles can be separated by infiltrating the porous fixed bed formed at the riffled area and large particle heavy minerals particles can be separated by staying atop the bed. When flow rates are higher, the contents of the separators are fluidized and heavy particles settle on the bed, causing gangue to be ejected once sufficient heavy particles have settled. At the highest flow rates, gangue is ejected regardless of heavy mineral retention. This observation was recorded by Zhou et al as well [17]. This suggests a range of particle behaviour which leads to increased concentration of heavy particles (heavy recovery), including particle size, fluidization, and light particle ejection [12], [15]. Comparison of the Falcon enhanced gravity separator and Knelson enhanced gravity separator showed that the Falcon was less sensitive to particle size effects and flow rates than the Knelson enhanced gravity separator [15]. An important conclusion to be drawn from these previous studies is that there is limited knowledge on the fundamental understanding and performance of these enhanced gravity separators, especially at lower and higher flow rates.

Analysis of the past literature [4], [8], [9], [15] showed that limited studies have been conducted on the impact of inclination angle on segregation performance of heavy fraction in enhanced gravity separator riffles. Additionally, there has been little scientific analysis of riffle designs adopted in the Knelson and Falcon enhanced gravity separators, which are the leading enhanced gravity separators in the industry [4]. Since little research has attempted to understand the impact of riffle design variations and inclination angle on the gravity separator, this study aims to improve these aspects of the separator. This would be crucial in enhancing the performance of these equipment and gravity separators that employ engineered riffled sections.

Understanding of the complex fluid-particle interaction of the dense slurry flow within the gravity concentrator is crucial to comprehend the effects of different parameters such as the inclination angle, inlet flow rate and riffle design. This fluid-solid particle interaction is influenced by forces such as the gravitational force, centrifugal force, viscous drag, and flow turbulence, where the centrifugal force is the dominant force in enhanced gravity separators. Given the difficulty in experimental analysis of a closed system such as the gravity separator, an inclined thin channel riffled setup with transparent walls is used for the experimental investigation of the fluid particle

interaction of the dense slurry flow. Use of such a setup can be justified by correlating the effect of force on the slurry flow, normal to the riffle in both thin channel and enhanced gravity separator, as analytically explained in the Section 2.2. Prior to describing the experimental setup and analysis, it is paramount to comprehend the particle-particle interaction in dry mixture (Section 2.3 Granular Segregation), particle-fluid interaction (Section 2.4 Hydraulic Transport) and bidensity particle laden flow (Section 2.5 Bidensity Particle Laden Flow) in the slurry flowing through the thin channel setup. As separation within enhanced gravity concentrators involves a combination of these phenomena, it is important to evaluate these interactions. Before proceeding further, it is also imperative to analyze the basic principle for gravity concentration by addressing the concentration criterion.

2.1   Gravity Concentration Criterion

Several mineral combinations are unresponsive to gravity separation, so mineral combinations, including mixtures, need to satisfy the concentration criterion (CC) as shown in equation (1) for separation using gravity.

$$\text{Concentration Criterion} = \frac{\text{SG of heavy particles} - \text{SG of fluid}}{\text{SG of light particles} - \text{SG of fluid}} \quad (1)$$

where SG denotes specific gravity. Commonly used CC ratios for minerals concentrated using gravity separation from a gangue (density of 2650 kg/m^3) are shown in Table 2.1. Table 2.2 shows the guidelines for this separation technique.

Table 2.1: CC of common minerals separated by gravity separation [11]

Minerals	Fluid	CC
Gold	Air	6.8
Gold	Water	10.3
Cassiterite	Water	3.5
Coal	Water	3.4
Hematite	Water	2.5

Table 2.2: Guide for gravity separation CC [18]

Concentration Criterion	Suitable to gravity separation
CC > 2.5	Simple down to 75 µm
1.75 < CC < 2.5	Possible down to 150 µm
1. 5 < CC < 1.75	Possible down to 1.7 mm
1.25 < CC < 1.5	Possible down to 6.35 mm
CC < 1.25	Impossible at any size
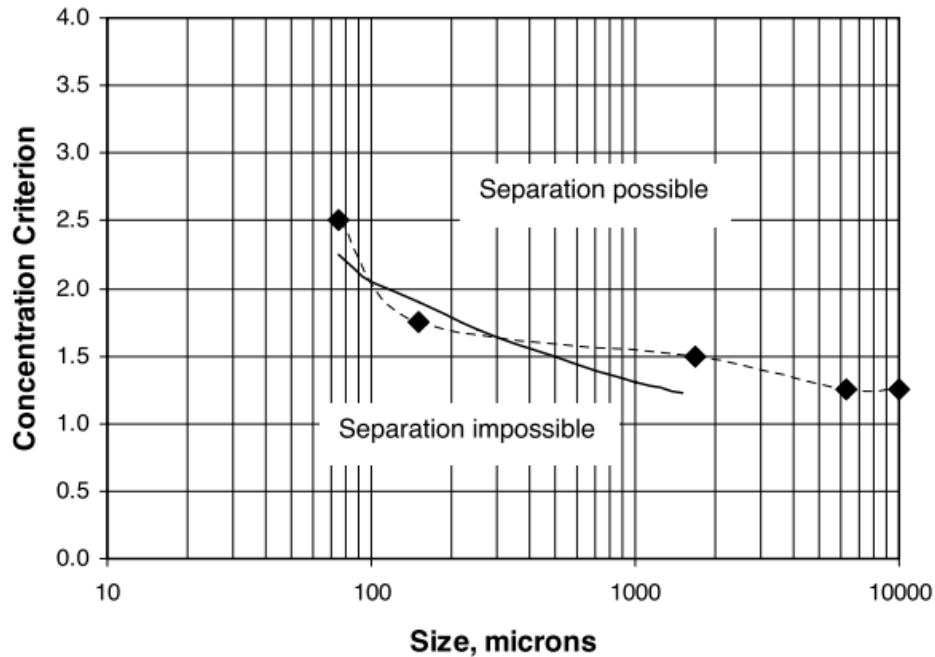
Graph 2.1: CC based on particle size. Solid line based on Burt's [19] work along with the data from Table 2.2 Reprinted from [11]

Since gold falls well within the range of concentration criterion, gold can be separated using gravity, especially with enhanced gravity separators. The slurry mixture used in this thesis can be separated using gravity as its heavy mineral component, steel shot particles (derivative of hematite), can also be separated using gravity concentration as shown in Table 2.1.

2.2 Mathematical Correlation of 1G and 200G

The enhanced gravity separators employ centrifugal force for concentration, which is an artificially generated gravitational field higher than 1G (where G is gravitational force field), where particle settling is elevated [4]. It is paramount to understand the theoretical settling velocities of spherical particles under a gravitational field of 1G and a centrifugal force field of 200G [4]. Based on this, a mathematical correlation between a 1G system and a 200G system allows a study conducted on a 1G system to be extrapolated to a 200G Falcon enhanced gravity separator as Majumder and Barnwal determined in their work [4].

Consider the mass of a single spherical particle in a mixture as denoted by m. When a particle with a mass m revolves at a radius r with an angular velocity ω, the particle experiences a centrifugal force $F_c = m\omega^2 r$ in the radial direction. Assuming that the centrifugal acceleration is much greater than the gravitational acceleration, the settling velocity of the particle (v) can be considered to be in the radial direction. The same particle under the influence of only gravitational force $F_g = mg_G$, where g_G is acceleration due to gravity would experience a particle settling velocity, v_g. The relative centrifugal force, G$_{CG}$, is the ratio of centrifugal to gravitational force, denoted by

$$G_{CG} = \frac{F_c}{F_g} = \frac{\omega^2 r}{g_G} \tag{2}$$

In a centrifugal field, the sedimentation of a spherical particle immersed in an incompressible fluid is governed by [4], [20]

$$\frac{dv}{dt} + \frac{18\mu}{\rho_p D_p^2} v = \frac{\omega^2 r}{\rho_p} (\rho_p - \rho_f) \tag{3}$$

In equation (3), ρ_p is the particle density, D_p is the particle diameter, μ is the viscosity of the suspending medium and ρ_f is the density of the fluid. As the acceleration term in equation (3) reaches zero, the terminal settling velocity of a small particle settling in the Stokes regime ($10^{-4} < $ Re $ < 0.4$) can be written as [4]

$$v = \frac{(\rho_p - \rho_f)D_p^2 \omega^2 r}{18\mu} \tag{4}$$

$$\text{Re} = \frac{D_p \rho_p v}{\mu} \tag{5}$$

where Re is the Reynolds number defined in equation (5). By incorporating equation (2) into equation (4), the equation for terminal settling velocity becomes [4]

$$v = G_{CG} v_g \tag{6}$$

where v_g represents the settling velocity of a particle under only gravitational force.

For a particle settling outside the Stokes regime, the system is modeled by applying particle movement mechanics through an incompressible fluid. Under these conditions, Hsu [20] derived the following correlations for terminal velocity under gravitational and centrifugal forces:

$$v = G_{CG}^{1/2} v_g \qquad\qquad 0.4 < \text{Re} < 5000 \tag{7}$$

$$v = G_{CG}^{1/3} v_g \qquad\qquad 500 < \text{Re} < 2 \times 10^5 \tag{8}$$

The settling velocity under gravitational force (v_g) is defined by equation (9) and (10) using Stokes' Law for fine particles (equation (9)), representing viscous resistance, and Newton's Law (equation (10)) for coarse particles, representing turbulent resistance [11].

$$v_g = \frac{g(\rho_p - \rho_f)D_p^{\,2}}{18\mu} \tag{9}$$

$$v_g = \sqrt{\frac{4g(\rho_p - \rho_f)D_p}{3C_D\rho_f}} \tag{10}$$

where C_D is the drag coefficient. Equation (10) is valid for Re > 1000 while Stokes' equation (9) applies for Re < 1. The settling velocities empirical relations are dependent on drag coefficients, which are expressed as

$$C_D = \frac{1}{3}\left(A + \sqrt{A^2 + \frac{16B}{\text{Re}_p}}\right)^2 \tag{11}$$

where Re_p is the Reynold's number of a particle. The drag coefficient is developed as a solution from the coefficients A and B. Table 2.3 depicts the empirical values of A and B that were obtained by Jiménez and Madsen [11], [21] for different shaped particles with Corey shape factor (CSF) of 0.7.

Table 2.3: Empirical values for coefficients A and B in equation (11) [21]

Roundness Factor	A	B
2.5 (crushed)	0.995	5.211
3.5 (natural)	0.954	5.121
6.0 (well rounded)	0.890	4.974
Spheres	0.794	4.606

By analyzing equations (6) to (8), it is evident that as centrifugal force increases, the particle settling velocity increases with the rate of increase dependent on the Reynolds number of the flow [22]. Figure 2.2 shows the theoretical settling velocities of pure coal, shale and pyrite with SGs of 1.3, 2.5, and 4.8, respectively, as described by Luttrell [23]. From this plot it is evident that as particle size reduces, centrifugal force has a more dominant effect on the particle settling velocity.
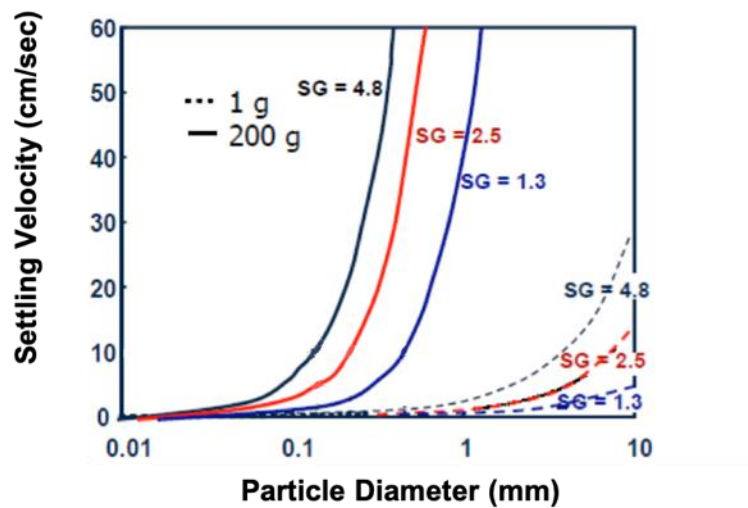
Figure 2.2: Effect of centrifugal force on particle settling velocities. Reprinted from [23], [24]

Since a correlation for settling velocity for particles under gravitational force (1G) and centrifugal force (200G) has been extended, a thin channel setup that employs 1G can be used as a baseline to further extend enhanced gravity separators that operate at higher Gs. This setup would be equivalent to a centrifugal concentrator with acceleration 1G.

2.3   Granular Segregation

Segregation of a granular material mixture with dissimilar densities, sizes or other physical material properties when they are flowing [25]–[28] or vibrating [29]–[31] was first reported in 1939 by Brown [32] and extensively studied by the engineering community [33]–[36]. In 1987, this phenomenon was brought to the attention of researchers through the "Brazil Nut Problem" (BNP) [37]. Interestingly, the results of this problem developed into the benchmark for granular segregation [31]. This kind of segregation is a common occurrence in industrial processes encompassing geophysical transport like debris flow [38], mineral transport [39], pyroclastic flow [40] and handling of bulk solids [41], [42].

Particle size [43] and density [44] are the critical factors that enable segregation in free surface flows along an inclined channel [45]–[49]. These factors lead to upward movement of larger particles in free surface flow of granular mixtures [25]. Most studies have investigated particle granular segregation in dry flow based on continuum mixture theory [50]–[52]. However, in 2013 and 2015, Larcher and Jenkins proposed granular segregation in the context of kinetic theory for dry, granular mixtures where all parameters are dependent on measured particle properties: material density, size and coefficient of restitution [53], [54]. Later in 2017, Larcher and Jenkins further enhanced the approach to particle-fluid flows that relies on measured particle properties [55].

Segregation of bidensity granular mixture on a slope is a factor of particle properties with minor variance in radii and rheology of the flow. The differences in radii and masses creates differences in flow depth and particle flux. Larcher and Jenkins also found that size differences play a greater role in segregation than mass differences as the particle flux is enhanced when the particles have similar volumes [55].

2.4   Hydraulic Transport

Industries such as food, fuel and mineral processing industry require transportation of mixtures of dispersed particles in a fluid over large distances [56], [57]. Classic examples of such conveyance of solid materials suspended in a liquid medium include slurry transportation of sand and mineral ores in the mining, china clay production, and pigment and paint production [57], [58]. Non-settling slurries and settling suspensions are the two types of hydraulic transport of particulate solids.

In the case of non-settling slurry, a homogenous mixture of a fluid with relatively fine particles ($D_p < 30$ μm) in high concentrations experiences a small amount of particle deposition due to strong particle-fluid and particle-particle interactions. In an adequate medium, transportation is often carried out in laminar or transitional flow even though they show non-Newtonian flow behaviour. In 1984, Ayazi characterized the non-Newtonian behaviour as factors of solid concentration, operating conditions, particle-fluid and particle-particle interactions, and fluid and particle properties [58].

For a settling suspension, a mixture of low-viscosity fluid and large size ($D_p > 40$ μm) or heavy particles, particles tend to settle to the bottom of the conveying system in the absence of sufficient turbulence in the fluid or low fluid velocity. The behaviour of suspensions depends on multiple things such as head losses, particle concentration and fluid flow conditions (Figure 2.3). In cases of disproportionately large and heavy particles, a solid concentration gradient will develop across the cross-section of the heterogeneous suspension in the pipe or channel. At lower fluid velocity above a critical value, the larger and heavy particles settle at the bottom and move along the floor of the system as a sliding bed [58].
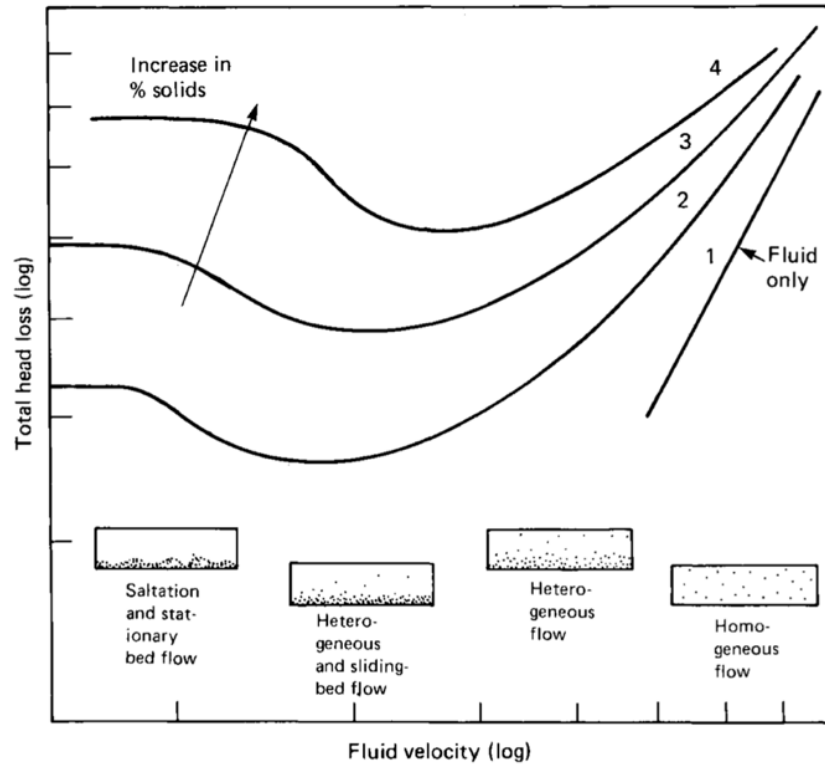
Figure 2.3: General pressure drop vs. fluid velocity curves for hydraulic transport of settling suspensions. Reprinted from [58]. Line 1: Frictional loss through the pipe of carrier fluid without particles. Lines 2–4: Trends in pressure drop for suspensions with increasing percentage of solids for a range of fluid velocities.

2.5   Bidensity Particle Laden Flow

Bidensity particle laden flow is a type of two-phase fluid flow, where one phase is constantly connected (carrier phase) and the other phase is diluted particles (dispersed or particle phase) [59]. In this flow, the diluted particle phase has particles with two distinguished density profiles. Previous studies on bidensity flow include the sedimentation [60]–[63] as well as resuspension of bidensity mixture in a constant shear flow [64].

Inclination angle of the flow has been shown to influence the mixing of the bidensity particle laden flow. Lower inclination angles lead to less mixed flow as observed by Lee et al., where they observed stratification of the bidensity mixture into separate layers at lower inclination angles [65]. Lee et al. experimentally and numerically deduced that particle segregation is greater in the settled regime than the ridged regime, with better mixing occurring in the ridged regime [66]. Applied to

14

mineral processing, bidensity particle laden flows at lower inclination angles would, in theory, result in better segregation into heavy minerals and gangue, leading to higher mineral recovery rates.

The competing effects of shear induced migration and gravitational settling within the case of bidensity mixtures were studied experimentally by Wong et al [66] where varying fractions of solids and inclination angles were used to analyze the interparticle interaction between the particles with different densities. Lee at al. further study the bifurcation behaviour of the settled and ridged regime within bidensity suspension flow [65]. However, this bifurcation behaviour is limited to low Reynolds number and highly viscous flows [65], [66]. There are very limited studies conducted on bidensity particle laden flow for high Reynolds number turbulent flow despite its potential implications in the industry. This study focuses on bidensity particle laden flow on an inclined plane, referred to as open thin channel flow as described in the next section.

2.6   Thin Channel Setup

The thin channel setup is a derivative of a commonly used equipment called a sluice. Sluices are one of the most simplified forms of gravity separators consisting of an inclined trough with openings at both ends [1]. A slurry consisting of solids and water is fed from the top while minerals separation can occur along the sloped surface. The separation that can be seen in this setup is dependent on the inclination angle, surface roughness, size and density of the particles, the solid-liquid ratio, length of the trough, thickness of the slurry flow, fluid velocity and fluid density [11], [43]. The fluid-particle interaction can be further enhanced using rough texture or cross-section riffles [67]. The thin channel flow can be considered as a flowing film under laminar or turbulent flow condition. Within the laminar flow, the fluid velocity gradient is varying in a parabolic manner along the thickness of the slurry flow. In turbulent flow, this velocity gradient is flatter but the velocity decreases closer to the slurry bed [11]. Figure 2.4 shows the impact of particle size and particle density on the segregation in the channel for a smooth surface when the flow is within the laminar regime [11]. In a sluice, after a period of time, some heavies may move with the light particles into the tailings as shown in Figure 2.5.
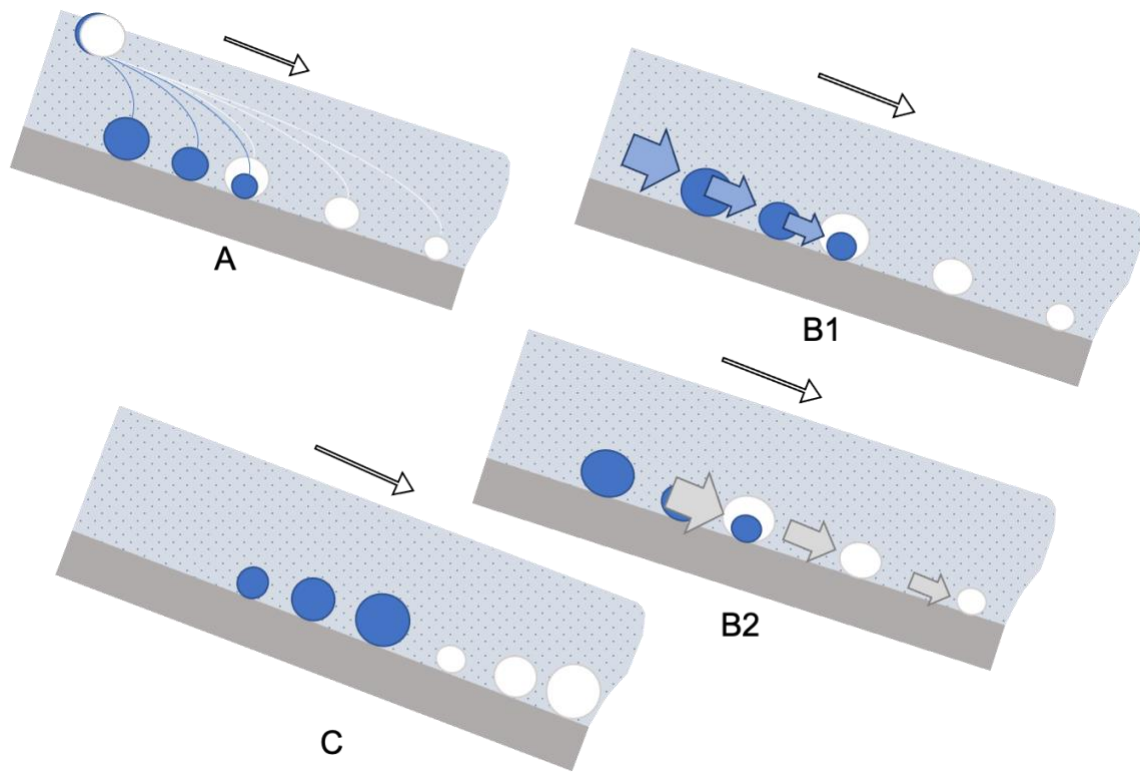
Figure 2.4: Impact of density, particle size and velocity of the fluid on particle segregation; ● – heavy particle & ○ – light particles. Image A depicts different settling rates of the particles. Image B1 & B2 shows the different forces being applied on the particles based on its size. Image C shows the final segregation in a thin channel
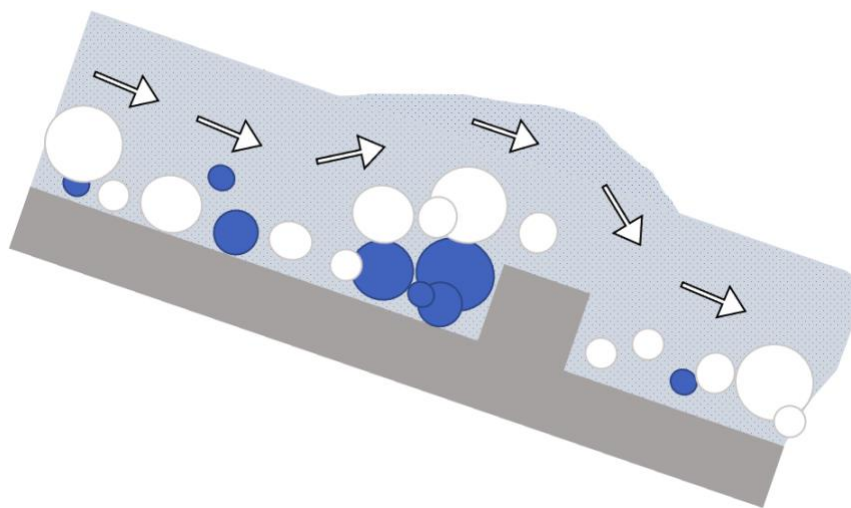
Figure 2.5: Impact of a riffle on segregation of lights and heavies in a thin channel flow

2.7 Summary

Slurry transportation characteristics and fluid flow behaviour in open and rectangular channels have been researched for many years [22]. Over the years, many researchers have concentrated on gravity-driven clear liquid flows [68]–[73] and pure granular flows [74]–[76] but very few have worked on particle-laden thin film flows [77]–[80]. The work on sedimentation in suspensions and settling of particles in quiescent liquids have gained noteworthy consideration [63], [81]–[85] but as previously stated, limited research have been focused on bidensity particle laden flow for high Reynolds number turbulent flow.

In other applications, lower inclination angles and lower flow rates have been suggested to increase heavy particle retention [45]. Altering these operating parameters does not appear to have been studied in an open thin channel or in enhanced gravity separators. This thesis extends findings from past literature by manipulating operating parameters to observe particle behaviour in the thin channel setup.

As established from past literature, there has been limited work on bidensity particle laden flows down horizontal channel which includes the turbulent characteristics of the fluid and that can be applied to dense slurry flow, further stating the importance of this study. The need for such an experimental study has also been advocated for by other researchers [55], [66].

Chapter 3: Research Methodology

3.1 Experimental Setup Overview

This section discusses the technical details of two experimental setups used in this study. Both setups consist of the thin channel segment, a mixing tank, an agitator (mixer), a pump, and connecting piping. The manipulated variables are riffle design, inclination angle, and flow rate in each experimental trial.

In experimental setup 1, high slurry flow rates of 22, 23 and 24 L/min were driven by a centrifugal pump. While keeping the pump rate constant, the feed rate to the thin channel segment was adjusted by controlling the flow rate of the slurry in the recirculation loop. In experimental setup 2, a low flow rate of 8 L/min was achieved by using a peristaltic pump. Both systems are designed to be robust and to ensure reproducibility of the results. The piping and tubing used in experimental setup 2 are designed to be shorter compared to setup 1 to minimize particle settling in these parts of the system.

3.1.1 Overall Experimental Setup
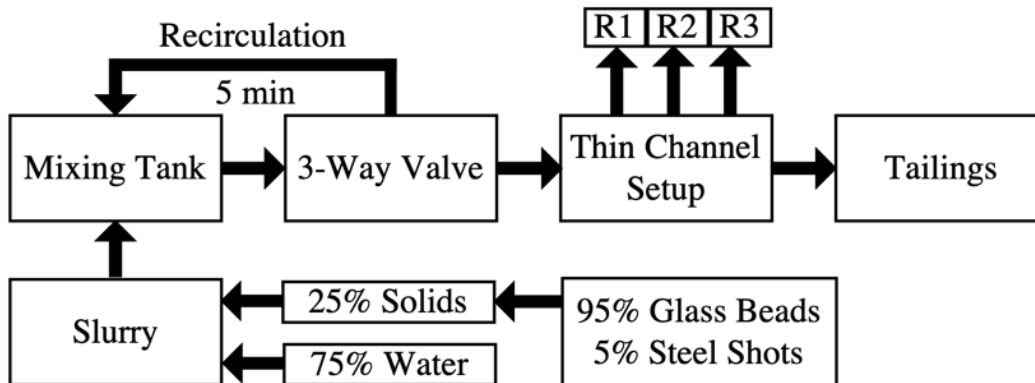
Figure 3.1: General procedure of the experiment setups

Both experimental setups follow a general procedure as shown in Figure 3.1. A tank containing the slurry mixture is constantly stirred or agitated. This solution is pumped through piping or tubing using a pump to a 3-way valve which is connected to the thin channel segment as well as a recirculation tube that brings the slurry back to the tank. The slurry is recirculated for 5 minutes

prior to the experimental trial. After this time, using the 3-way valve connected to the thin channel, the slurry enters the system as a homogeneous mixture. Each trial in experimental setup 1 is 10 seconds long and each trial in experimental setup 2 is 5 seconds long. These timings are based on the time required for the riffles to be compact with particles and establish a statistically stationary flow over the riffles. Once the experimental trial is complete, the particle mixtures from each of the three riffles and outlet (tailings) are meticulously removed and collected in separate trays. The samples in trays are dewatered using a vacuum filter and an oven. The light and heavy particles are separated from each dry sample using a neodymium magnet and then weighed. This data is tabulated for further analysis.

Figure 3.2 provides a pictorial overview of setup 1. The centrifugal pump used in this setup is the Sepro iPump with 25 L tank capacity. The slurry is pumped to the system through tubing 1 (orange arrow) and exits through tubing 2 (blue arrow) while valve 1 is closed and valve 2 is completely open. This setup allows the iPump to work as an agitator and a pump simultaneously. After the mixture has become homogenous, valve 1 is opened to allow the mixture to pass through the flow meter and re-enter the pump through tubing 3 (green arrow). This allows the experimenter to achieve the desired flow by adjusting valve 1 and valve 2 before allowing any slurry to enter the thin channel. Once the desired flow rate is achieved and the system has reached equilibrium, the 3-way valve is opened to allow the slurry to pass to the thin channel through tubing 4, which represents the start of the experiment. After 10 seconds, the 3-way valve is closed, and slurry is diverted back to the pump through tubing 3 at the end of the experiment. The samples from the riffles are collected as previously stated for further analysis.

An overview of experimental setup 2 is shown in Figure 3.3. A slurry mixture is prepared in the mixing tank and particles are kept in the suspension using a Caframo RZR1 overhead stirrer running at 1900 RPM. A ball valve at the bottom of the mixing tank is opened to allow the mixture to enter Sepro's C15 peristaltic pump from which the slurry is pumped back into the mixing tank via a 3-way valve until the system reaches equilibrium. Then, the slurry is diverted to the thin channel via a 3-way valve, representing the start of the experiment. After 5 seconds, the 3-way valve is turned back to the slurry recirculation position, representing the end of the experiment. The samples from the riffles are collected as previously stated for further analysis.
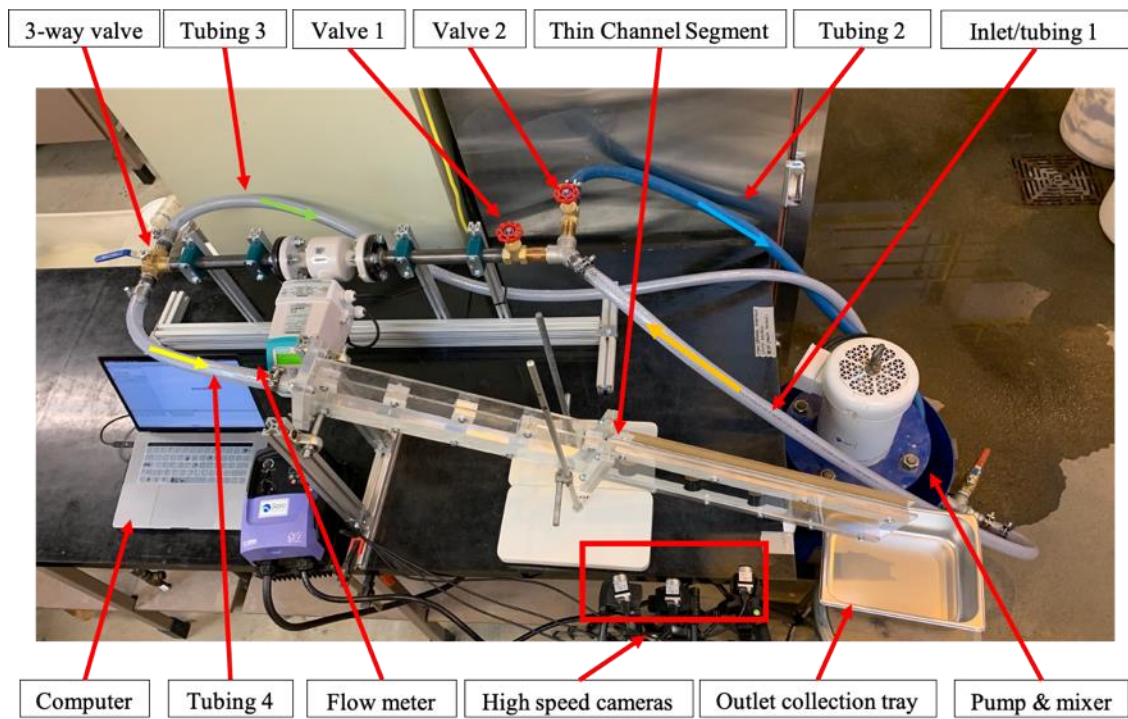
Figure 3.2: Experimental setup 1
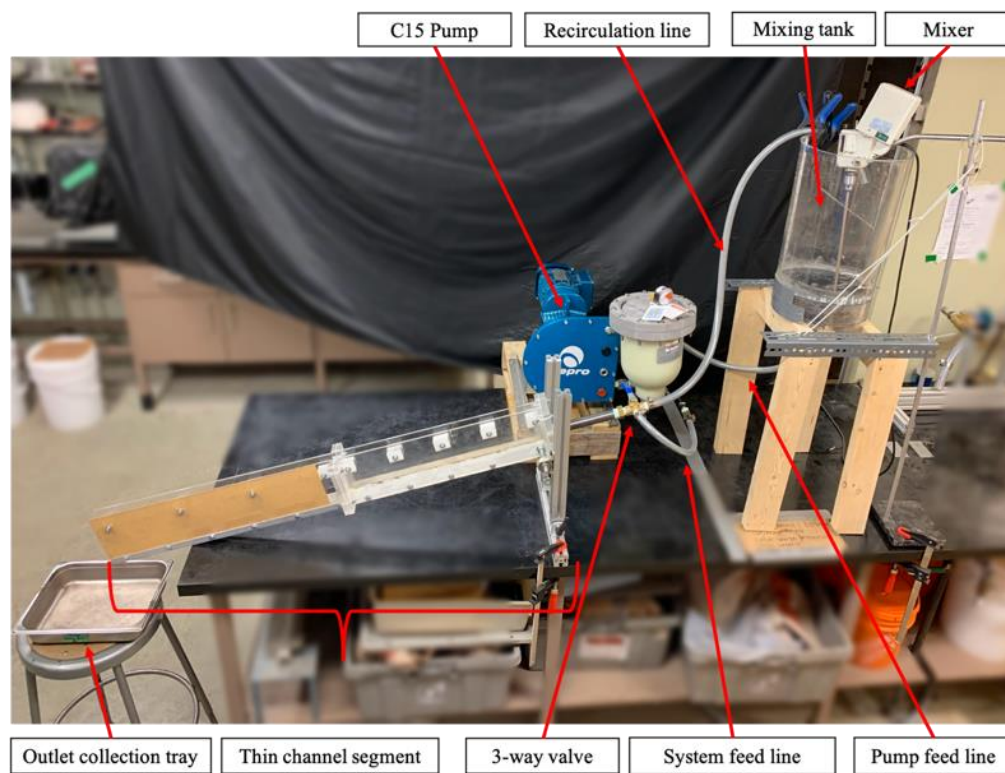
Figure 3.3: Experimental setup 2

3.1.2   Thin Channel Segment

The thin channel portion of the experimental setup consists of 2 parts: the sluice with a flat segment followed by a riffled segment, and the stand to adjust the inclination angle (Figure 3.4).
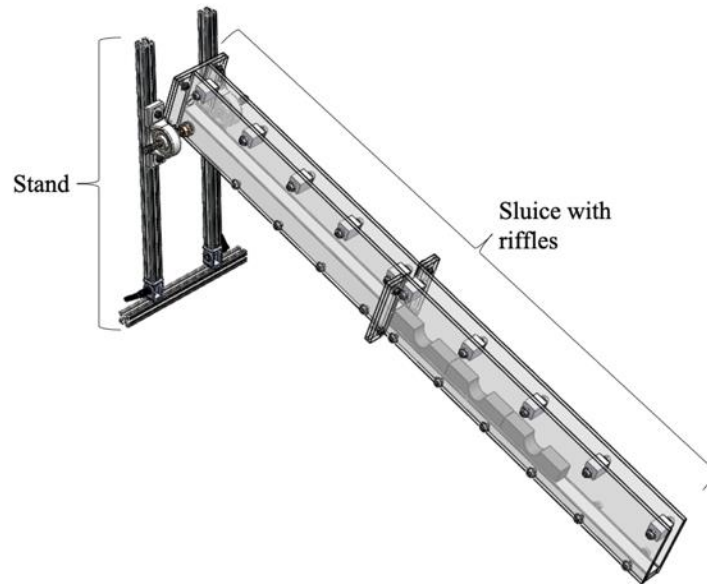
Figure 3.4: Isometric view of the thin channel segment

The sluice is attached to the stand using a threaded rod that is nested within two mounted ball bearings that are secured on railings attached to the base of the stand using locking pivots. The locking pivots allow fine-tuning of the roll, pitch, yaw, and inclination angle of the thin channel. By sliding the ball bearings along the vertical aluminum extrusion rails, the thin channel's inclination angle is adjusted. The base of the stand is secured to a workbench using C-clamps.

The thin channel segment is 120.65 cm long, 2.54 cm wide, and 15.24 cm tall (Figure 3.5). The walls of the channel are made of transparent acrylic sheets for monitoring particle behaviour and fluid flow. The first section of the thin channel allows the slurry flow to fully develop before entering the second section, as elaborated further in Section 3.2.1. The second section consists of three riffles named R1, R2, and R3. One of the side panels in the second section of the channel is removable, thus allowing different riffle designs to be tested. The aluminum base in the second section has a 3.05 cm deep cutout that is intended for placing the riffles in such a way that a fully developed flow in the first section enters the second section smoothly (Figure 3.5). The distance

from the inlet of the thin channel to the first riffle is 62.86 cm with the center-to-center gap between each riffle being 15 cm.
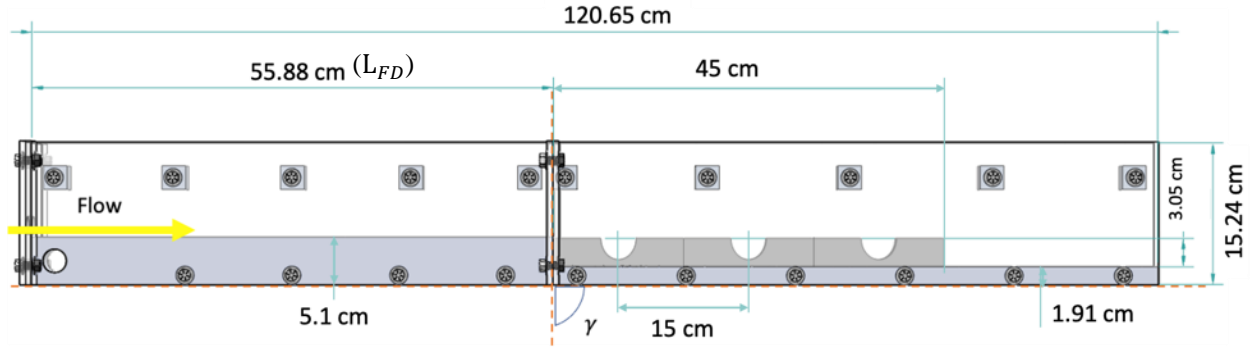
Figure 3.5: Front view of the thin channel segment

3.2   Operating Conditions

3.2.1   Flow Stabilization

The flow that enters the riffled section needs to be fully developed to ensure minimization of the flow fluctuations caused by the turbulence leading to increased reproducibility of the experiments. This also ensures that trials are conducted as consistently as possible, so each riffle design experiences similar flow behavior. To achieve this, the length of the flow developing zone (L_{FD} shown in Figure 3.5) has been designed based on the correlation between Reynolds number (Re) and Froude number (F) that was developed by Kirkgöz and Ardiçlioğlu [86] and is given as

$$\frac{L_{FD}}{D_{CF}} = 76 - 0.0001 \frac{Re}{F} \tag{12}$$

where L_{FD} is length of the flow developing zone and D_{CF} is the depth of the flow. The calculated value of the flow developing zone is 53.10 cm for a slurry velocity of 24 L/min. The actual length of the flow developing zone is 55.88 cm in the experimental setup to account for any margin of error and to allow testing using a wider range of flow velocities. The average height of the liquid film is 7 mm and with an average height fluctuation of ± 1 mm. The calculation is provided in detail in Appendix A

3.2.2   Inclination Angle

The inclination angle (γ) is a critical parameter investigated in this study as it plays a significant role in segregation of bidensity particle laden flows [65]. To better understand the impact of

segregation at various slopes, inclination angles of 9º, 12º, and 15º on heavy particle recovery are analyzed for various riffle designs and flow rates. These angles are selected based on the current bowl geometry of conventional enhanced gravity separators.

3.2.3   Flow Rates

The slurry flow rates for the experiments were chosen based on the best efficiency point (BEP) of the pumps in the experiment setups. The flow rates were adjusted using the variable-frequency drive (VFD) of the pump. For experimental setup 1, the slurry flow rates chosen were 22, 23, and 24 L/min by setting the VFD of the iPump at 55, 57.5, and 60 Hz, respectively. These flows were in turbulence regime (A.1). For experimental setup 2, an average volumetric flow rate of 8 L/min was achieved at 60 Hz on the VFD for the C15 peristaltic pump. This flow was in transitional regime (A.1). Analysis of riffles design on heavy particle recovery at various flow rates furthers the understanding of the impact of both bowl design and slurry flow regime on separation efficiency in enhanced gravity separation units.

3.3   Material and Slurry Properties

The slurry mixture constituents are water, glass beads, and steel shots; steel shots with density of 7800 kg/m^3 are used as heavy particle and glass beads with density of 2600 kg/m^3 as light particle. These material substitutions are selected due to their uniform shape, size, and ease of recovery.

A slurry mixture with 25% of solids consisting of a bidensity blend of glass beads (95% mass fraction), steel shots (5% mass fraction), and water is prepared in the respective mixing tanks for experimental setups 1 and 2. As shown in equation (13), the CC of the mixture is 4.25, hence gravity separation is easily possible as described in Section 2.1.

$$CC = \frac{7800 - 1000}{2600 - 1000} = 4.25 \tag{13}$$

The particle size distribution of glass beads is shown in Table 3.1 and their morphology is shown in Figure 3.6. The particle size distribution of steel shots is shown in Table 3.2 and their morphology is shown in Figure 3.7. The overall particle size range for the solids used in this study goes between 212 µm and 300 µm (narrow distribution). The particle size distribution curve of both glass beads and steel shots are shown in Graph 3.1.

Table 3.1: Particle size distribution – glass beads

Sieve Opening (μm)	Material Retained (g)	Cumulative Mass Retained (g)	Percentage Passing (%)
600	0	0	100
425	2	2	99.8
300	8	10	99
212	838	848	15.2
150	132	980	2
106	19	999	0.1
75	1	1000	0
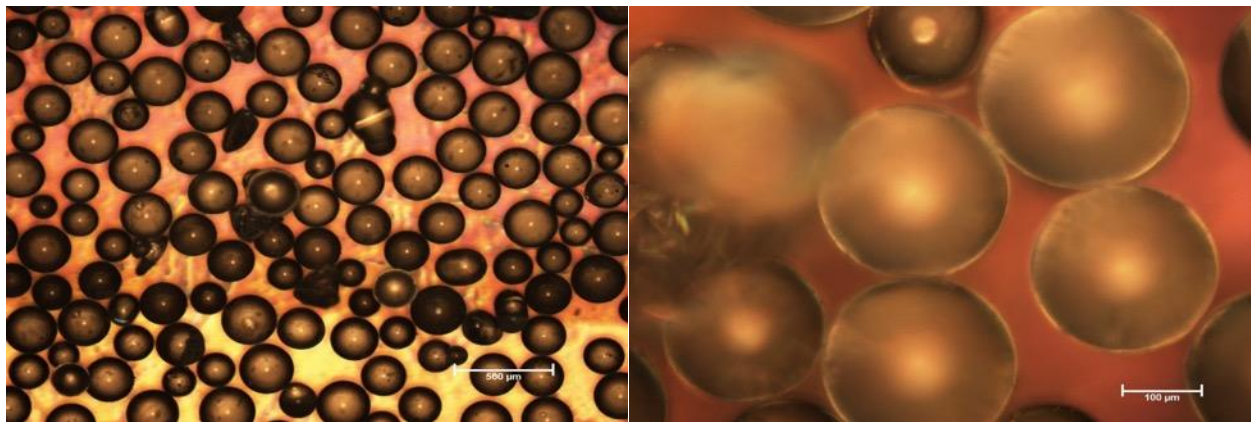
Figure 3.6: Morphology of glass beads

Table 3.2: Particle size distribution – steel shots

Sieve Opening (μm)	Material Retained (g)	Cumulative Mass Retained (g)	Percentage Passing (%)
600	0	0	100
425	379	379	62.1
300	593	972	2.8
212	28	1000	0
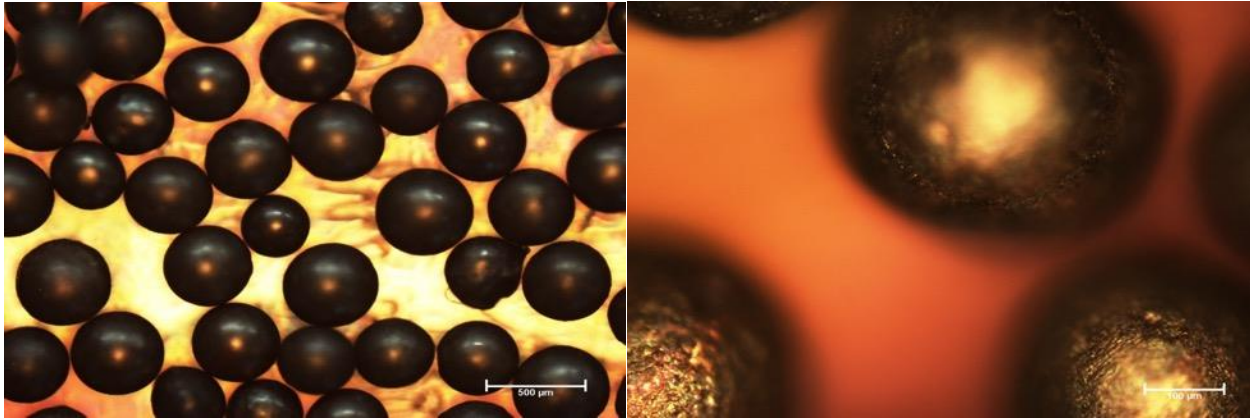
Figure 3.7: Morphology of steel shots
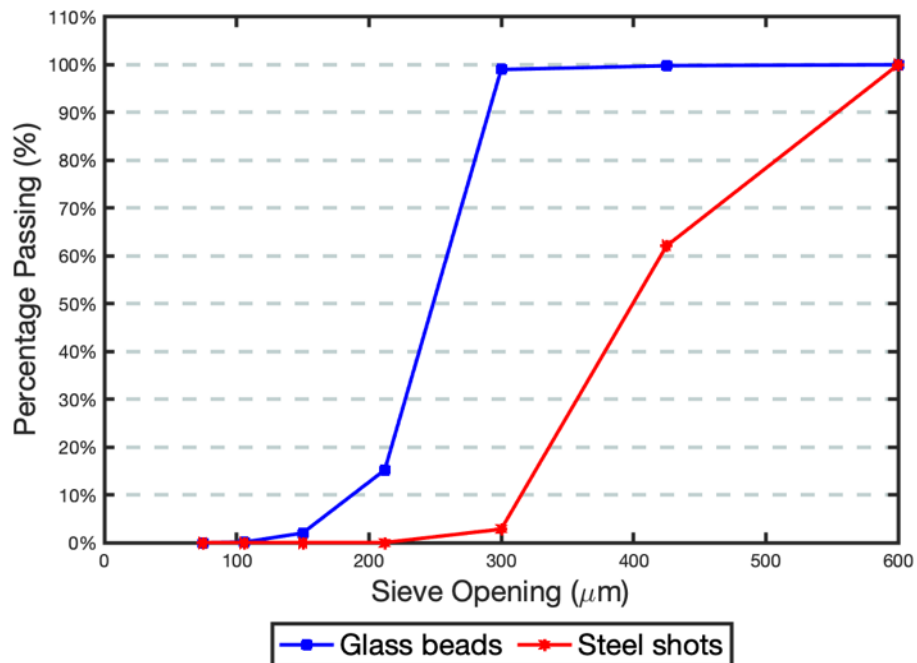
Graph 3.1: Particle size distribution curve of glass beads and steel shots

When preparing the mixture for setup 1, 15 kg of water is added to the tank and the centrifugal pump is turned on. Next, a mixture of 5 kg of solids consisting of 4.75 kg glass beads and 0.25 kg steel shots is added to the tank. For setup 2, 7.5 kg of water is added to the mixing tank. The stirrer and pump are turned on. Then 2.5 kg of solids consisting of 2.375 kg of glass beads and 0.125 kg of steel shots are added to the mixing tank.

3.4 Riffle Designs

The riffles are 3D printed using an Ultimaker S5 with tough black polylactic acid (PLA). Various riffle designs were considered, and the following nine designs were extensively tested. Each design was developed consecutively based on experimental observations of riffle design V1's performance and bidensity particle laden flow behaviour. The geometry of the riffle section block is illustrated in Figure 3.8 and all riffle contours under consideration is depicted in Figure 3.9. All riffles are designed with a volume of 17.37 cm^3 as described in Table 3.3.
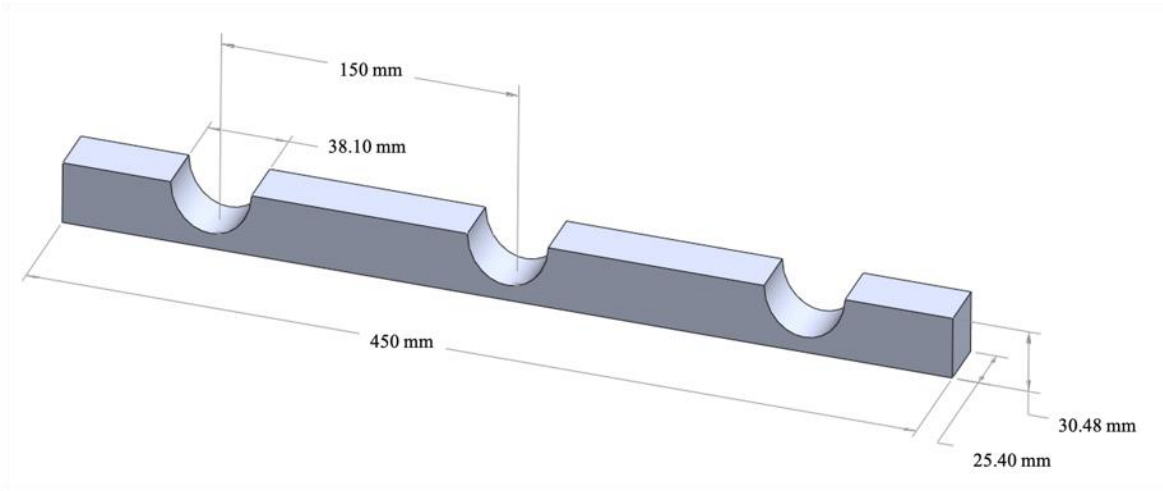
Figure 3.8: Riffle section block of the thin channel segment

As illustrated in Figure 3.9, design V1 is a semi-elliptical shaped riffle, based on simple geometry and used as a baseline for the heavy particle recovery. Riffle design V1.1 is a derivative of design V1. The elliptical shape from design 1 is rotated 30° clockwise from its center line. Comparable to design V1.1, the elliptical shape from design 1.2 is rotated 30° counterclockwise from its center line to form this shape. Design V2 is a trapezoidal design with the opening narrower than the base of the riffle. This design was derived from the results of experiments conducted on riffle design V1. Design V3 is octagonal and derived from the combined geometric features of designs V1 and V2. The riffle is more circular shaped than design V2. Design V4 was developed to smooth out the corners of design V3's octagonal shape. It is analogous to design V1, but the entry and exit points of the riffle are curved into the center of the riffle. Design V5 is based on the current riffle design used in the Falcon gravity separator, as shown in Figure 3.10. This is a trapezoidal shape with the opening wider than the base and smoothed edges inside the riffle.
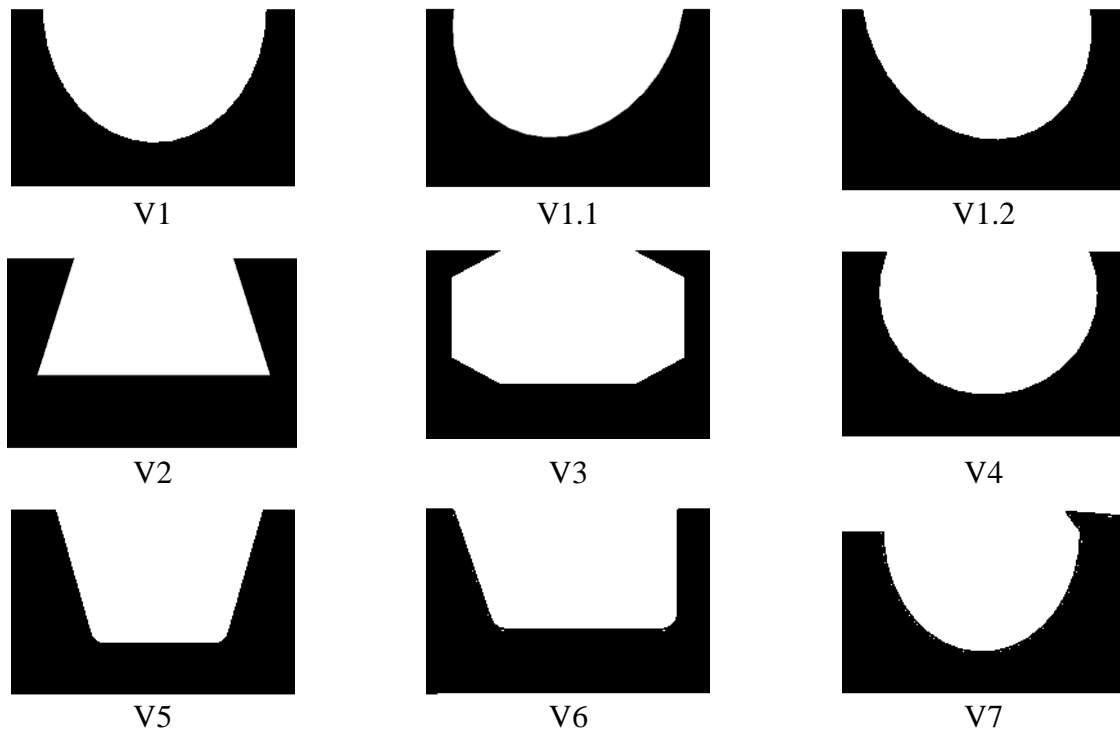
Figure 3.9: Riffle designs contours. Refer Appendix C for more details.

Table 3.3: Riffle design parameters

Design	Riffle volume (cm³)	Central depth (mm)	Riffle opening width (mm)	Area of opening (mm²)
V1		22.86	38.10	967.74
V1.1		21.70	39.64	1006.86
V1.2		21.70	39.64	1006.86
V2		18.80	29.50	749.30
V3	17.37	21.34	20.07	509.78
V4		23.80	31.75	806.45
V5		22.10	38.10	967.74
V6		19.81	38.10	967.74
V7		22.86	35.10	891.54
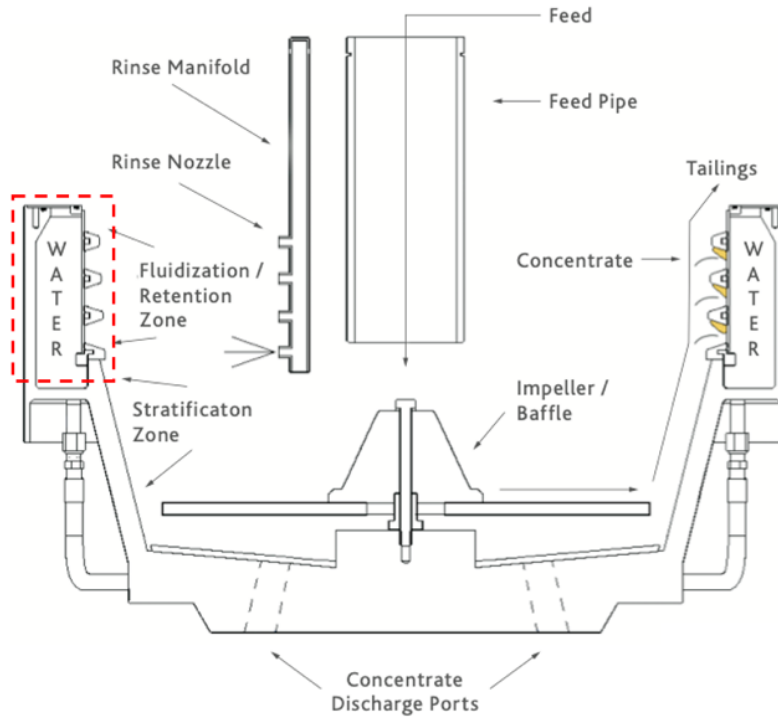
Figure 3.10: Riffles on the Falcon enhanced gravity separator. Reprinted from [16].

Riffle design V6 is derived from design V5 and incorporates attributes of all the previous designs. This design gauges the performance of design V5 when a restriction is implemented on the exit edge of the riffle. Design V7 is a byproduct of design V1 with a lip at the exit edge of the riffle.

3.5 Design of Experiments

A full factorial design of experiments (DOE) provides an in-depth analysis of all 3 factors (riffle design, flow rate, and inclination angle) under investigation. These responses are analyzed to assess each key effect and interaction effect of these manipulated variables.

Table 3.4: Design of experiments for experimental setup 1

Number of flow rates considered	3
Number of riffle designs considered	9
Number of inclination angles considered	3
Total number of trial cases	**81**

Experimental setup 1 tested 9 designs at 3 different flow rates and 3 different inclination angles, as shown in Table 3.4. This resulted in 81 distinct test cases based on a full factorial DOE. A detailed DOE table is presented in Appendix B.1.

Table 3.5: Design of experiments for experimental setup 2

Number of flow rates considered	1
Number of riffle designs considered	9
Number of inclination angles considered	2
Total number of trial cases	**18**

Experimental setup 2 tested 9 designs using 1 flow rate and 2 inclination angles, as shown in Table 3.5, resulting in 18 distinct test cases. A detailed DOE table for the experimental setup 2 is presented in Appendix B.2. The pump and its accompanying dampener in setup 2 could not be set to produce stable flow at lower flow rates, therefore the flow rates lower than 8 L/min were not investigated in this setup. Additionally, the 9° inclination angle in setup 2 was not pursued because initial tests showed the particles creating finite slopes, making accurate data collection improbable as was the case with the 6° inclination angle in experimental setup 1. This phenomenon is further analyzed in the Section 4.10.

3.6 Performance Indices

The performance indices used to measure heavy particle concentration performance of the thin channel setup with different riffle designs are presented below. The main analyses are heavy recovery, mass yield, enrichment factor, light rejection, and separation efficiency.

Mass yield in riffle i, Y_i, (equation (14)) describes the total amount of solid particles retained in riffle i compared to the total amount of solid particles present in the feed.

$$Y_i = \frac{M_i}{M_f} \tag{14}$$

where M_i is the total mass of solids accumulated in riffle i over the duration of the experiment and M_f is the total mass of solids present in the feed over the duration of the experiment. Total mass yield, Y_{total}, can be calculated as the sum of mass yields of individual riffles, $Y_{total} = \sum Y_i$.

Enrichment factor for riffle i, EF_i (equation (15)) provides a ratio between the fraction of heavy particles in riffle i, h_i, and the fraction of heavy particles in the feed, h_f. Total enrichment factor, EF_{total}, can be calculated as the sum of enrichment factors of individual riffles, $EF_{total} = \sum EF_i$ where $h_{i\_total} = \sum h_i$ and $h_{f\_total} = \sum h_f$.

$$EF_i = \frac{h_i}{h_f} \tag{15}$$

For the bidensity mixture of light and heavy particles considered in this study, the following relationships are true:

$$h_f + l_f = 1; \; h_i + l_i = 1; \; h_c + l_c = 1; \; h_t + l_t = 1 \tag{16}$$

where, l_f, l_i, l_c, and l_t are fraction of light particles in the feed, riffle i, all riffles (concentrate), and tailings, respectively. Similarly, h_f, h_i, h_c, and h_t can be defined as fraction of heavy particles in the feed, riffle i, all riffles (concentrate), and tailings, respectively.

The heavy particle recovery in riffle i, Rh_i, and total heavy recovery, Rh_{total}, can be calculated from mass yield and enrichment factors using following equations:

$$Rh_i = EF_i \cdot Y_i \tag{17}$$

$$Rh_{total} = EF_{total} \cdot Y_{total} \tag{18}$$

Similarly, the light particle recovery in riffle i, Rl_i, and total light recovery, Rl_{total}, can be calculated as follows:

$$Rl_i = \frac{l_i}{l_f} \cdot Y_i \tag{19}$$

$$Rl_{total} = \frac{l_c}{l_f} \cdot Y_{total} \tag{20}$$

Overall separation efficiency for the device (equation (21)) can be determined by calculating the difference between total heavies and total lights recoveries in the riffles (concentrate).

$$SE_{total} = Rh_{total} - Rl_{total} \tag{21}$$

To understand particle behaviour in the riffles based on elapsed time, a dimensionless parameter T is used, where T is a ratio of time over total experimental time. This dimensionless time would allow a better comparison of phenomena in both experimental setups 1 and 2 as experiments on each setup were performed over different time periods.

3.7 Assessment of Experimental Errors

For a significant portion of cases in both setups, multiple trials were conducted to determine the margin of error in the experimental data. The average standard deviations for the enrichment factor of heavy particles of 15 distinct cases for setup 1, and 2 distinct cases for setup 2 are less than 5%. The average standard deviation for the enrichment factor of heavy particles of each riffle across designs and setups is approximately 7%. These deviations are well within the acceptable range for such experimental studies. Full analysis is presented in Appendix D and Appendix E

While in the acceptable range, this error margin may have come from different aspects of the experiment. Experimental work is inherently prone to human error. It is improbable to have the exact operating conditions present in the desired ways in each experimental trial. The inlet to the thin channel was controlled and timed manually, a possible source of human error. Additionally, experimental setup 1 employed a centrifugal pump for mixing and pumping, however, the slurry density experienced by the thin channel varied during trials. Similarly, mixing and pumping of slurry in experimental setup 2 also supplied varying slurry densities to the thin channel. As previously described, enrichment factor of heavy particles was calculated based on the reconciliated slurry density that the thin channel was exposed to, thus limiting the impact of experimental error.

The thin channel setup experiences 1G force and has been established to mathematically correlate to the 200G Falcon enhanced gravity separator. The data from the 1G setup may not perfectly scale up to the 200G system. The 1G setup provides a platform to analyze various riffle geometries and their relating attributes in a lab setting. Findings from the lab-scale setup can be correlated to potential behaviour in enhanced gravity separators that operate at 200G.

High-speed camera data made it evident that in setup 1, riffle R1 collected more heavy particles but erosion caused the heavies to be pushed to riffle R2. Erosion describes the phenomenon where the settled particles in the riffles are pushed out by a sudden flow influx. This occurred when the 3-way valve was turned off at the end of each experiment. Setup 1 experienced significantly more erosion than setup 2 due to higher flow rates used in the setup.

Setup 2 was developed to ensure that the thin channel was being exposed to a consistent, heterogeneous slurry mixture since the centrifugal pump in setup 1 was not able to do this consistently. Setup 2 used the C15 peristaltic pump, allowing low flow rate test conditions, which to a certain extent, mitigated the impact of erosion in the riffles at the end of each trial. The Falcon enhanced gravity separator would retain heavy particles better at a higher flow rate as the particles are under a higher G-force. Hence, the data from setup 2 is a better approximation for heavy particle segregation that could occur at the riffled section of the Falcon enhanced gravity separator bowl.

Chapter 4: Results

4.1 Introduction

The system's performance is analyzed based on measures of performance indices introduced in Section 3.6. To analyze the impact of flow rate, inclination angle, and riffle design, the riffled section of the thin channel segment is fitted with 3 identical riffles under the tag names R1, R2, and R3 based on the order in which the riffles are exposed to the slurry flow (Figure 4.1). As the slurry contains light (glass beads, 95% w/w) and heavy (steel shots, 5% w/w) particles, the unit's separation performance is considered superior if both recovery of heavy particles and grade of heavy particles in riffles are maximized, or when the separation efficiency index approaches 100%.
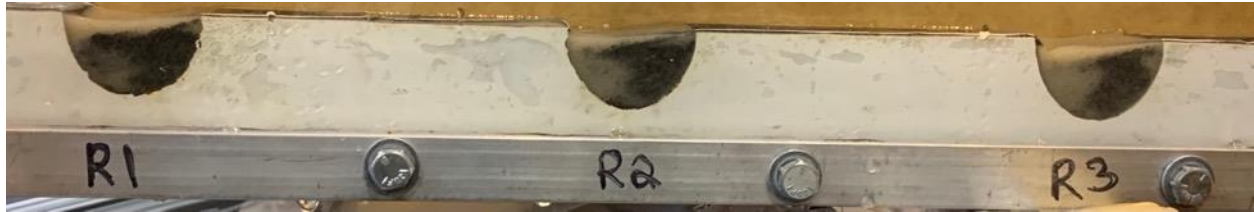
Figure 4.1: Riffle order in thin channel segment. Riffles are identical, any perceived variation is due to imaging discrepancies

4.2 Grade-Recovery of Heavy Particles for Each Riffle

Graph 4.1 depicts that at 24 L/min, as the fraction of heavy particles in each riffle increases, the heavy particle recovery in each riffle also increases. The highest heavy particle recovery per single riffle is obtained by design V4's R1 at 9º inclination angle, while the highest fraction of heavy particles in a riffle was achieved by design V1.2's R2 at 15º inclination angle. In general, it is observed that the highest heavy particle recovery in the riffles is at 9º inclination angle (red marks in Graph 4.1). On the other hand, the lowest heavy particle recoveries are recorded at 15º inclination angle, but the drop in recovery is typically followed by an increase in heavy grade (green marks in Graph 4.1). Heavy particle recovery is generally higher for R1 and R2 in comparison with R3 across all designs and inclination angles.
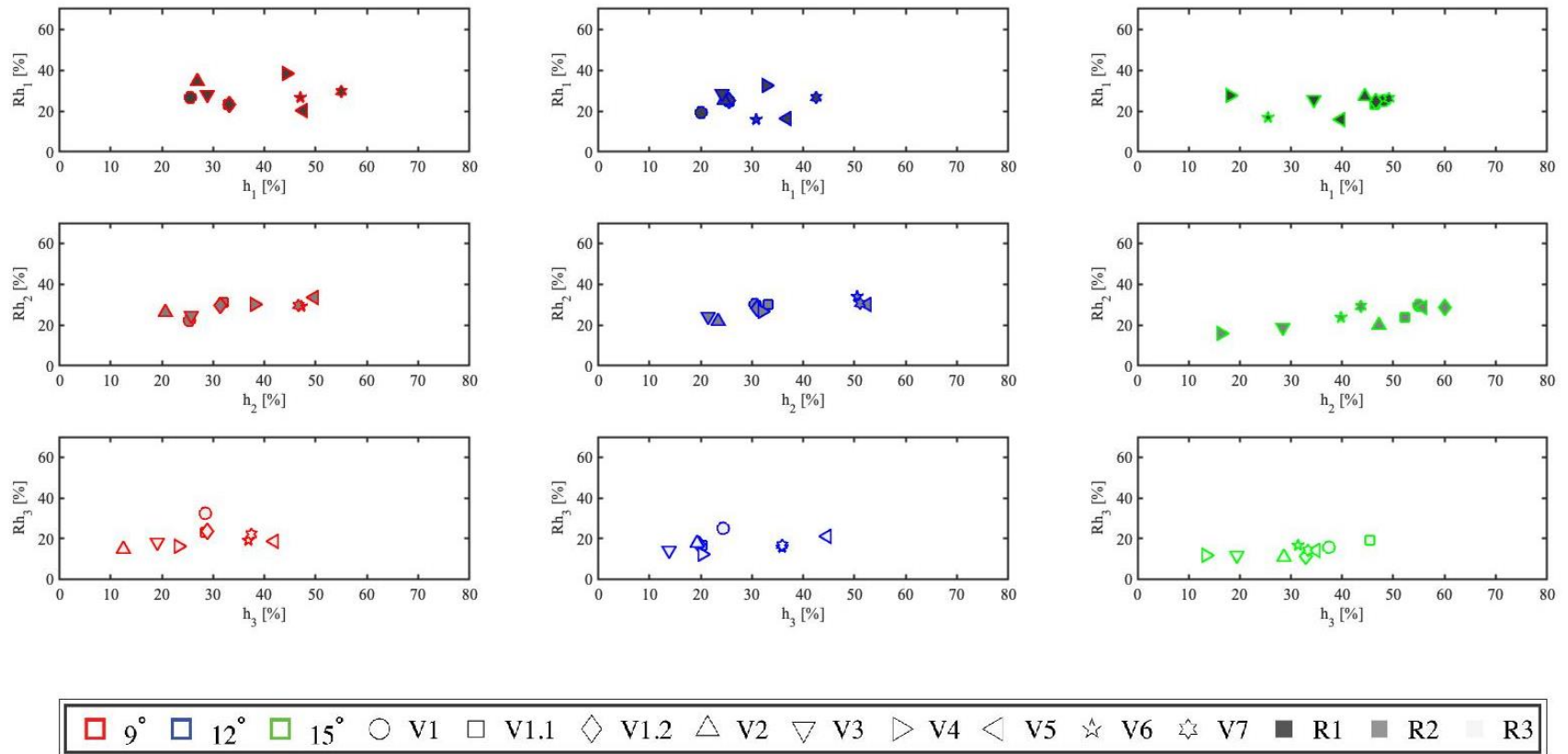
Graph 4.1: Grade-recovery of heavy particles for each riffle for 24 L/min
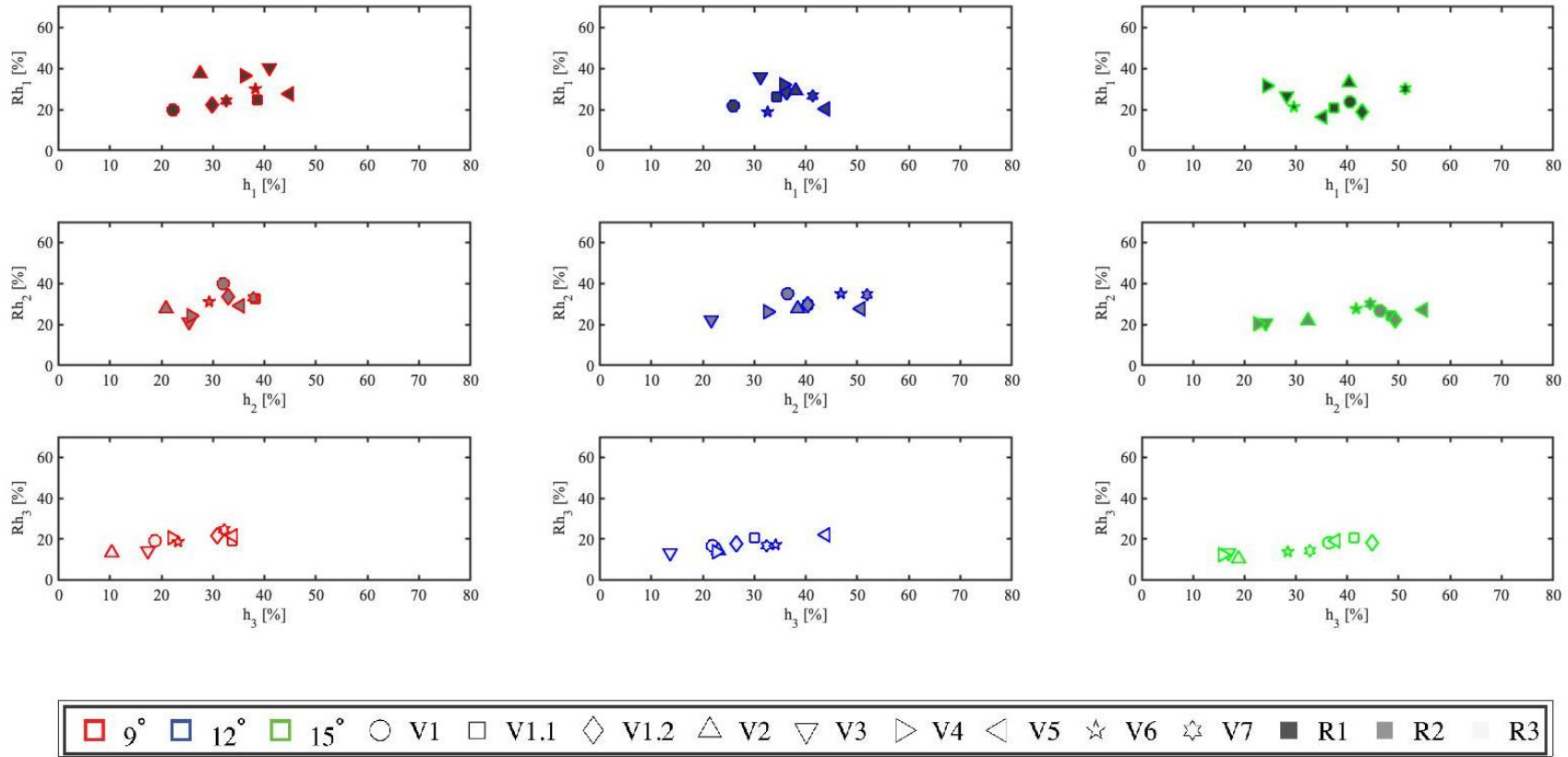
Graph 4.2: Grade-recovery of heavy particles for each riffle for 23 L/min

Similar trends can be observed for tests operated at 23 L/min and 22 L/min feed flow rate as shown in Graph 4.2 and Graph 4.3. For 23 L/min feed flow rate, the highest heavy particle recovery is obtained by design V3's R1 at 9° inclination angle, while the highest fraction of heavy particles was recovered by design V5's R2 at 15° inclination angle. For 22 L/min flow rate, the highest heavy particle recovery is obtained by design V2's R1 at 9° inclination angle, while the highest fraction of heavy particles was recovered by design V5's R2 at 12° inclination angle. While in general, consistently lower heavy particle recovery is found across all designs at 15° inclination angle,

there is improvement in both fraction of heavy particles and recovery of heavy particles at 9º and 12º inclination angles in riffles R1 and R2. This indicates superior performance. R1 of the designs tested at 9º inclination angle at the 22 L/min flow rate show the best performance, with the grade-recovery curve more closely following a linear trend (Graph 4.3), which may be attributed to increased residence time in the sluice.
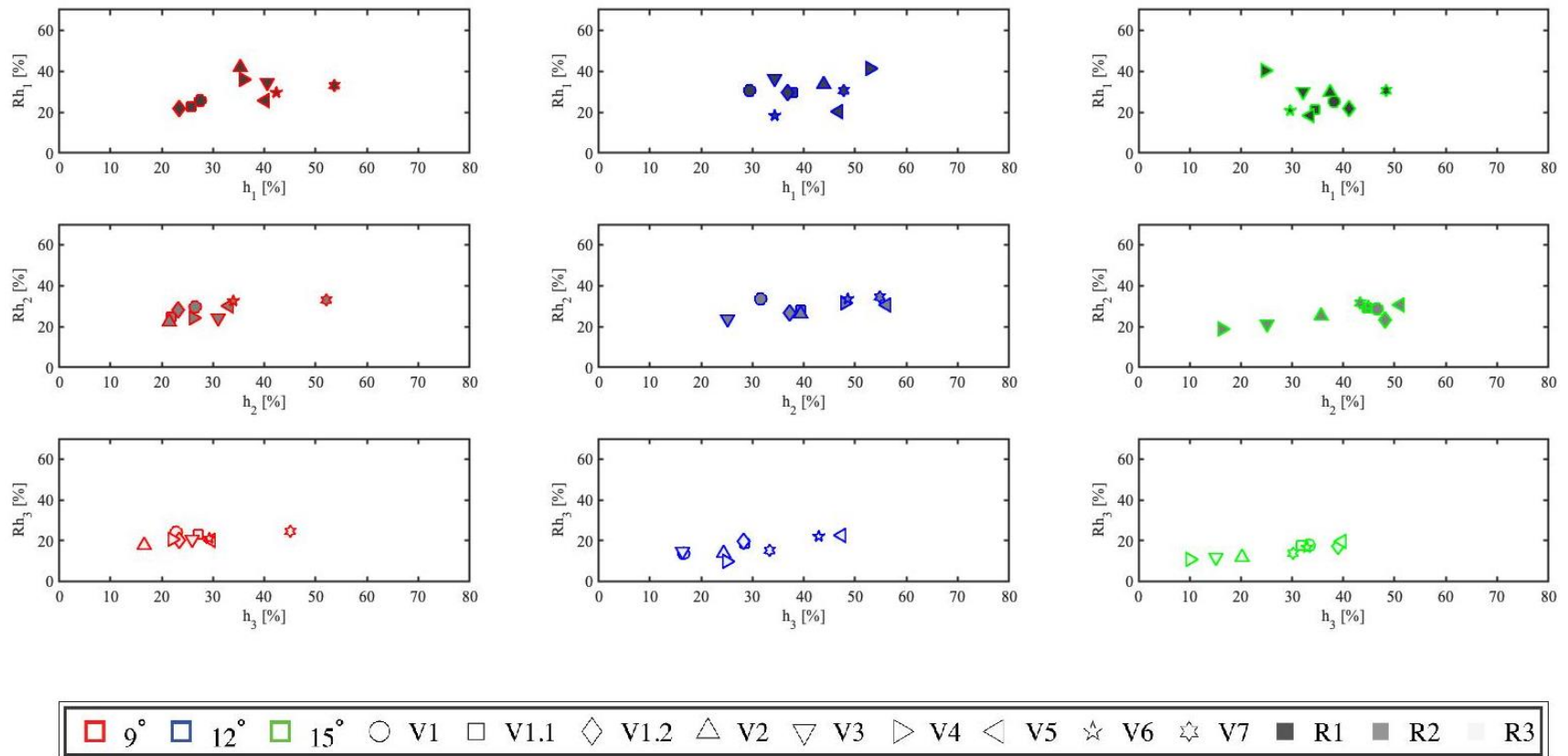
Graph 4.3: Grade-recovery of heavy particles for each riffle for 22 L/min
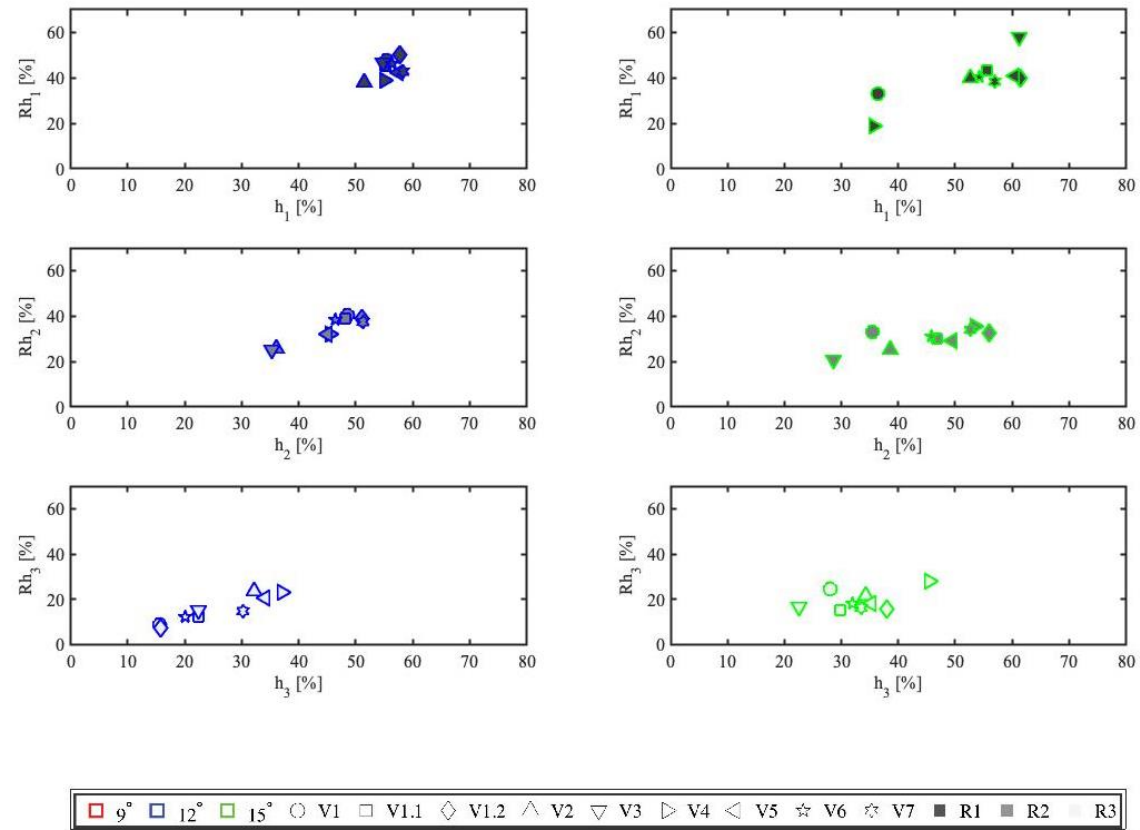
Graph 4.4: Grade-recovery of heavy particles for each riffle for 8 L/min

The per riffle grade-recovery of heavy particle at 8 L/min flow rate is given in Graph 4.4 for the two inclination angles tested. While similar trends and relationships relative to the channel inclination angle and riffle order of other flow rates can be observed at this flow rate. Significantly reduced scatter in the data and increased magnitude of both heavy particle recovery and fraction of heavy particles in each riffle can be noticed for the same riffle designs as well.

R1 and R2 at 8 L/min have significantly better performance than the same riffles at the higher flow rates. This is possibly due to the more stable flow of the second pump, along with lower flow rate, leading to lower turbulence of the flow in the channel and increased residence time. The shorter experimental trial time may have also played a role. Grade-recovery of heavy particles across all designs and for two tested inclination angles are shown to follow similar trends within the 5% experimental error margin, with riffles R1 and R2 having the highest fraction of heavy particles and heavy particle recovery in comparison with the last riffle in series.

At lower flow rates, it is likely that the sliding and heterogeneous bed formed in the flow developing zone produced a fully developed flow in which the heavy particles segregated to the bottom layer, the light particle formed the center layer, and a fluid-only layer resided in the top region of the flow. As a result, R1 and R2 are likely entrapping heavy particles that have already been segregated in the flow, resulting in these riffles collecting most of the heavy particles in the feed. In the meantime, the slurry consisting mainly of light particles may start filling R3 and compacting this riffle with light particles. Due to low flow rate, the slurry flow does not have enough velocity to displace the light particles that are packed within R3. Figures in Section 4.9 further supports this hypothesis, showing greater accumulation of heavy particles in R1 and R2 compared to R3.
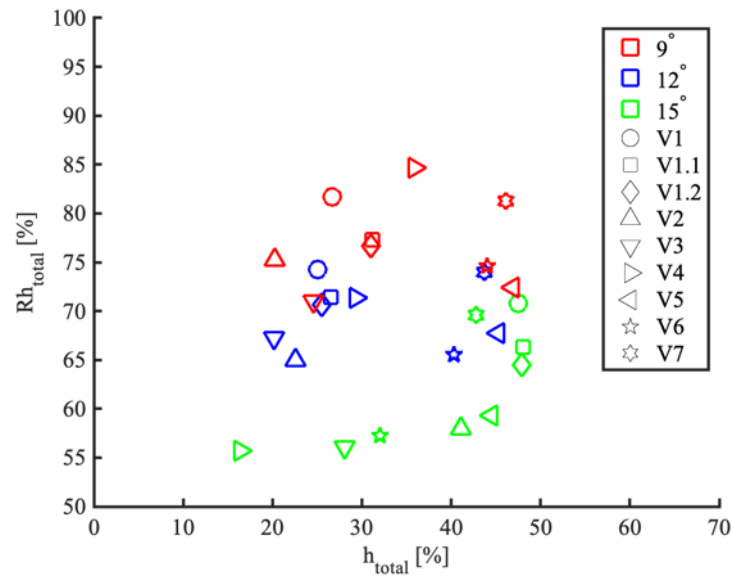
4.3   Grade-Recovery of Heavy Particles for Complete System

Grade-recovery of heavy particles for the complete system is presented in Graph 4.5 and Graph 4.6 for the flow rates of 24 L/min and 23 L/min, respectively. For both flow rates, as the total fraction of heavy particles across riffles increases, total recovery of heavy particles in all riffles increases slightly. The exception to this is for designs at 9º inclination angle at 24 L/min, which show a more linear curve. This suggests that riffle design at these flow rates had minimal impact on total recovery and total fraction of heavy particles. Inclination angle had a stronger effect on these indices, with 15º inclination angle experiencing the lowest total grade-recovery of heavy particles, 9º inclination angle showing the highest total grade-recovery of heavy particles, and 12º inclination angle falling in between. For the flow rate of 24 L/min, design V1.1 at 15º inclination angle retained the highest total fraction of heavy particles while design V4 at 9º inclination angle obtained the highest total recovery of heavy particles. For 23 L/min, design V5 at 15º inclination

angle retained the highest total fraction of heavy particles while design V7 at 9º inclination angle obtained the highest total recovery of heavy particles. A similar trend is observed at the flow rate of 22 L/min (Graph 4.7). At this flow rate, design V7 at 9º inclination angle had the highest total fraction and the highest total grade of heavy particles.

Graph 4.5: Grade-recovery of heavy particles for complete system at 24 L/min
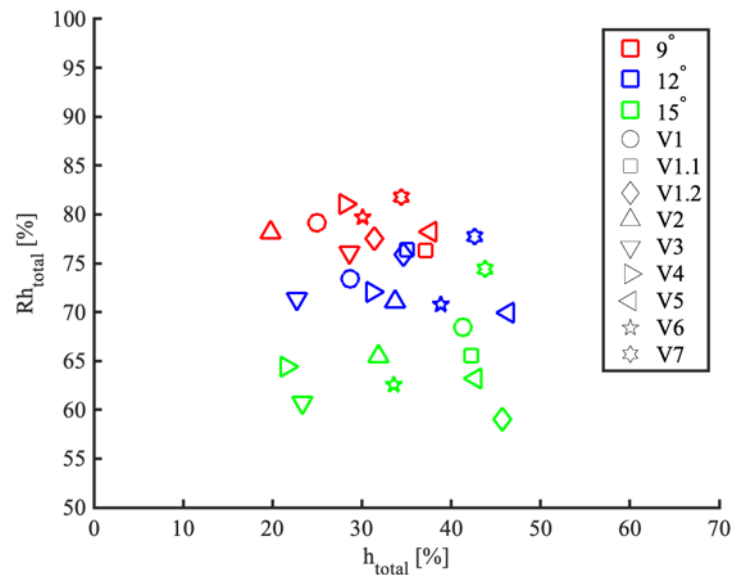
Graph 4.6: Grade-recovery of heavy particles for complete system at 23 L/min
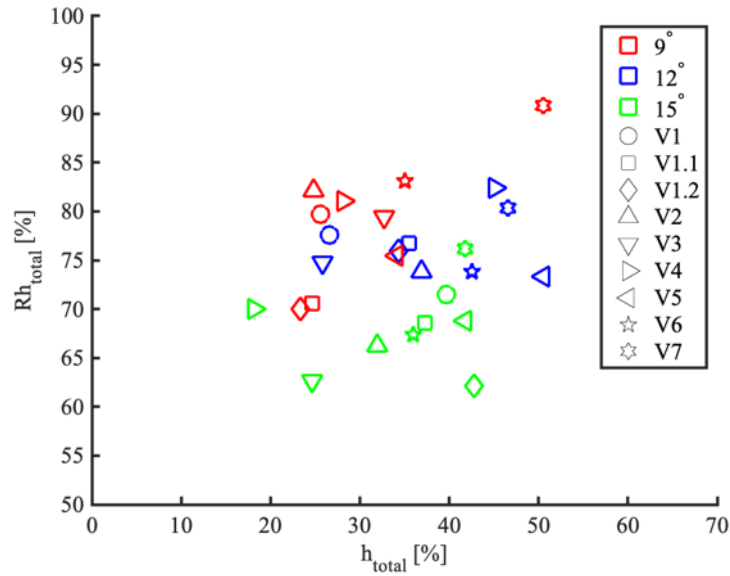
Graph 4.7: Grade-recovery of heavy particles for complete system at 22 L/min
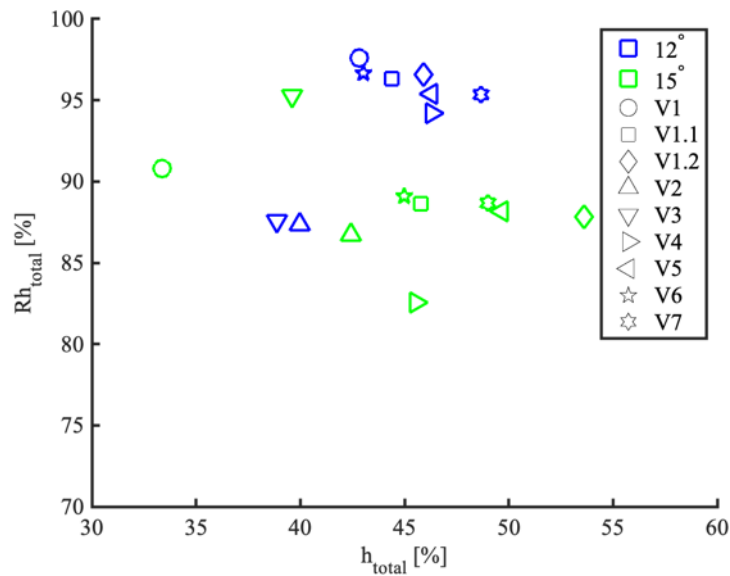
Graph 4.8: Grade-recovery of heavy particles for complete system at 8 L/min

Graph 4.8 demonstrates the overall performance of the system at 8 L/min for the two inclination angles tested at this flow rate. This performance index seems to be influenced by inclination angle for most designs, such that 12° inclination angle experiences greater total grade-recovery of heavy particles than at 15° inclination angle, but some designs did not follow this trend. Design V3 had higher total grade-recovery of heavy particles at 15° inclination angle than at 12° inclination angle, and design V2 had similar total grade-recovery of heavy particles regardless of inclination angle.

Improved performance of design V3 may be due to the angle of the flow aligning with the geometry of the riffle opening at certain inclination angles. Despite having a lower fraction of heavy particles, the designs at 12º inclination angle maintain high total recovery of heavy particles at the flow rate of 8 L/min, implying that there is a stronger relationship between low flow rate, low inclination angle, and total recovery of heavy particles in the riffles.

Comparing grade-recovery of heavy particles for the complete system for the different flow rates indicates that the lowest inclination angle tested for a given flow rate produces the best grade-recovery of heavy particles for the system. Also, when considering 9º inclination angle, as flow rate decreases, grade-recovery of heavy particles for the system improves. This is most evident when comparing design V7's performance at 9º inclination angle at 24 L/min (Graph 4.5) and 22 L/min (Graph 4.7). A similar result is shown at 8 L/min, where total recovery of heavy particles at 12º inclination angle is the highest across inclination angles.

As previously mentioned, the low flow rate and low inclination angle may reduce the slurry flow velocity, allowing the slurry to segregate before entering the riffles. This segregation may allow riffles to collect and retain more heavy particles. Design V7's performance may be due to the raised lip at the exit edge of the riffle entrapping heavy particles more efficiently while allowing light particles to exit.

4.4   Mass Yield – Recovery of Heavy Particles for Each Riffle

At 24 L/min, the mass yield increases as the heavy particle recovery increases. Design V5's R2 at 9º inclination angle had the highest mass yield while design V4's R1 at 9º inclination angle obtained the highest recovery of heavy particles (Graph 4.9). At 23 L/min, design V1.1's R2 at 9º inclination angle had the highest mass yield while design V3's R1 at 9º inclination angle obtained the highest recovery of heavy particles (Graph 4.10). At 22 L/min, design V7's riffles at 9º inclination angle had the highest mass yields while design V2's R1 at 9º inclination angle obtained the highest recovery of heavy particles (Graph 4.11). At 8 L/min, design V1.2's R1 at 12º inclination angle had the highest mass yield while design V3's R1 at 15º inclination angle obtained the highest recovery of heavy particles (Graph 4.12).
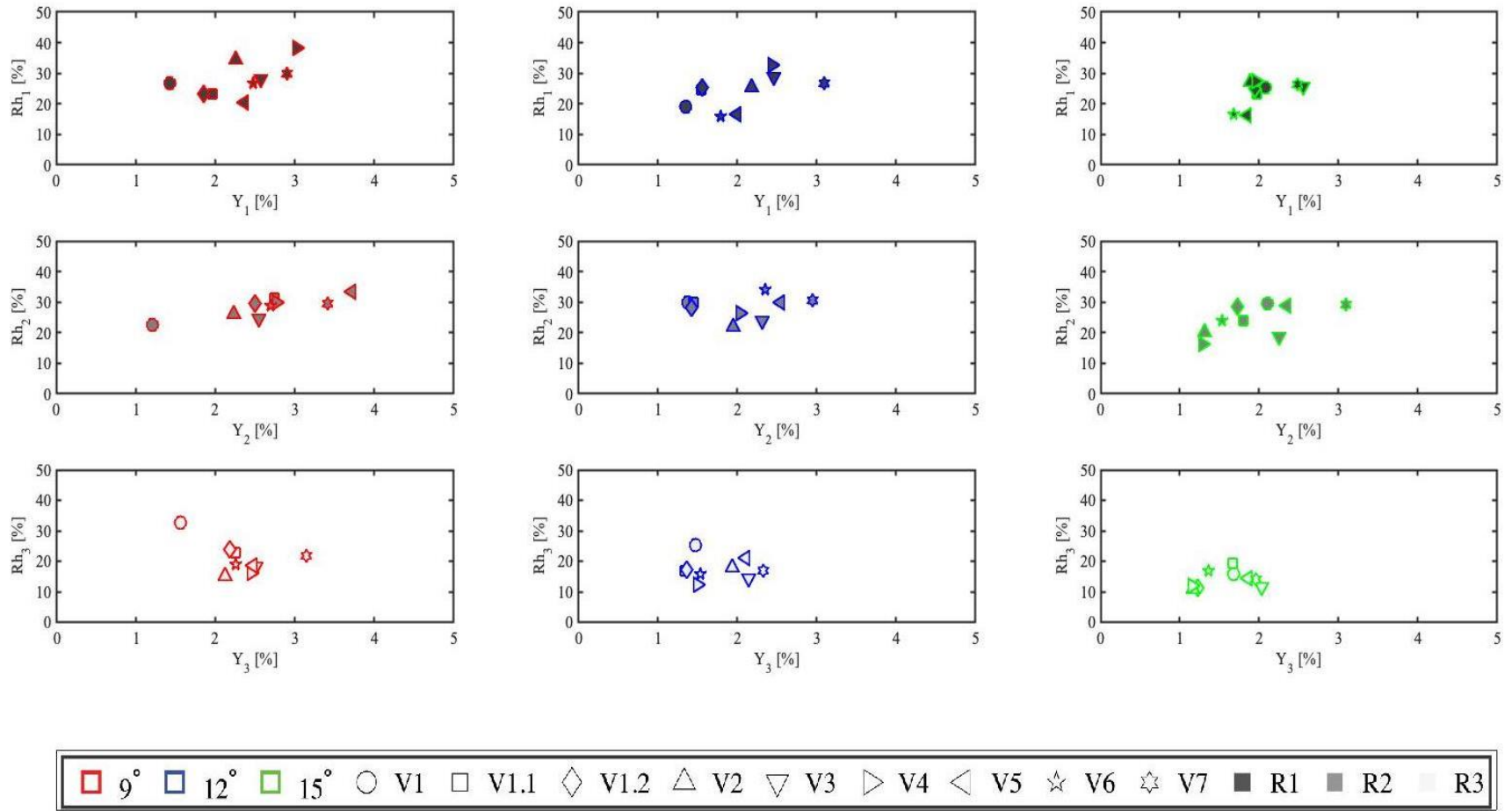
Graph 4.9: Mass yield-recovery of heavy particles for each riffle at 24 L/min

At flow rates of 24 L/min, 23 L/min, and 22 L/min, designs at 9º inclination angle had the highest mass yield and recovery of heavy particles, indicating superior performance. At these flow rates, designs at 15º inclination angle tended to have lower mass yield and

recovery of heavy particles, though at 22 L/min designs at 12º inclination angle performed worse than at other flow rates (Graph 4.11). The low flow rate coupled with the low inclination angle may have resulted in better performance for the reasons previously mentioned.
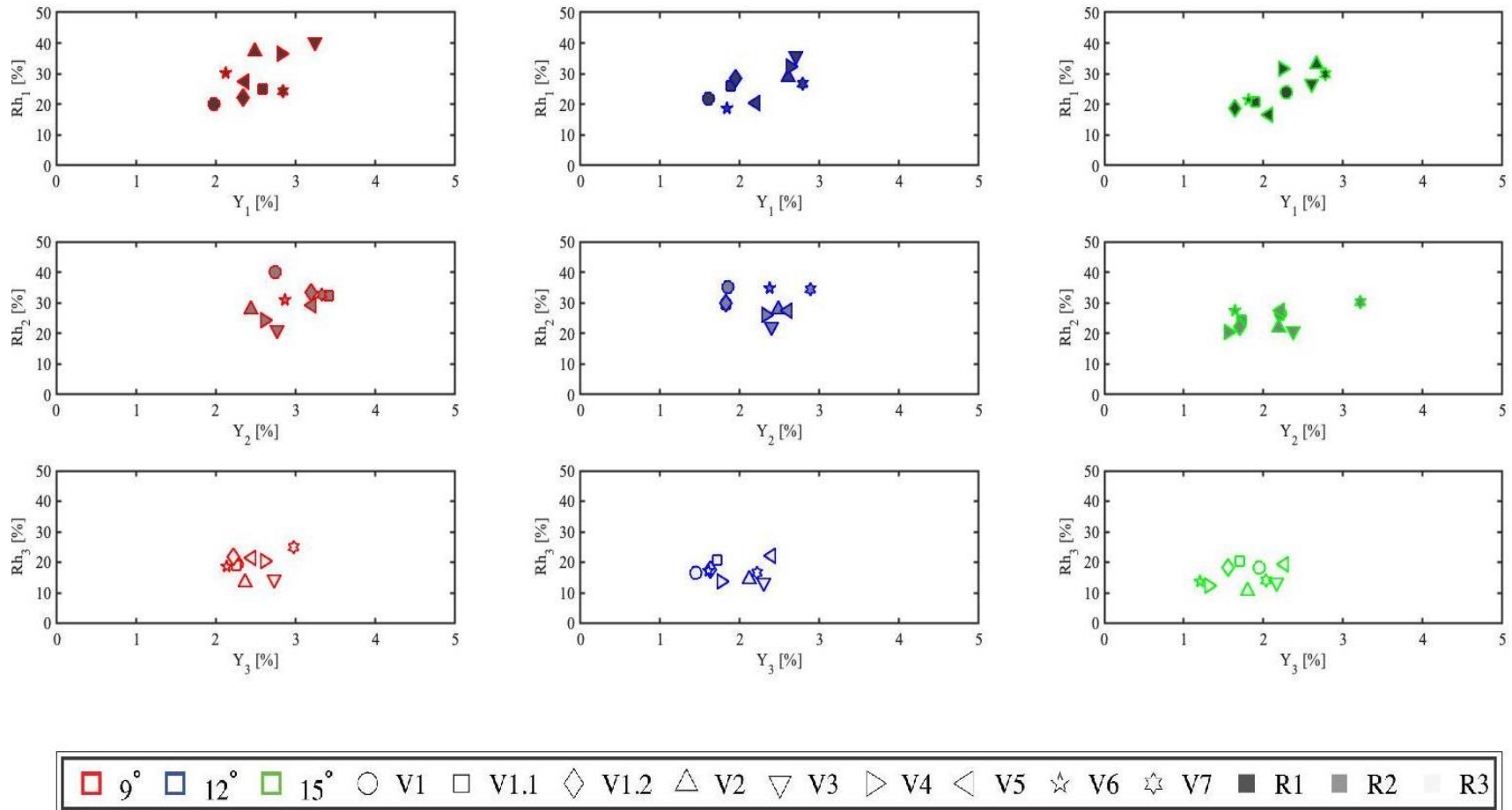
Graph 4.10: Mass yield-recovery of heavy particles for each riffle at 23 L/min
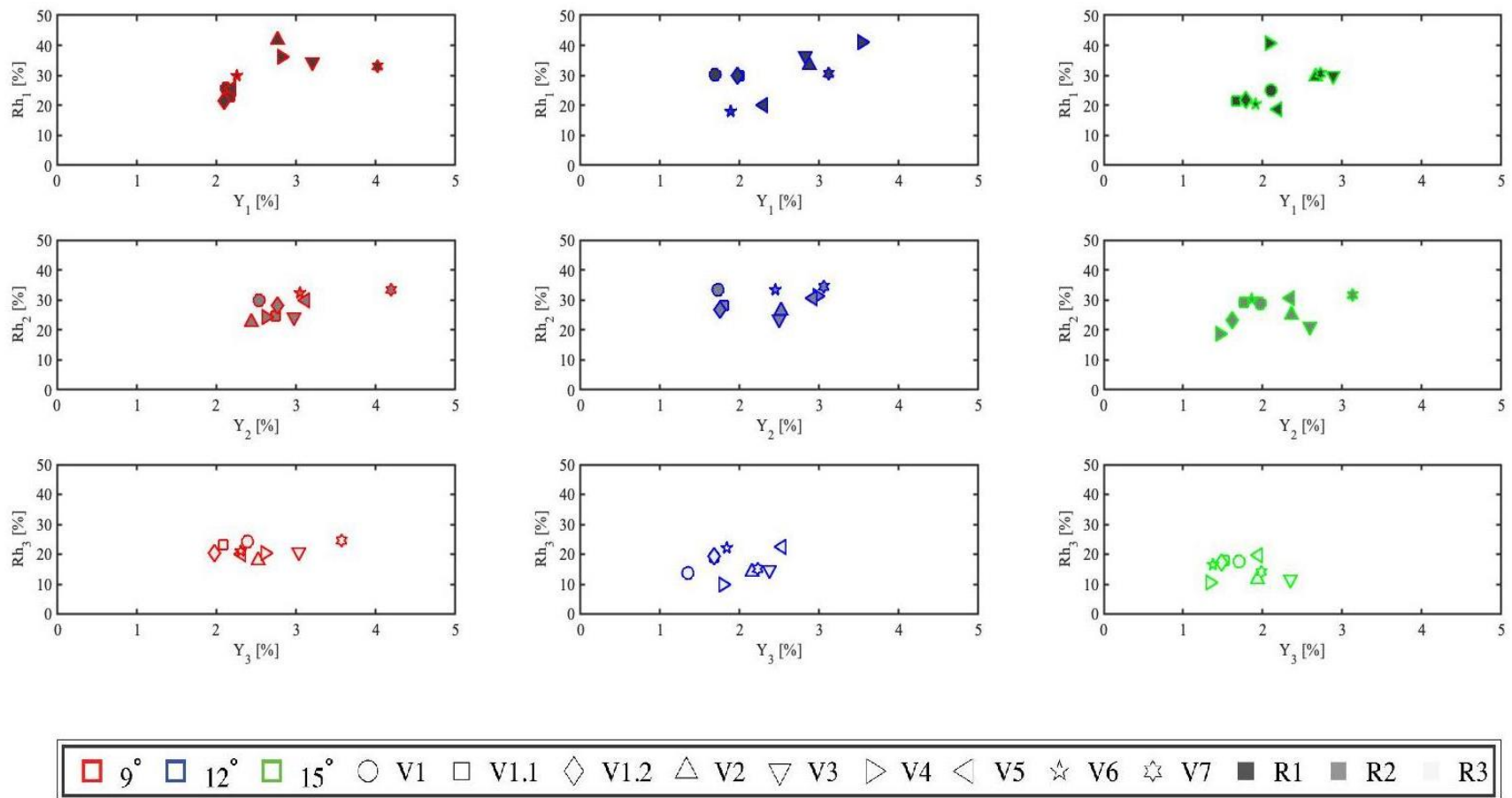
Graph 4.11: Mass yield-recovery of heavy particles for each riffle at 22 L/min
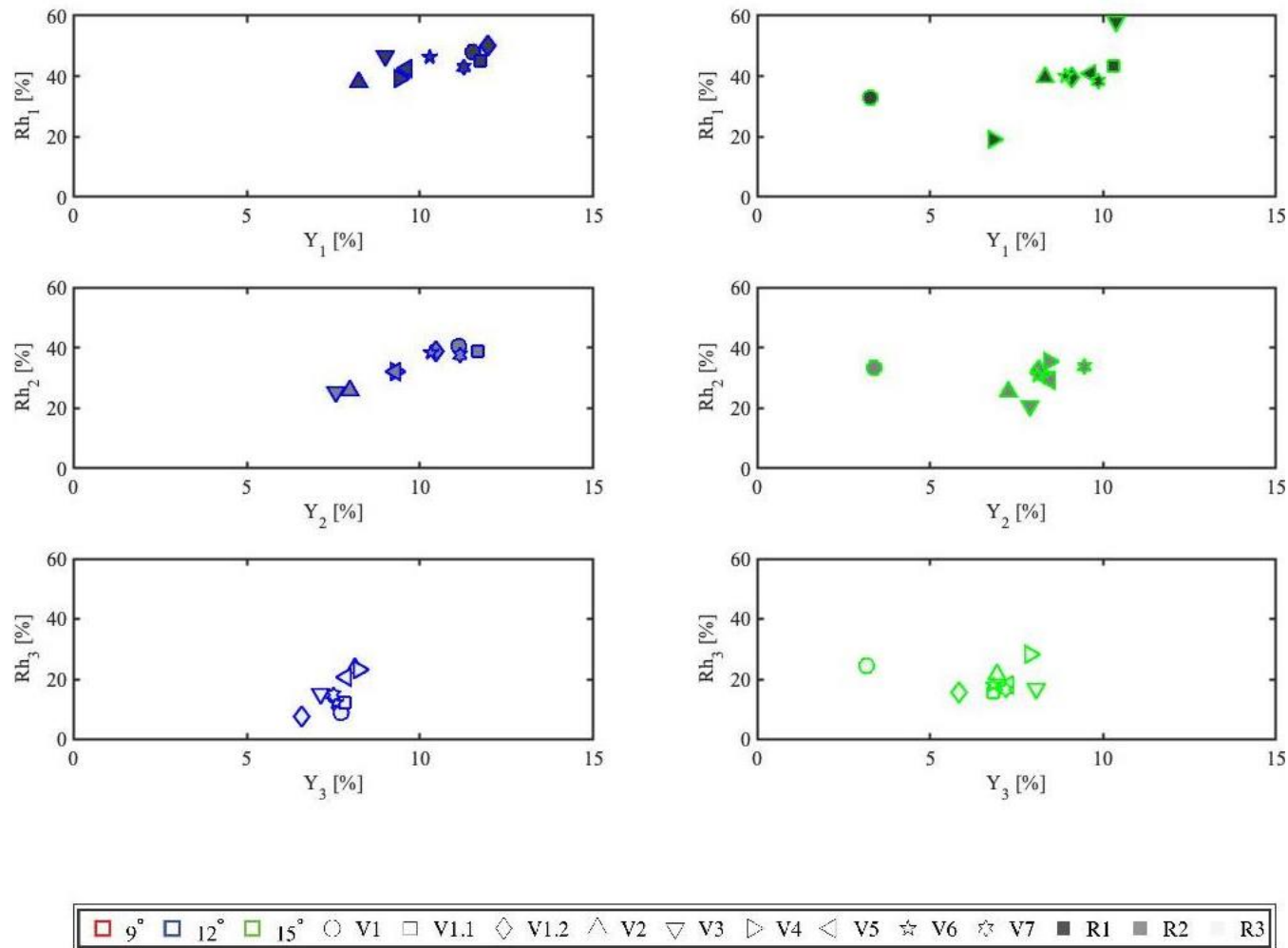
Graph 4.12: Mass yield-recovery of heavy particles for each riffle at 8 L/min

At 8 L/min, recovery of heavy particles increases steeply with minimal increase in mass yield. Designs at 12° inclination angle at 8 L/min have the best performance at this flow rate, indicating the low inclination angle results in better performance (Graph 4.12).

The superior performance of design V7 may be attributed to its geometry as previously mentioned. The semi-elliptical shape creates recirculation zones that retain heavy particles while allowing the light particles to exit. As seen in the grade-recovery of heavy particles per riffle, R1 and R2 consistently have better performance than R3 for all flow rates. Again, this suggests the slurry entering R1 deposits heavy particles until the riffle becomes compact and by the time the slurry enters R3, it contains fewer heavy particles.

4.5   Total Mass Yield – Total Recovery of Heavy Particles

At 9° inclination angle for flow rates of 24 L/min (Graph 4.13), 23 L/min (Graph 4.14), and 22 L/min (Graph 4.15), the system experienced the highest total mass yield and highest total recovery of heavy particles in all riffles. As the flow rate reduced, there was minimal change in total recovery of heavy particles for a given inclination angle. Similarly for the flow rate of 8 L/min (Graph 4.16), designs at 12° inclination angle performed the best for total mass yield and total recovery of heavy particles. The lowest inclination angle tested at 8 L/min (12° inclination angle) showed the highest total recovery of heavy particles at this flow rate, suggesting the low inclination angle contributed significantly to better system performance.
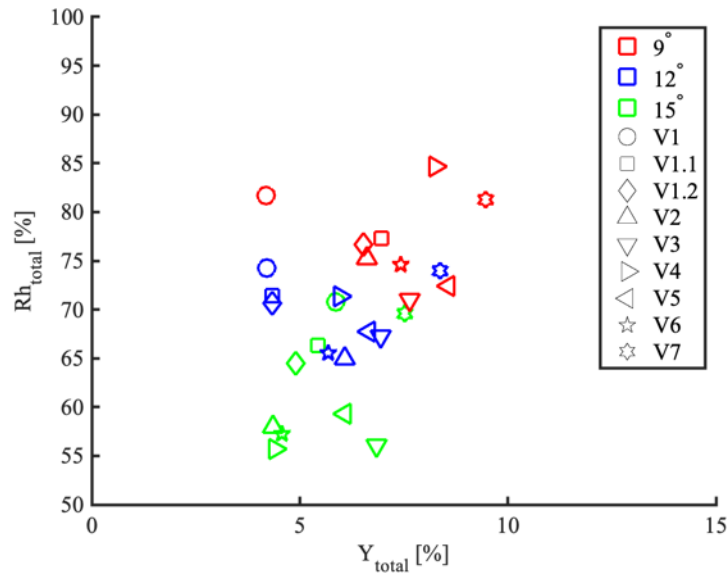
Graph 4.13: Total mass yield-total recovery of heavy particles at 24 L/min

Across the flow rates used in setup 1, designs at 15° inclination angle demonstrated the lowest total recovery of heavy particles and total mass yield. However, comparing higher flow rates (24 L/min)

46

with lower flow rates (22 L/min) for designs at 15º inclination angle shows that total recovery of heavy particles in all riffles systematically increases with the reduction in flow rate, suggesting lower flow rate results in better performance at this inclination angle. The unique contributions of flow rate to the system performance are likely due to the previously mentioned phenomena such as increased residence time and greater particle segregation in the flow.
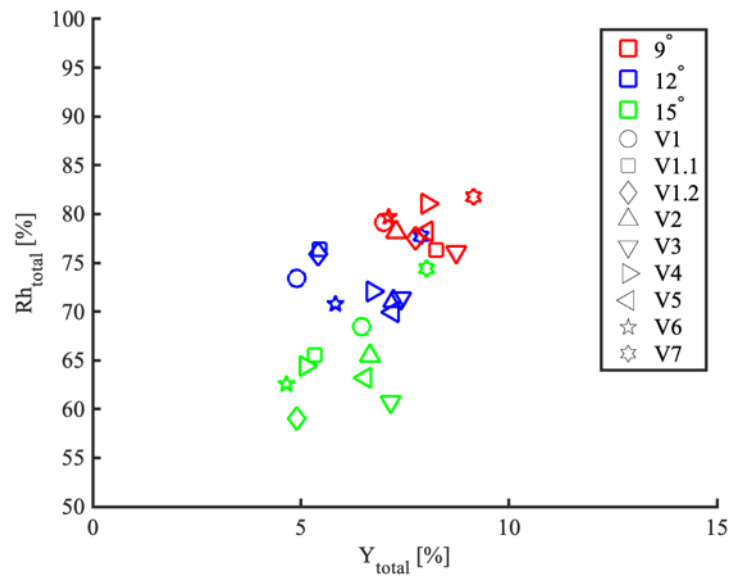
Graph 4.14: Total mass yield-total recovery of heavy particles at 23 L/min
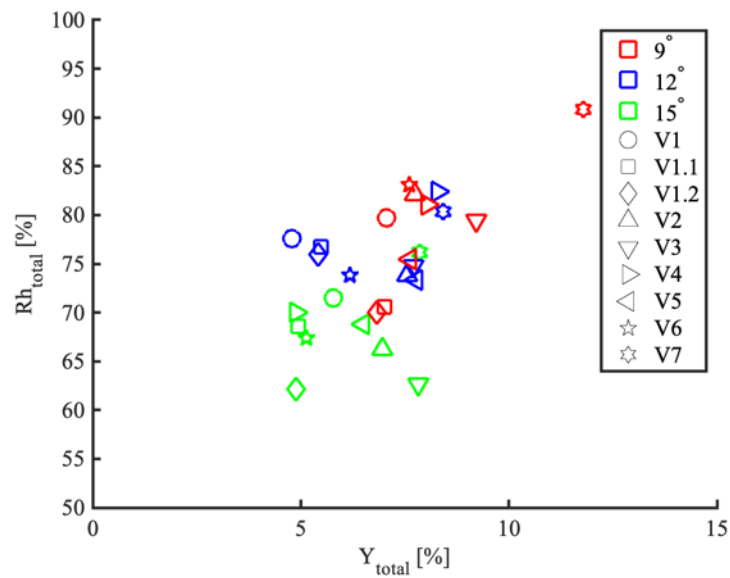
Graph 4.15: Total mass yield-total recovery of heavy particles at 22 L/min
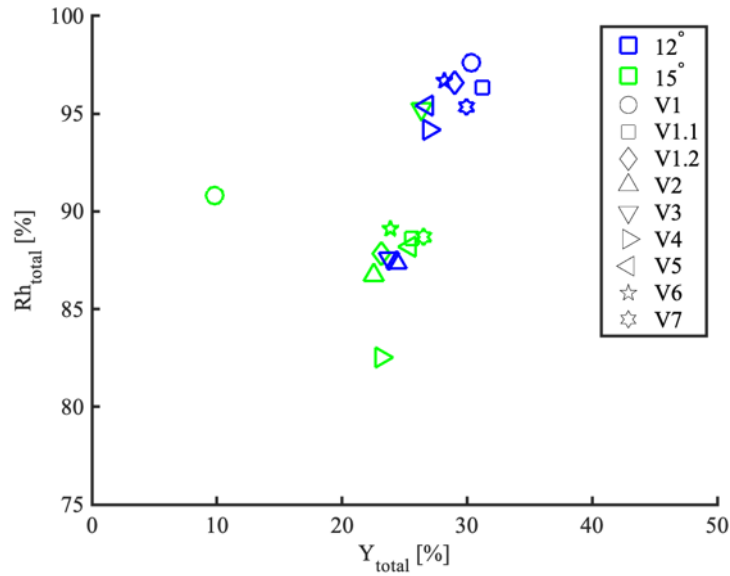
Graph 4.16: Total mass yield-total recovery of heavy particles at 8 L/min

For the flow rates 22 L/min, 23 L/min, and 24 L/min, design V7 at 9° inclination angle was consistently one of the best performing designs. This is likely due to design V7's geometry, as previously mentioned, coupled with the low inclination angle.

Most designs at 12° inclination angle at the flow rate of 8 L/min performed similarly well, with total mass yield and total recovery of heavy particles being consistently high. Design V1 at 15° inclination angle is considered an outlier because it is far outside the general total mass yield and total recovery of heavy particles trend seen in Graph 4.16. It could be inferred that a higher proportion of design V1's mass yield was heavy as opposed to light particles, resulting in its performance on this index. This may be due to the larger riffle opening allowing more heavy particles to enter and be entrapped within the riffle. However, this is not seen in other performance indices, suggesting it is an outlier. For this flow rate, it appears riffle design had minimal impact on performance and that lower inclination angle was more influential. This further state the influences of inclination angle and flow rate on the system performance.

4.6   Grade-Enrichment Factor of Heavy Particles for Each Riffle

At 24 L/min, design V1.2's R2 retained the highest fraction of heavy particles while design V1's R2 had the highest enrichment factor, as seen in Graph 4.17. Graph 4.18 shows that at 23 L/min, design V5's R2 retained the highest fraction of heavy particles while design V1's R2 had the

highest enrichment factor. At 22 L/min, design V5's R2 retained the highest fraction of heavy particles while design V4's R1 had the highest enrichment factor (Graph 4.19). In general, R1 and R2 for most cases perform the best, suggesting the first two riffles in the series collected the highest fraction of heavy particles and had the best enrichment factors.

At the flow rates of 24 L/min, 23 L/min, and 22 L/min, differences in enrichment factor can be seen at different flow rates and designs. At 12º inclination angle and 15º inclination angle, there is greater variation in design performance than at 9º inclination angle, suggesting riffle design contributes more to heavy particle retention and enrichment factor at the higher inclination angles. Across these flow rates in setup 1, design V1 has a high enrichment factor in several conditions. Design V1 performs well at 9º inclination angle and 12º inclination angle but not at 15º inclination angle, suggesting its performance may be partly due to the lower inclination angles. At 9º inclination angle and 12º inclination angle, the larger riffle opening, and semi-elliptical shape may have enhanced heavy particle retention and separation such that it had a higher fraction of heavy particles retained. Riffle design minimally impacted grade enrichment factor when considering single riffles at the inclination angles and flow rates tested.
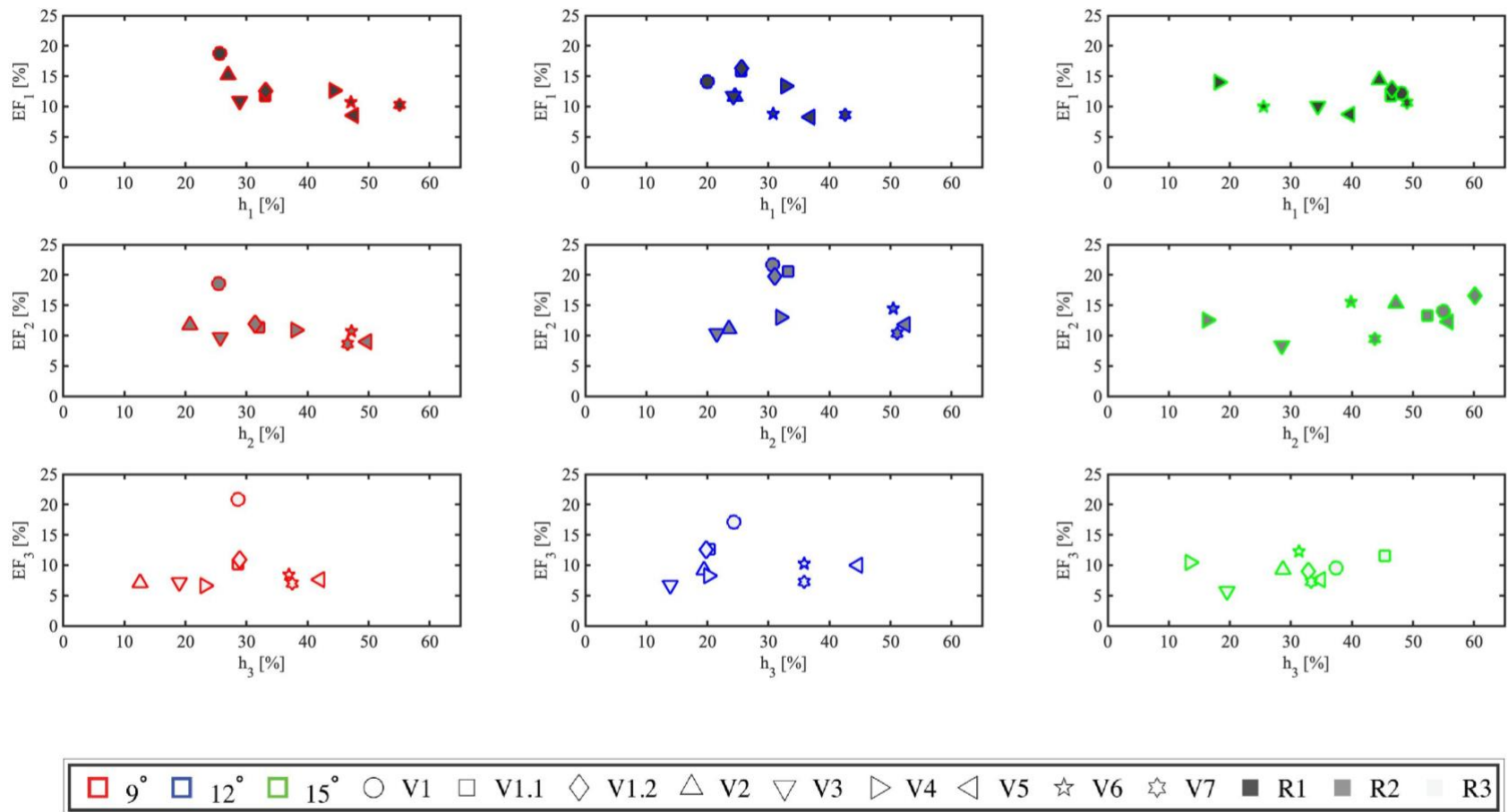
Graph 4.17: Grade-enrichment factor of heavy particles for each riffle at 24 L/min
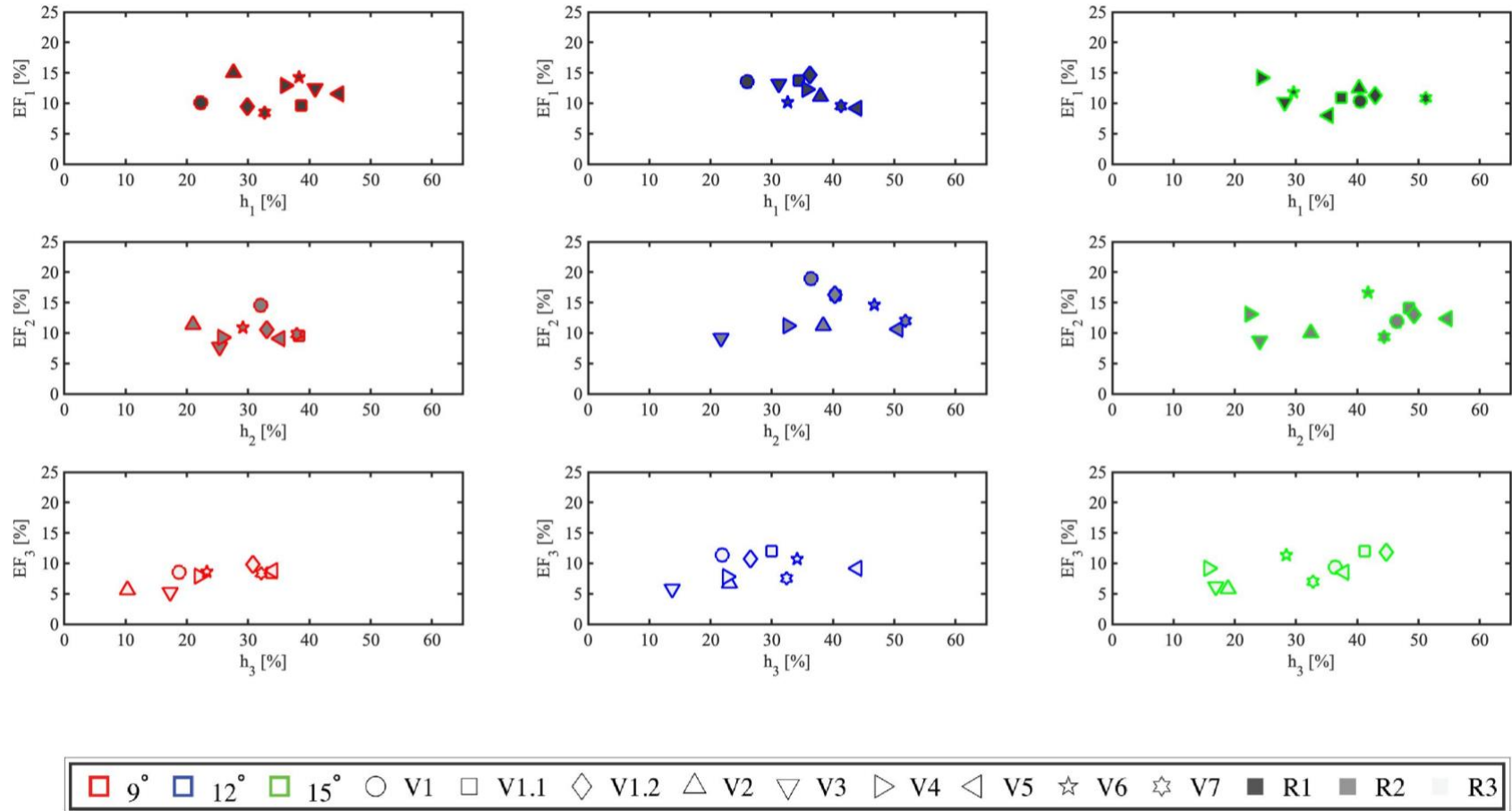
Graph 4.18: Grade-enrichment factor of heavy particles for each riffle at 23 L/min
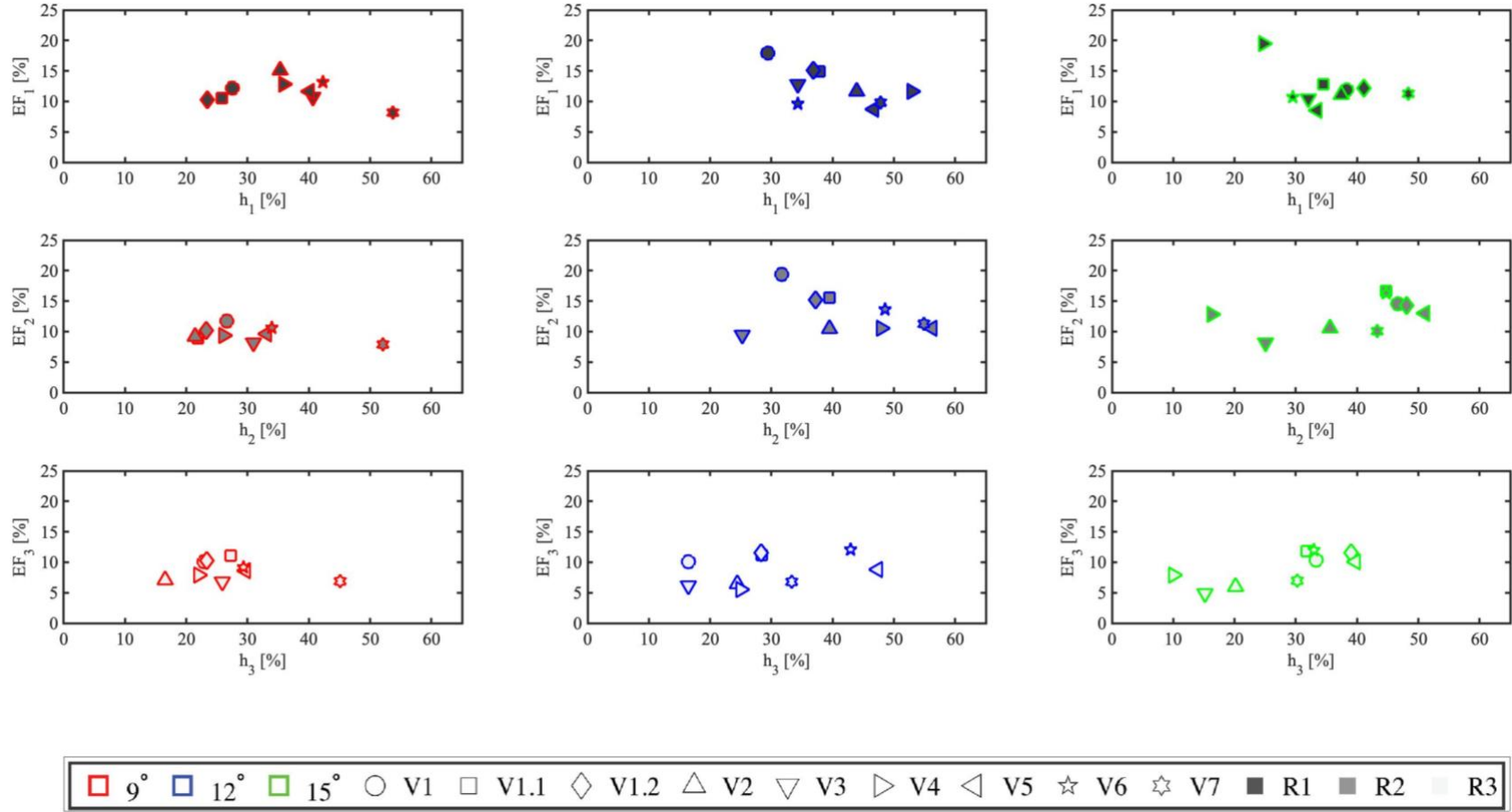
Graph 4.19: Grade-enrichment factor of heavy particles for each riffle at 22 L/min

Graph 4.20: Grade-enrichment factor of heavy particles for each riffle at 8 L/min

At 8 L/min, design V1.2's R1 retained the highest fraction of heavy particles while design V1's riffles at 15° inclination angle had the highest enrichment factors. Design V1's performance is likely partly due to its geometries, as previously mentioned, along with the low flow rate allowing the flow to segregate more before reaching the riffles. The grade of heavy particles and enrichment factor for riffles and designs at different inclination angles is closely clustered in a linear curve, as shown in Graph 4.20. It appears at both 12° inclination angle and 15° inclination angle, there is high and low performance, suggesting for these parameters' inclination angle has minimal effect on enrichment factor and grade of heavy particles in each riffle.

For this performance index, there is no consistent inclination angle that performs better than the others. The grade-enrichment factor of heavy particles for designs and inclination angles are clustered together, without clear separation in performance among inclination angle and designs. This suggests a minimal impact of inclination angle on grade-enrichment factor of heavy particles for single riffles.

4.7   Grade-Enrichment Factor of Heavy Particles for Complete System

For all flow rates and inclination angles, grade-enrichment factor of heavy particles follows a flattened curve such that the increase in total grade of heavy particles in all riffles has minimal increase in total enrichment factor.

Graph 4.21 shows the grade-enrichment factor of heavy particles for the complete system at 24 L/min. It appears the best performing design was design V2 at 15° inclination angle. Design V1.1 at 15° inclination angle had the highest total fraction of heavy particles while design V1 at 9° inclination angle had the highest total enrichment factor. At 23 L/min, design V5 had the highest total fraction of heavy particles while design V1 had the highest total enrichment factor (Graph 4.22). Designs V1 and its variations at 15° inclination angle seem to have the best performance on this measure. At the flow rate of 22 L/min, the best performing designs are at 12° inclination angle and 15° inclination angle (Graph 4.23). Design V1.2 at 15° inclination angle appears to slightly outperform design V6 at 12° inclination angle, while design V7 had the highest total fraction of heavy particles and design V1 had the highest total enrichment factor.
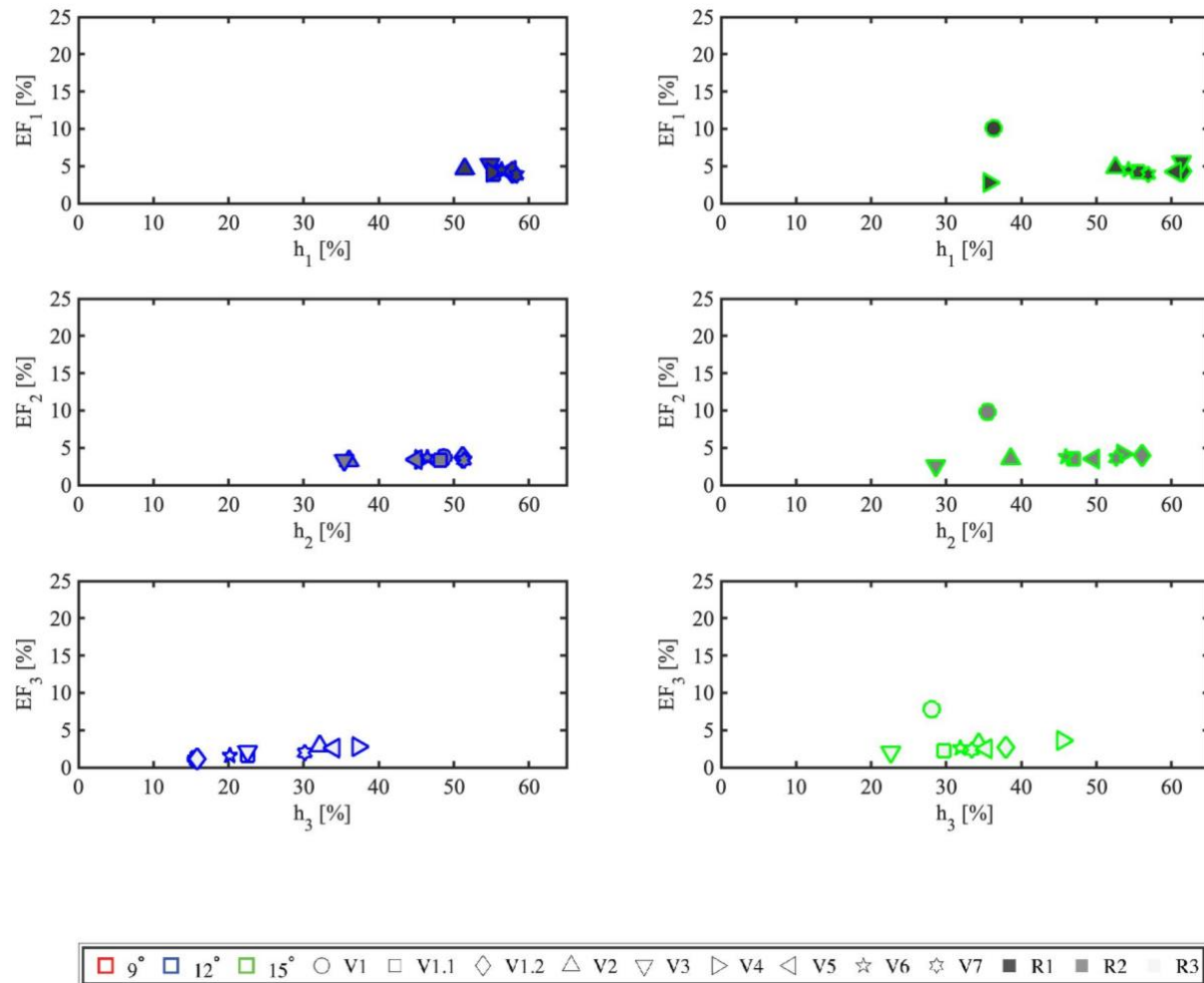
Graph 4.21: Grade-enrichment factor of heavy particles for complete system at 24 L/min
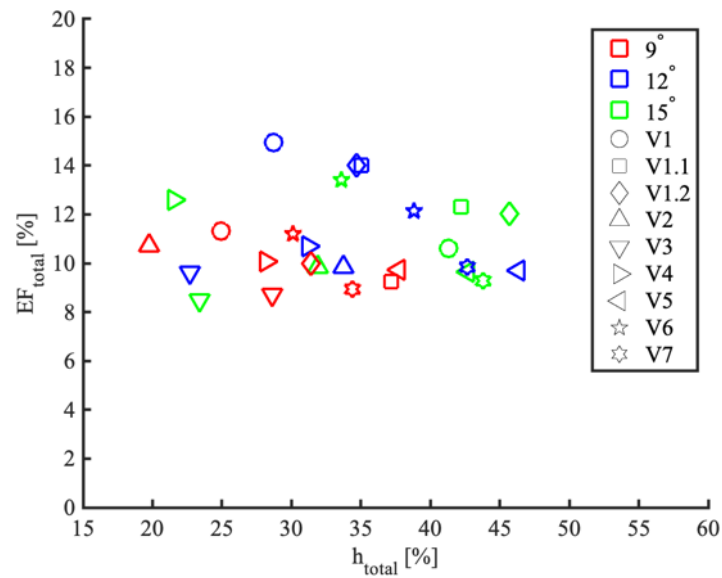
Graph 4.22: Grade-enrichment factor of heavy particles for complete system at 23 L/min

Design V1's performance across the flow rates in setup 1 suggest it is more efficient at collecting and retaining heavy particles. As mentioned, this may be due to its geometries. Design V1 does not perform exceptionally well at 15° inclination angle though, suggesting the lower inclination angles enhance design V1's ability to retain heavy particles. While riffle geometry appears to contribute to design performance, in this case inclination angle has a stronger impact on

55

enrichment factor of heavy particles. This may be due to the lower inclination angles leading to a reduced flow velocity that in turn allows the flow to segregate before reaching the riffled section.
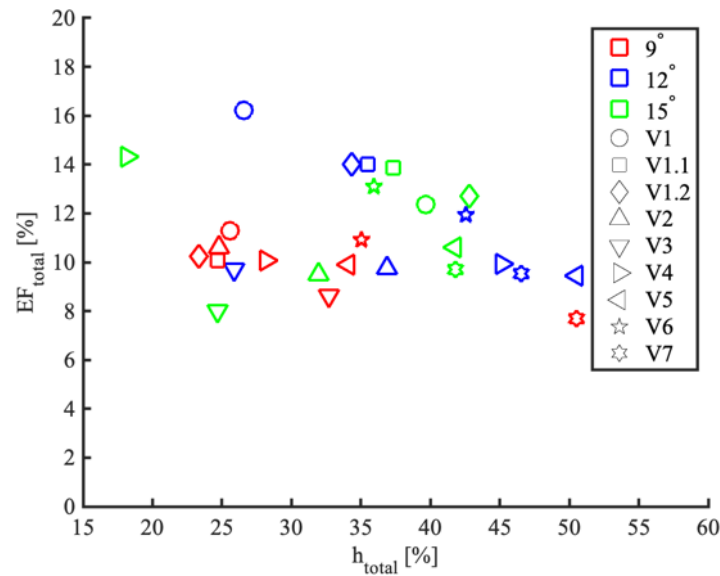
Graph 4.23: Grade-enrichment factor of heavy particles for complete system at 22 L/min

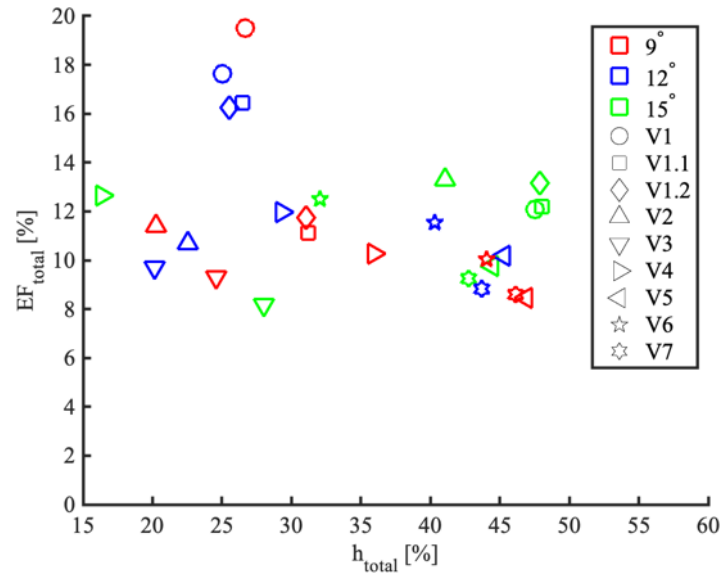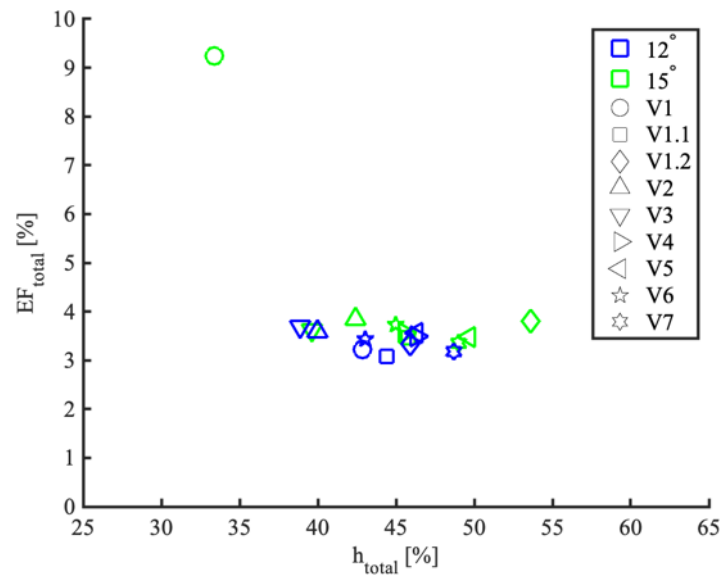Graph 4.24: Grade-enrichment factor of heavy particles for complete system at 8 L/min

Graph 4.24 illustrates the grade-enrichment factor of heavy particles for the complete system at 8 L/min. Design V1.2 had the highest total fraction of heavy particles while design V1 had the highest total enrichment factor of heavy particles. Design V1's enrichment factor of heavy

particles at 15° inclination angle may be an outlier, however, based on the tight trends in the other results. Aside from this result, inclination angle does not appear to strongly influence enrichment factor at this flow rate. This could be due to the low flow rate having a stronger influence on enrichment factor of heavy particles than inclination angle.

4.8   Grade-Separation Efficiency of Heavy Particles for Complete System

Graph 4.25 demonstrates the grade-separation efficiency of heavy particles for the complete system at 24 L/min. Design V1.1 had the highest total fraction of heavy particles while Design V4 had the highest separation efficiency of heavy particles in riffles. Designs at 9° inclination angle and 12° inclination angle appear to follow a trend where separation efficiency of heavy particles increases significantly but total grade of heavy particles increases minimally. At 15° inclination angle, the opposite trend is observed where designs show greater increases in total grade of heavy particles and minimal increases in separation efficiency of heavy particles in riffles.
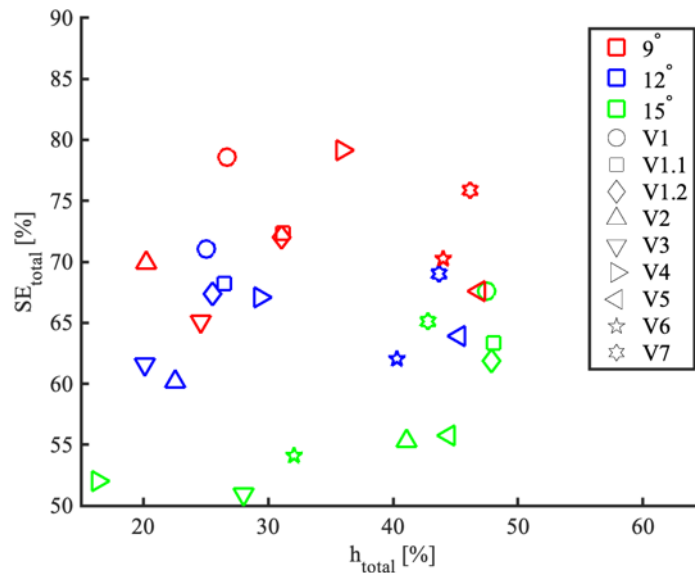
Graph 4.25: Grade-separation efficiency of heavy particles for complete system at 24 L/min

Graph 4.26 shows grade-separation efficiency of heavy particles in riffles for the system at 23 L/min. For all inclination angles at this flow rate, separation efficiency of heavy particles increases minimally in relation to the increases in total grade of heavy particles, suggesting similar separation efficiencies regardless of total heavy grade at this flow rate.
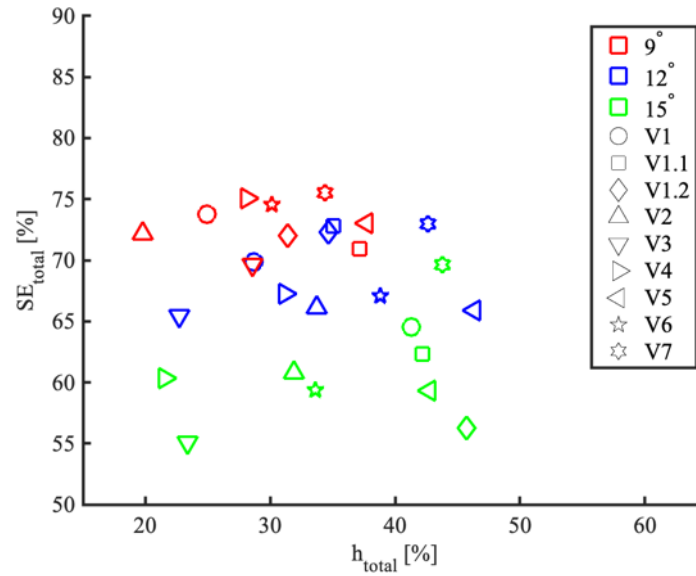
Graph 4.26: Grade-separation efficiency of heavy particles for complete system at 23 L/min
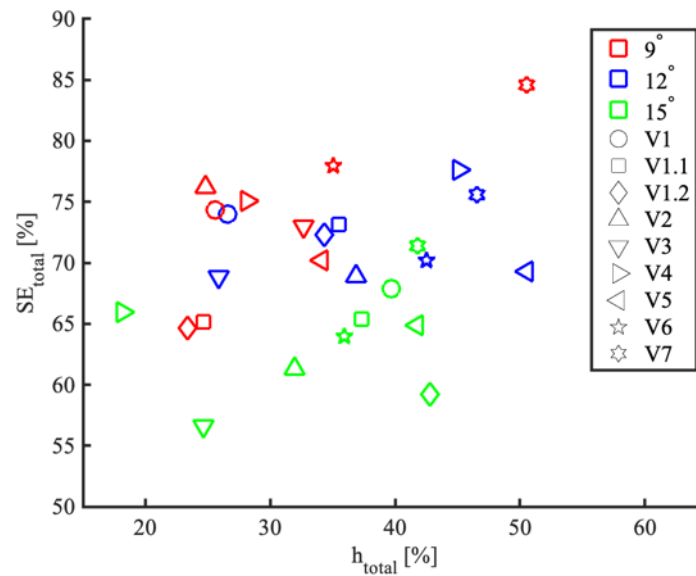
Graph 4.27: Grade-separation efficiency of heavy particles for complete system at 22 L/min

At 22 L/min, grade-separation efficiency of heavy particles follows a more consistent trend, as shown in Graph 4.27. Designs at 15° inclination angle generally show a linear trend, suggesting a clearer ranking of riffle design performance at this inclination angle and flow rate. At all inclination angles, design V7 performs consistently well. For designs at 12° inclination angle, it appears there is minimal increase in separation efficiency of heavy particles while total grade of heavy particles increases significantly.

58

At flow rates of 24 L/min, 23 L/min, and 22 L/min, design V7 at 9º inclination angle performed best with respect to grade-separation efficiency of heavy particles (Graph 4.25, Graph 4.26, Graph 4.27). As previously mentioned, design V7's geometry likely increases its ability to entrap heavy particles while allowing light particles to exit.

Graph 4.28 shows the grade-separation efficiency of heavy particles for the complete system at 8 L/min. At this flow rate, designs at 12º inclination angle had better grade-separation efficiency of heavy particles with minimal impact from the riffle design itself. This suggests that low flow rate and low inclination angle significantly contributed to increased separation efficiency of heavy particles while riffle design had minimal impact. Design V1 at 15º inclination angle is far outside the general range of separation efficiencies at this flow rate, hence this is treated as an outlier. Separation efficiency of heavy particles was generally lower for designs at 15º inclination angle.
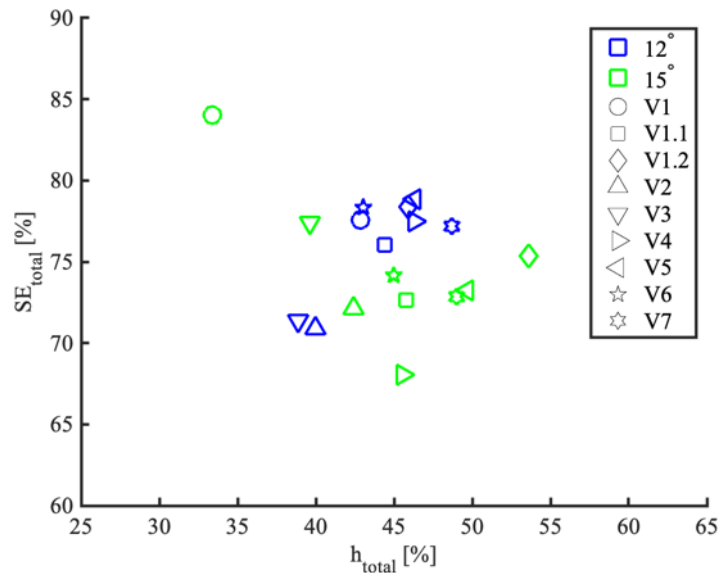
Graph 4.28: Grade-separation efficiency of heavy particles for complete system at 8 L/min

In general, for the flow rates tested in setup 1, separation efficiency of heavy particles increases as flow rate reduces such that separation efficiency of heavy particles at 22 L/min is higher than at 24 L/min. For these conditions, higher inclination angles (15º inclination angle) had lower separation efficiency of heavy particles than lower inclination angles (9º inclination angle), indicating lower inclination angles improve performance on this index. A similar trend is observed at the flow rate of 8 L/min, where designs at 12º inclination angle perform better in general than

designs at 15° inclination angle. The difference in performance is smaller at this flow rate, which may indicate inclination angle has a weaker effect on separation efficiency of heavy particles when the flow rate is low.

4.9   Volumetric Analysis

The volumetric analysis is conducted at 12° inclination angle and 8 L/min flow rate as most riffle designs performed well in this condition. This is supported by analysis of the performance indices. This representation provides a 2D perspective on heavy particle retention in the riffles over the course of the experiment. In all the figures in this section, the time stamp $T = 0$ represents the riffles at the start of the experiment. $T = 0.5$ depicts the riffles halfway through the experiment. $T > 1$ illustrates the riffles when the experimental trials have concluded. The pie chart with the $T > 1$ time stamp depicts the volumetric particle retention of each riffle based on the quantitative data collected. This section also provides a visual perspective on heavy accumulation at different riffles by various riffle design.
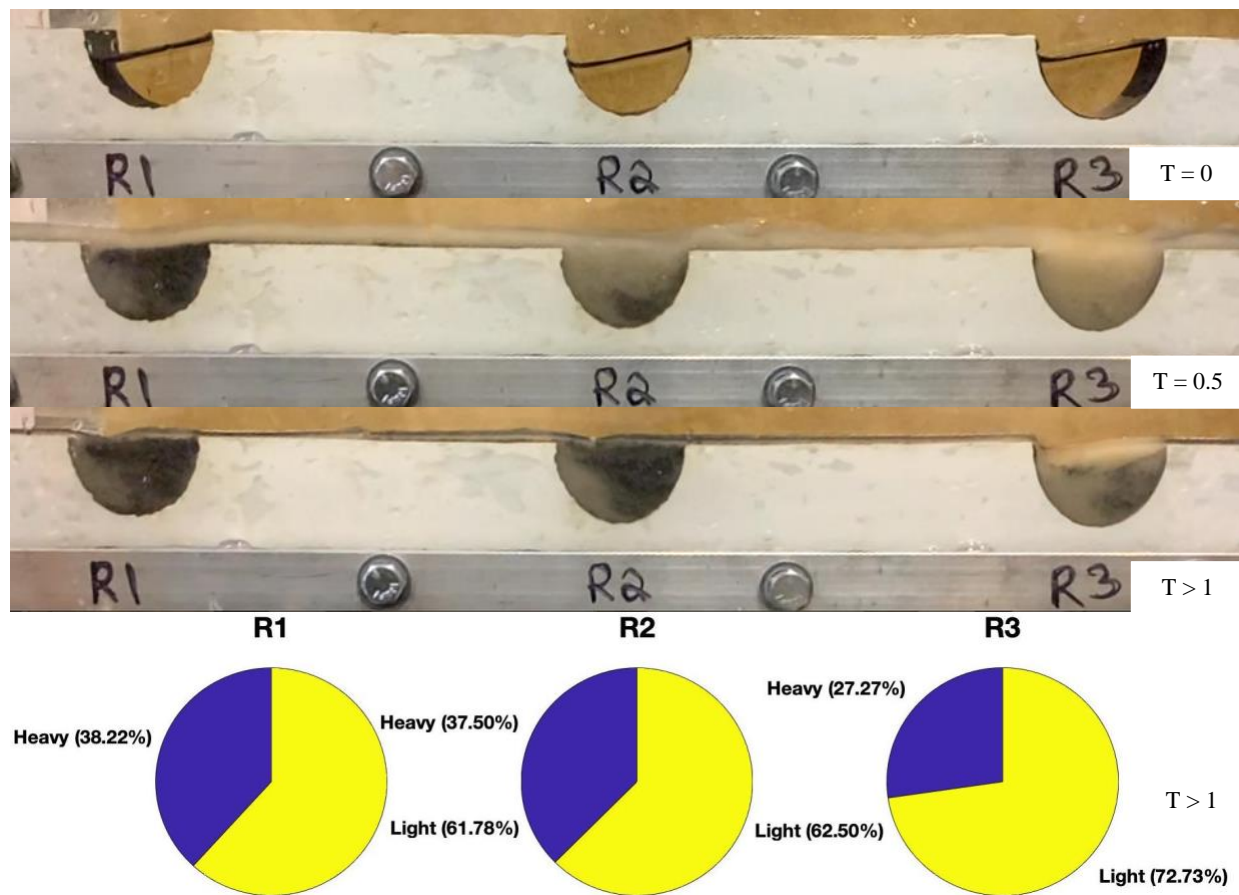
Figure 4.2: Performance of design V1 at different experimental stages

As Figure 4.2 illustrates, R1 retains the highest fraction of heavies by volume, followed by R2 and R3. The heavy accumulation progression as illustrated by the images at different time stamps supports this data.
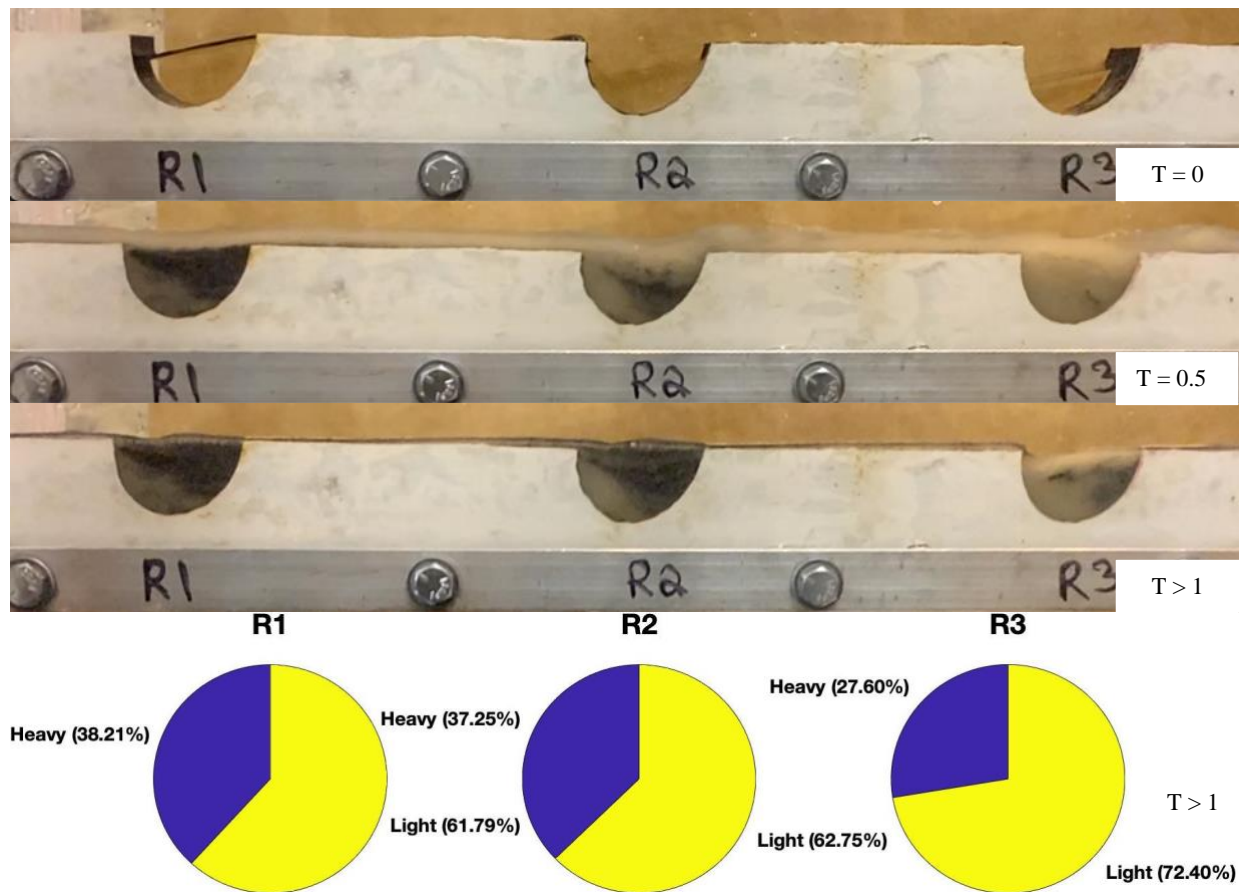
Figure 4.3: Performance of design V1.1 at different experimental stages

Figure 4.3 shows that R1 retains the highest fraction of heavies by volume, followed by R2 and R3. The heavy accumulation in the riffles is illustrated by the images at different time stamps and supports this data.
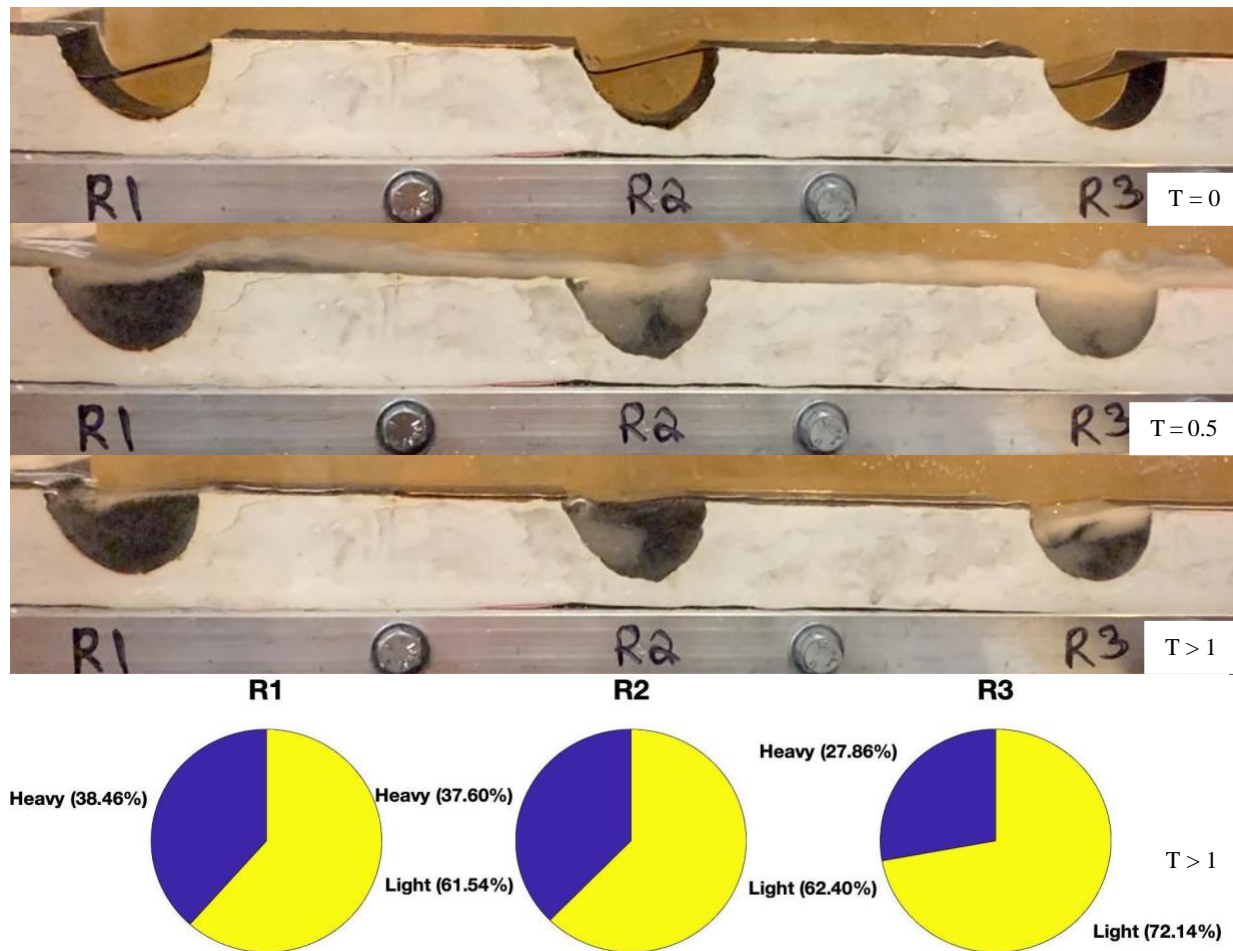
Figure 4.4: Performance of design V1.2 at different experimental stages

In Figure 4.4, R1 retains the highest fraction of heavies by volume, followed by R2 and R3. In R1, the heavy particles appear to be well-concentrated compared to the other riffles. Heavy formation in R2 and R3 appear more stratified.
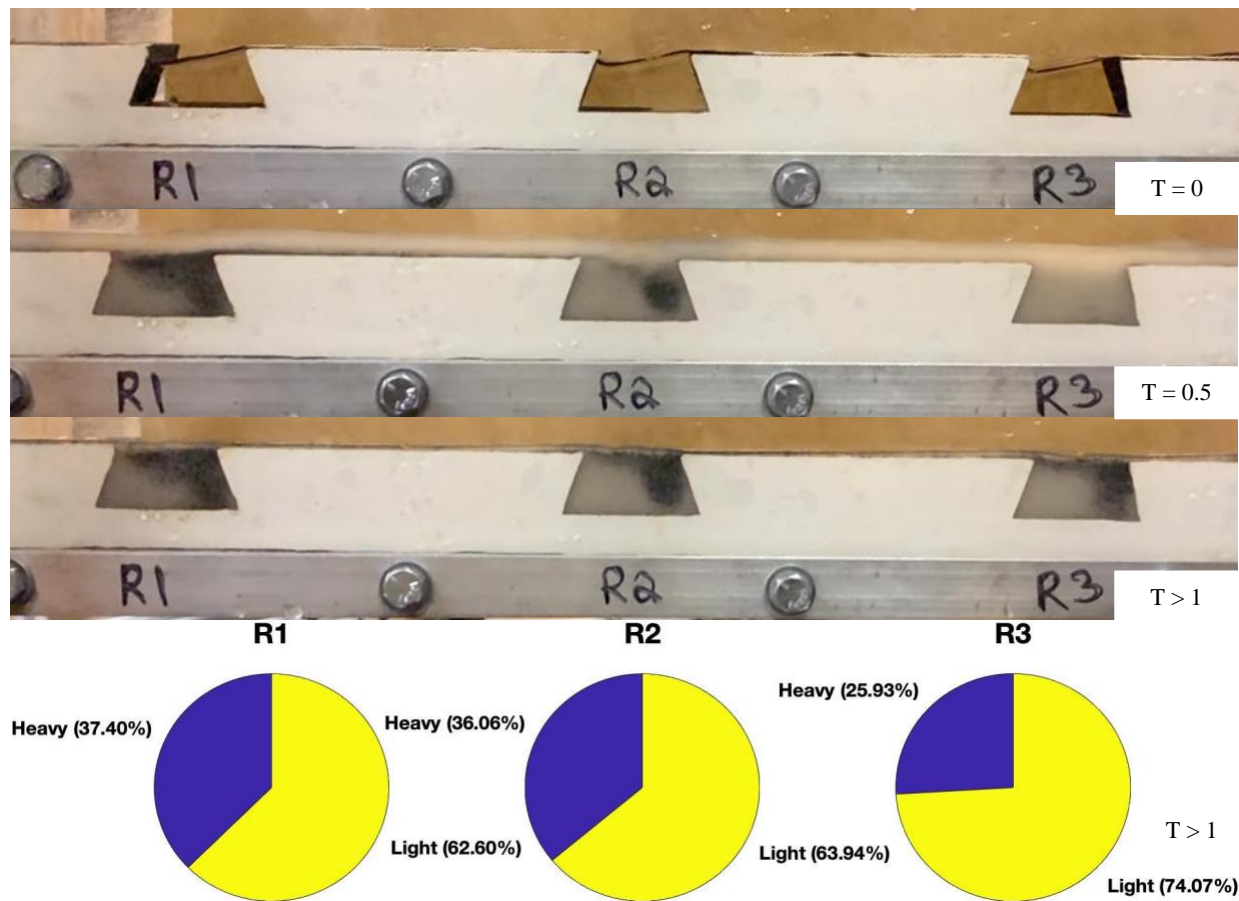
Figure 4.5: Performance of design V2 at different experimental stages

R1 retains the highest fraction of heavies by volume, followed by R2 and R3, as shown in Figure 4.5. All riffles seem to have stratified heavy and light particle concentrations.
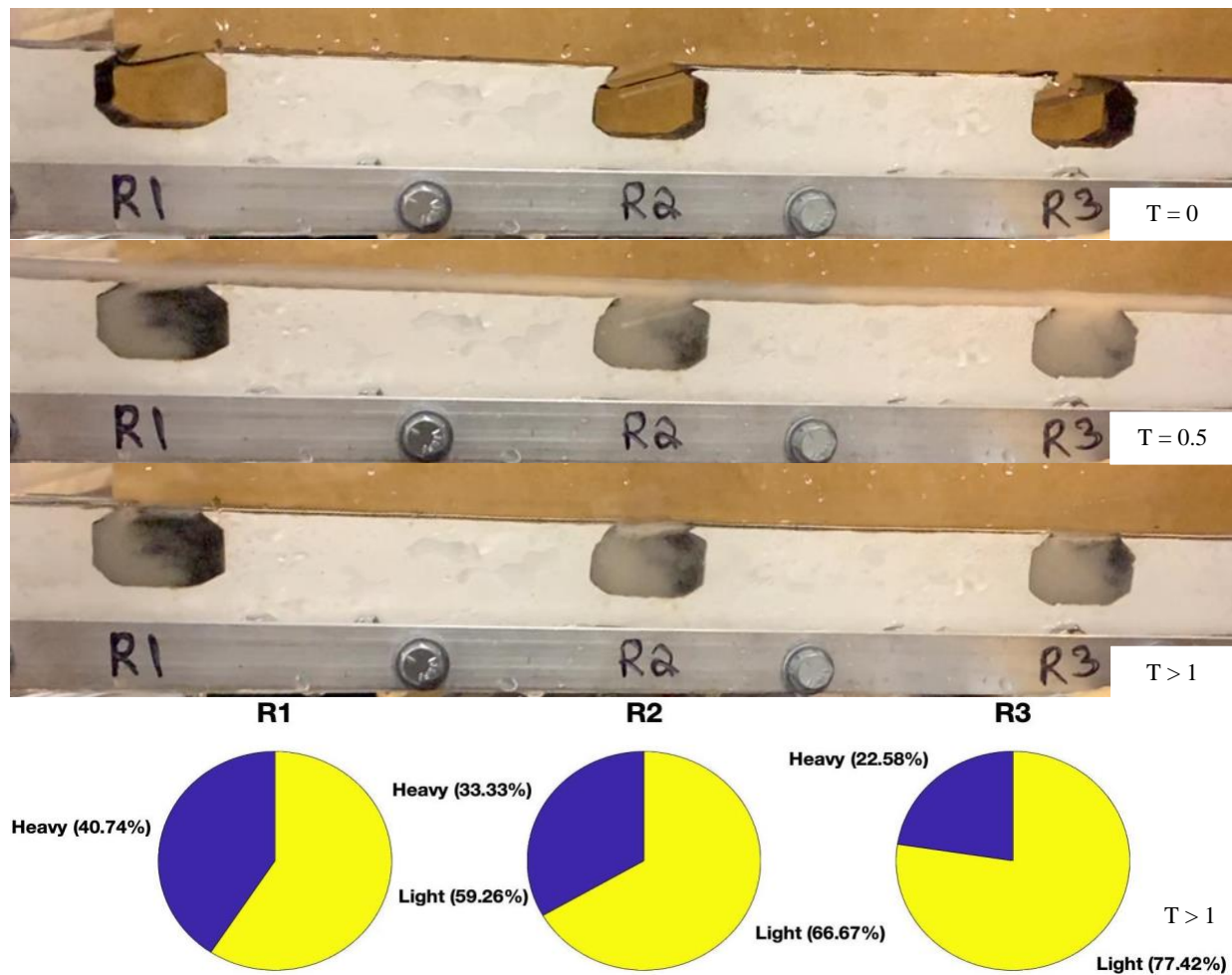
Figure 4.6: Performance of design V3 at different experimental stages

R1 retains the highest fraction of heavies by volume, followed by R2 and R3, as illustrated by Figure 4.6. The heavy accumulation progression as illustrated by the images at different time stamps supports this data. The particles in R1 seem to be the most stratified, followed by R2 and R3.
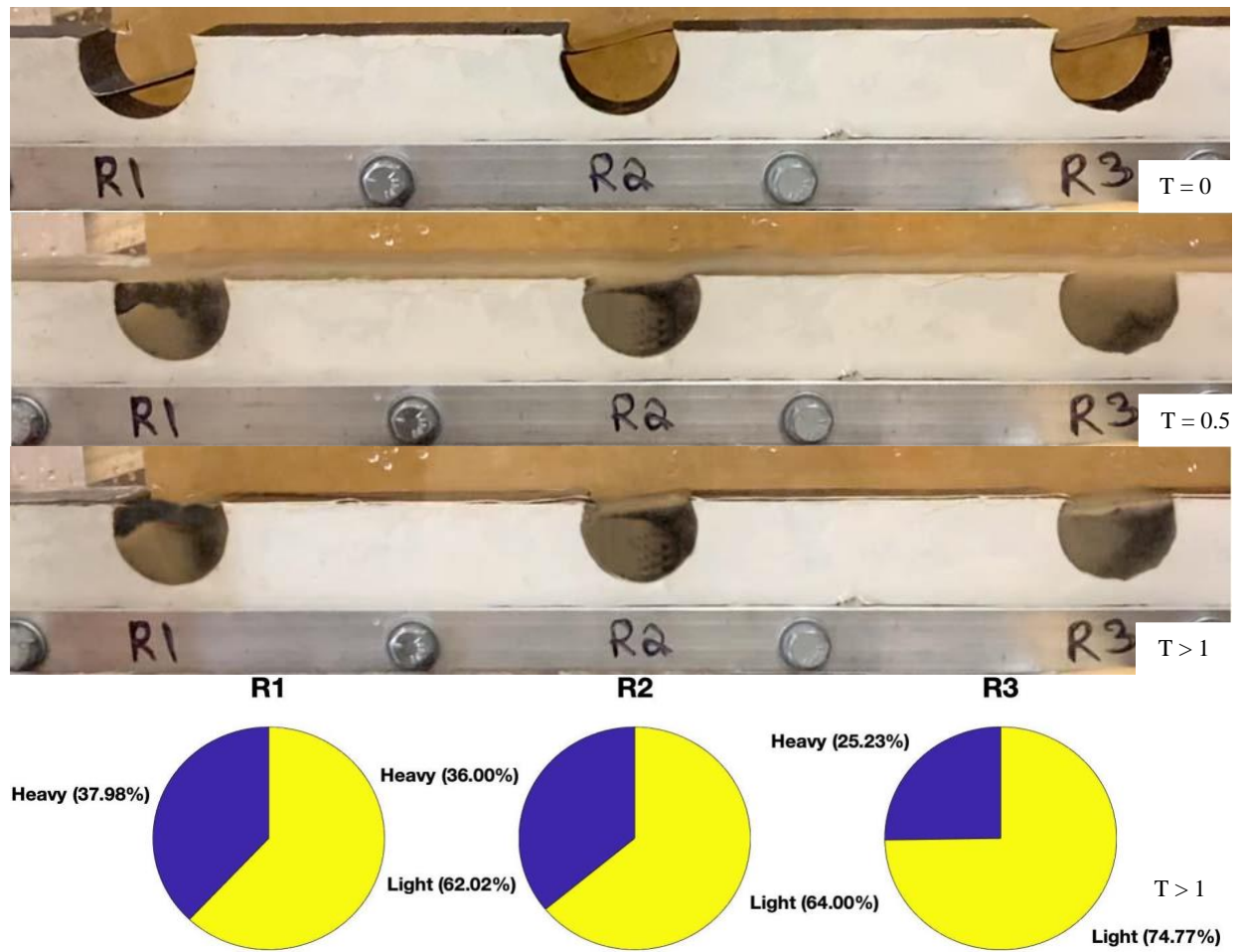
Figure 4.7: Performance of design V4 at different experimental stages

Figure 4.7 depicts that R1 retains the highest fraction of heavies by volume, followed by R2 and R3. R1 and R2 appear to be the most stratified, followed by R3.
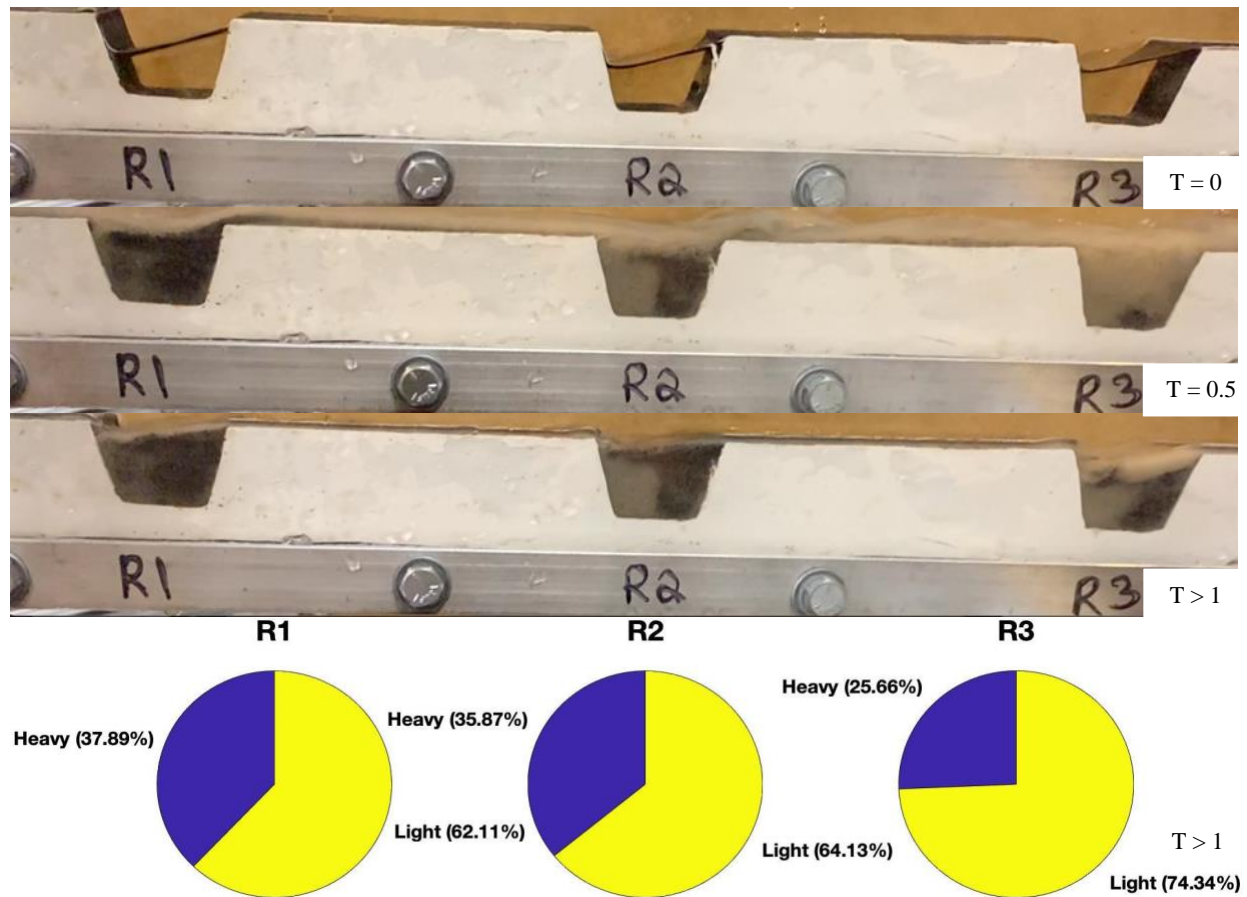
Figure 4.8: Performance of design V5 at different experimental stages

As seen in Figure 4.8, R1 retains the highest fraction of heavies by volume, followed by R2 and R3. R2 appears to most stratified while R1 appears to have well-packed heavy particles.
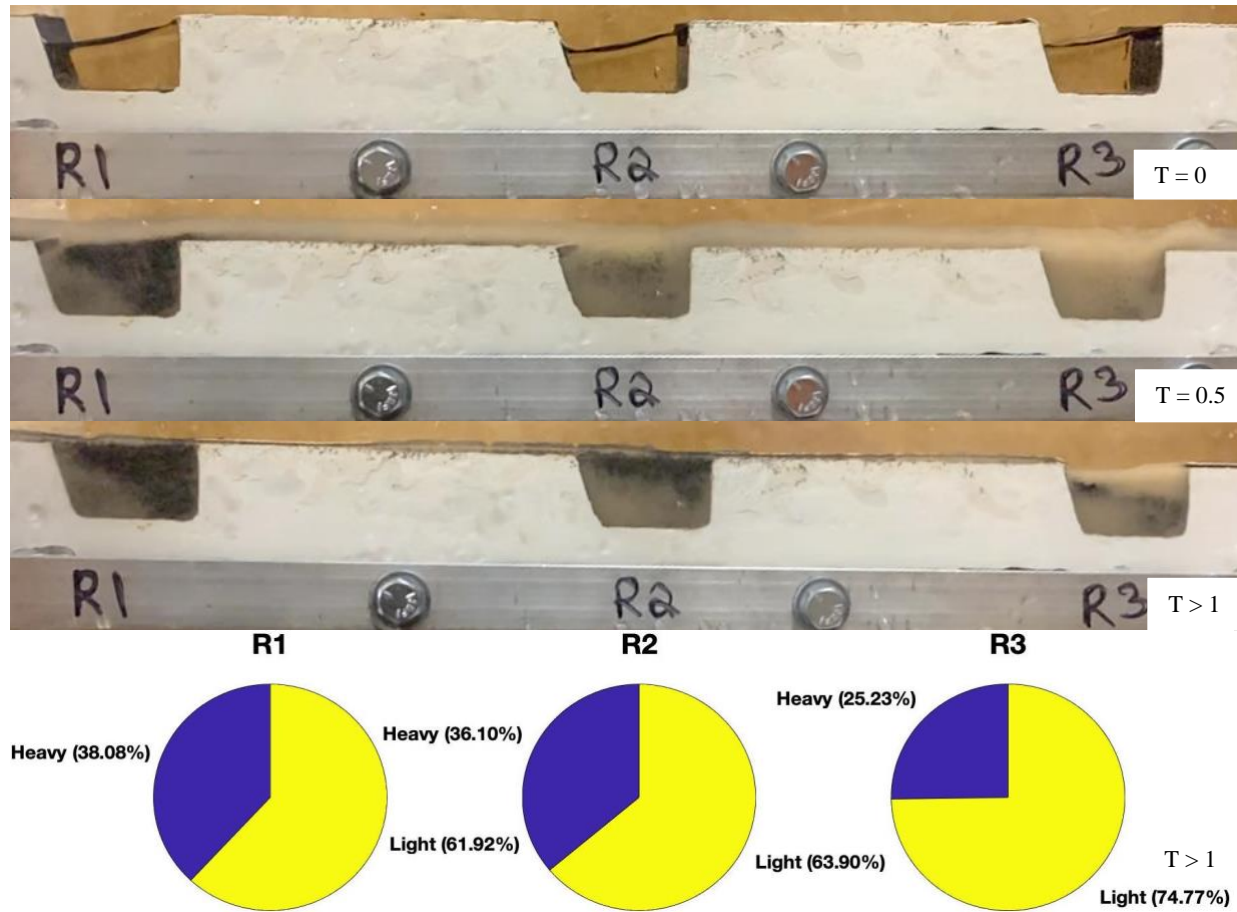
Figure 4.9: Performance of design V6 at different experimental stages

Figure 4.9 shows that R1 retains the highest fraction of heavies by volume, followed by R2 and R3. The heavy accumulation progression as illustrated by the images at different time stamps supports this data. R1 has the most well-packed heavy particles, followed by R2. R3 appears to have slight stratification of heavy particles.
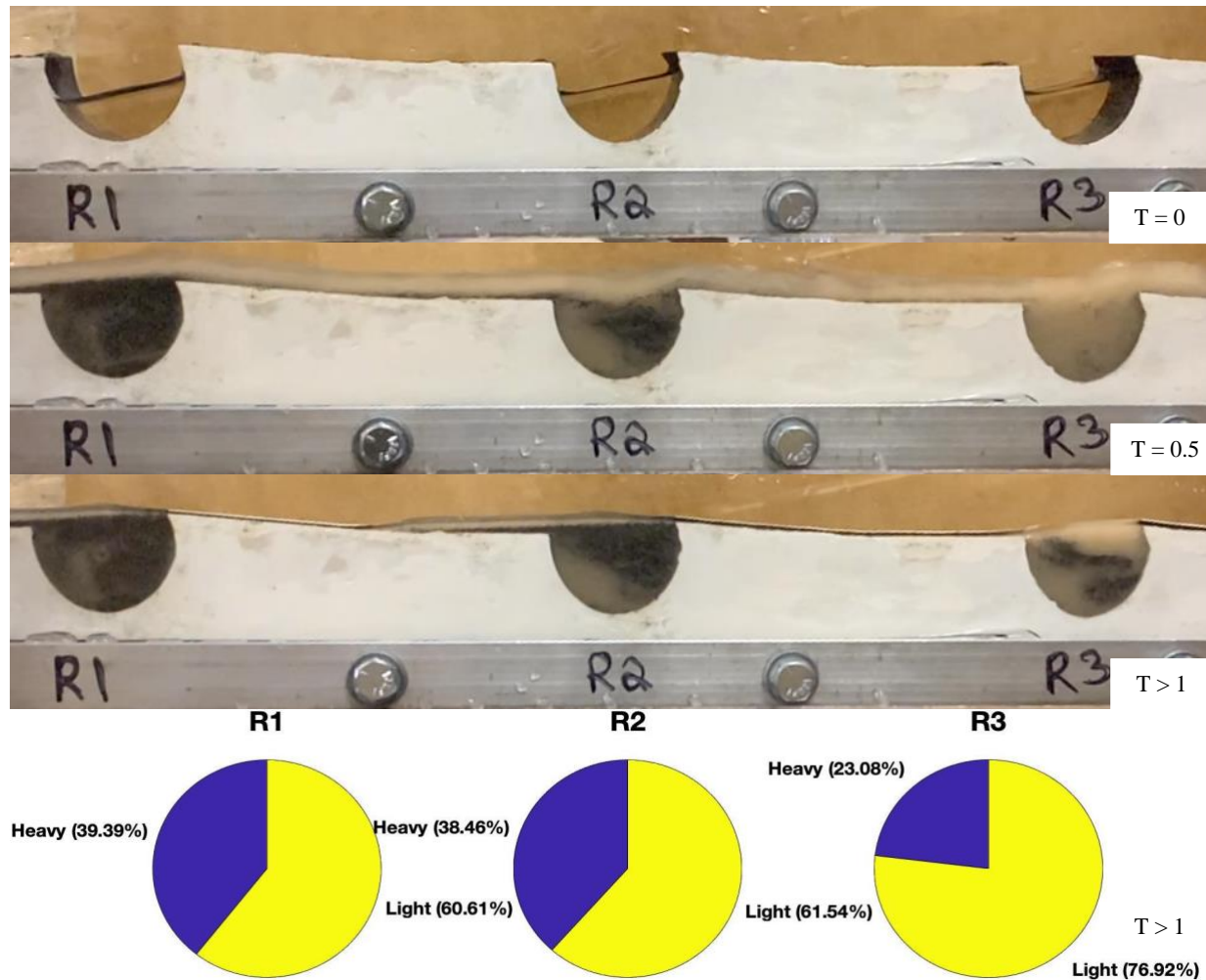
Figure 4.10: Performance of design V7 at different experimental stages

R1 appears to retain the most heavies and have a well-packed riffle compared to R2 and R3, as shown in Figure 4.10. This hypothesis seems to be strengthened by R1 having the highest fraction of heavy retention by volume, followed by R2 and R3. The heavy accumulation progression as illustrated by the images at different time stamps supports this data. Some riffles seem to be densely packed with heavies from the 2D perspective, but the volumetric analysis shows a consistent proportion of heavy and light particles for the designs.

4.10 Effect of Inclination Angle

Inclination angle impacted performance indices as expected based on previous literature described in Chapter 2. As the inclination angle decreased, performance indices generally improved. More heavy particles were retained in the riffles, possibly due to the flow angle aligning with the riffle

shape more closely than at higher inclination angles. Additionally, low inclination angles may have reduced the velocity of the flow, allowing it to be slow enough that particles begin to segregate as they enter the riffles.

There is a point at which inclination angles become too low to accurately measure heavy particle retention. As previously established [87], solids form hills with finite slopes at extremely low inclination angles, thus limiting the ability to accurately measure the solid concentration in the riffles. During the experiments, the solids in the slurry formed hills with finite slopes in trials conducted at 6° inclination angle for setup 1 (Figure 4.11) and at 9° inclination angle for setup 2. As a result, these trials were discontinued due to difficulty in accurately measuring the heavy particle retention in the riffles.
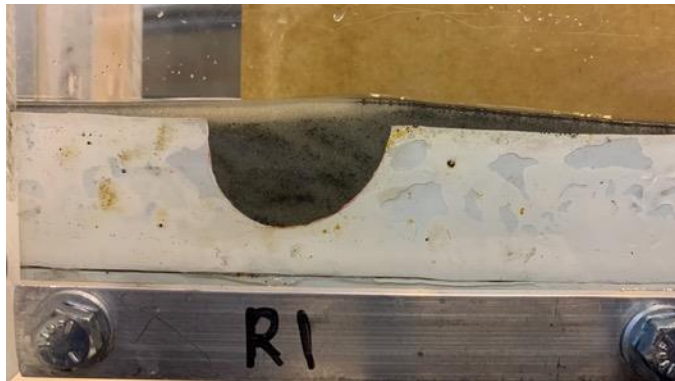
Figure 4.11: Solids forming finite slopes at lower inclination angles of the thin channel

Similarly, studies were attempted at inclination angles of 18° and higher, but the riffles were retaining very few particles at all flow rates analyzed. In addition, the shearing effect on the slurry flow from the valve shut-off caused high amounts of erosion from the riffles which could not be quantified or reproduced. Thus, the experiments were conducted at inclination angles of 9°, 12°, and 15° for experimental setup 1 and inclination angles of 12° and 15° were studied for experimental setup 2.

4.11 Effect of Flow Rate

In setup 1, the best performance occurred at 22 L/min. Performance at the flow rate of 8 L/min in setup 2 was consistently high, though because of the differing setups, results cannot be directly

compared between setups 1 and 2. At high flow rates, such as 24 L/min, it may be that very little heavy particles are trapped in the riffles because the flow is not segregated before it reaches the riffles, unlike at low flow rates. As a result, segregation of heavy particles would have to primarily occur within the riffles, relying on the riffle's geometry to concentrate the heavies. As previously stated, the formation of a sliding and heterogeneous bed in the flow developing zone likely produced a fully developed flow with heavy particles segregating to the bottom layer, the light particle forming the center layer, and a fluid-only layer residing in the top region of the flow at low flow rates. This common flow behaviour of bidensity particle laden flow seemed to allow certain riffle geometries to perform better compared to the others at low flow rates.

4.12 Effect of Riffle Shape

Design V1 and its variations along with design V7 tended to outperform the other riffle designs. This may be due to the semi-elliptical shape creating a recirculation zone within the riffle that forces heavy particles to remain in the riffle until they settle. Designs V2, V3, and V4 may have had lower heavy particle retention rates due to smaller riffle openings, possibly limiting the flow from freely entering the riffle. This may have resulted in limited vortices within the riffle, which could have led to the riffles filling faster but not expelling light particles. Once the riffles were filled, they became compact with particles and established a statistically stationary flow over the riffles.

Design V4 may have performed better at high flow rates and lower inclination angles due to its more circular shape, possibly allowing vortices to form within the riffle that aid heavy particle settling. Design V5 is used as a comparison design since this design is used in the riffled section of the Falcon enhanced gravity separator. Compared to the other designs in this study, design V5 performed moderately well, suggesting improvements can be made to its design. Design V6 is a derivative of design V5, and it performed similarly to design V5. Enhanced heavy particle capture and retention of design V7 may be attributed to the boundary layer of heavy and light particles segregation aligning with the raised lip at the riffle exit point.

Chapter 5: Conclusion

The objective of this thesis was to study the behaviour and characteristic separation of heavy and light particles in an open thin channel setup. Particle behaviour in the riffled section of the thin channel setup was studied by varying flow rate, inclination angle, and riffle geometries. Riffle designs were developed to increase heavy particle retention, with testing intended to determine which design yielded the highest enrichment factor, mass yield, and separation efficiency of heavy particles.

In this study, it was observed that lower inclination angles (9° inclination vs. 15° inclination) and lower flow rates (22 L/min vs. 24 L/min in setup 1; 8 L/min in setup 2) resulted in better mineral recovery, coinciding with previous research. Falcon enhanced gravity separators could use these results to modify the bowl's angle and flow rate to retain the highest fraction of heavy particles in the riffled section. Similarly, any gravity separators employing engineered riffle sections could benefit from the findings in this study.

Designs V1 and its variations along with design V7 can be considered superior riffle designs based on the analyses conducted in this research. The semi-elliptical shape in both these designs appeared to efficiently capture and retain heavy particles while allowing light particles to exit the riffle, leading to high heavy particle recovery. Design V7 included a raised lip at the riffle exit which seems to have enhanced heavy particle entrapment more than design V1. Specifically, the raised lip prevented heavy particles from exiting the riffle while allowing light particles to exit. Asymmetrical shapes such as design V7 have the potential to simultaneously allow particles to enter the riffle while trapping heavy particles within the riffle, creating effective particle segregation.

This thesis found a strong relationship between low flow rates and low inclination angles as primary influences on mineral recovery using a riffled thin channel setup, with semi-elliptical riffle design producing the best results. The particle behaviour observations in this thesis can serve as a foundation for study on Falcon enhanced gravity separator geometry as well as any devices that employ engineered riffles for gravity separation.

Chapter 6: Future Research

This research provides valuable insight into bidensity particle laden flow behaviour in a riffled thin channel setup. In this study, only a few parameters were analyzed, thus opening avenues for future research into the impact of various slurry densities, spacing between riffles, non-identical riffles in the same trial run, and mono-sized or poly-sized particles. The experiments were conducted as a batch process, like how existing Falcon enhanced gravity separators perform, however, future studies can be conducted on a continuous system.

Developing a method to continuously extract heavy particles from the riffles would allow Falcon enhanced gravity separators to operate without interruptions for mineral recovery, increasing processing efficiency and saving capital. The impact of vibration on particle segregation is well analyzed phenomenon, thus using accordion riffles may enhance the performance of the riffled sections. This would be an interesting development in mineral processing. If fluidization of the riffled section with air is performed, this would revolutionize the industry as it would save significant capital and energy in the dewatering process.

This thesis provides experimental support for some operating parameters and further experimental work can expand the possibilities for optimizing gravity separation.

Bibliography

[1]   S. K. Haldar, "Mineral Processing," in *Mineral Exploration*, Elsevier, 2018, pp. 259–290.

[2]   B. A. Wills and J. A. Finch, *Wills' Mineral Processing Technology*, Eighth. Elsevier, 2016.

[3]   M. Zhou, O. Kökkılıç, R. Langlois, and K. E. Waters, "Size-by-size analysis of dry gravity separation using a 3-in. Knelson Concentrator," *Miner. Eng.*, vol. 91, pp. 42–54, May 2016, doi: 10.1016/j.mineng.2015.10.022.

[4]   A. K. Majumder and J. P. Barnwal, "Modeling of Enhanced Gravity Concentrators–Present Status," *Miner. Process. Extr. Metall. Rev.*, vol. 27, no. 1, pp. 61–86, Jan. 2006, doi: 10.1080/08827500500339307.

[5]   P. Ahlerup, T. Baskaran, and A. Bigsten, "Gold Mining and Education: A Long-run Resource Curse in Africa?," *J. Dev. Stud.*, vol. 56, no. 9, pp. 1745–1762, Sep. 2020, doi: 10.1080/00220388.2019.1696959.

[6]   C. Gasparrini, *Gold and Other Precious Metals*, vol. 53, no. 9. Berlin, Heidelberg: Springer Berlin Heidelberg, 1993.

[7]   I. Alp, O. Celep, H. Deveci, and M. Vicil, "Recovery of gold from a free-milling ore by centrifugal gravity separator," *Iran. J. Sci. Technol. Trans. B Eng.*, vol. 32, no. 1, pp. 67–71, 2008.

[8]   L. Huang and N. Mejiab, "Characterizing gravity recoverable PGMS and gold in grinding circuit," *Iran. J. Sci. Technol. Trans. B Eng.*, vol. 29, Dec. 2005.

[9]   A. R. Laplante and N. Nickoletopoulos, "Validation of a falcon model with a synthetic ore," *Can. Metall. Q.*, vol. 36, no. 1, pp. 7–13, 1997, doi: https://doi.org/10.1016/S0008-4433(96)00031-6.

[10]   A. Falconer, "Gravity Separation: Old Technique/New Methods," *Phys. Sep. Sci. Eng.*, vol. 12, no. 1, pp. 31–48, Jan. 2003, doi: 10.1080/1478647031000104293.

[11]   A. Gupta and D. S. Yan, "Gravity Separation," in *Mineral Processing Design and Operation*, Elsevier, 2006, pp. 494–554.

[12]   D. Schriner and C. Anderson, "Centrifugal Concentration of Rare Earth Minerals from Calcitic Gangue," *J. Metall. Eng.*, vol. 4, no. 0, p. 69, 2015, doi: 10.14355/me.2015.04.009.

[13]   "The Legend Of Knelson Concentrators," *GCA*, 2019. https://www.gca.gold/legend-of-knelson/# (accessed Feb. 03, 2021).

[14] J. Boehnke, "The falcon semi-batch gravity concentrator," *Mineral processing and aggregate specialist - Sepro Minerals Systems Corp*, 2014. https://minerals.seprosystems.com/wp-content/uploads/2020/05/Introduction-to-the-Falcon-Semi-Batch-Gravity-Concentrator.pdf (accessed Feb. 03, 2021).

[15] P. Ancia, J. Frenay, and P. Dandois, "Comparison of Knelson and Falcon centrifugal separators," in *Innovation in Physical Separation Technologies, Richard Mozley symposium volume*, 1997, pp. 53 – 62.

[16] S. M. S. Corp., "Falcon Semi - Batch (SB) Concentrators," 2018. https://minerals.seprosystems.com/wp-content/uploads/2019/09/Falcon_SB_Concentrator_2018-1-1.pdf.

[17] M. Zhou, O. Kökkiliç, R. Langlois, and K. E. Waters, "Size-by-size analysis of dry gravity separation using a 3-in. Knelson Concentrator," *Miner. Eng.*, vol. 91, pp. 42–54, 2016, doi: 10.1016/j.mineng.2015.10.022.

[18] A. F. Taggart, *Handbook of Mineral Dressing. Ores and Industrial Minerals.* New York, 1945.

[19] R. O. Burt, *Gravity Concentration Technology*. Elsevier, 1984.

[20] A. Weissberger, H. W. Hsu, E. S. Perry, and B. W. Rossiter, *Separations by Centrifugal Phenomena*. Wiley, 1981.

[21] J. A. Jiménez and O. S. Madsen, "A Simple Formula to Estimate Settling Velocity of Natural Sediments," *J. Waterw. Port, Coastal, Ocean Eng.*, vol. 129, no. 2, pp. 70–78, Mar. 2003, doi: 10.1061/(ASCE)0733-950X(2003)129:2(70).

[22] A. K. Majumder, G. J. Lyman, M. Brennan, and P. N. Holtham, "Modeling of flowing film concentrators," *Int. J. Miner. Process.*, vol. 80, no. 1, pp. 71–77, Aug. 2006, doi: 10.1016/j.minpro.2006.01.009.

[23] G. H. Luttrell, D. I. Phillips, and R. Honaker, "Enhanced gravity separators: New alternatives for fine coal cleaning," in *12th International Coal Preparation Conference*, 1995, pp. 281–292.

[24] "AMIT 145: Lesson 4 Gravity Separation," *Mining Mill Operator Training*, 2021. https://millops.community.uaf.edu/amit-145/amit-145-lesson-4/.

[25] J. A. Drahun and J. Bridgwater, "The mechanisms of free surface segregation," *Powder Technol.*, vol. 36, no. 1, pp. 39–53, 1983, doi: 10.1016/0032-5910(83)80007-2.

[26] K. M. Hill, A. Caprihan, and J. Kakalios, "Bulk segregation in rotated granular material measured by magnetic resonance imaging," *Phys. Rev. Lett.*, vol. 78, no. 1, pp. 50–53, 1997, doi: 10.1103/PhysRevLett.78.50.

[27] J. . . Ottino and D. V Khakhar, "Mixing and Segregation of Granular Materials," *Annu. Rev. Fluid Mech.*, vol. 32, no. 1, pp. 55–91, Jan. 2000, doi: 10.1146/annurev.fluid.32.1.55.

[28] S. W. Meier, R. M. Lueptow, and J. M. Ottino, "A dynamical systems approach to mixing and segregation of granular materials in tumblers," *Adv. Phys.*, vol. 56, no. 5, pp. 757–827, 2007, doi: 10.1080/00018730701611677.

[29] K. Ahmad and I. J. Smalley, "Observation of particle segregation in vibrated granular systems," *Powder Technol.*, vol. 8, no. 1–2, pp. 69–75, Aug. 1973, doi: 10.1016/0032-5910(73)80064-6.

[30] J. B. Knight, H. M. Jaeger, and S. R. Nagel, "Vibration-induced size separation in granular media: The convection connection," *Phys. Rev. Lett.*, vol. 70, no. 24, pp. 3728–3731, 1993, doi: 10.1103/PhysRevLett.70.3728.

[31] D. A. Huerta and J. C. Ruiz-Suárez, "Vibration-Induced Granular Segregation: A Phenomenon Driven by Three Mechanisms," *Phys. Rev. Lett.*, vol. 92, no. 11, pp. 1–4, 2004, doi: 10.1103/PhysRevLett.92.114301.

[32] R. L. Brown, "The fundamental principles of segregation," *Inst. Fuel*, vol. 13, pp. 15–19, 1939.

[33] J. C. Williams, "The segregation of particulate materials. A review," *Powder Technol.*, vol. 15, no. 2, pp. 245–251, 1976, doi: 10.1016/0032-5910(76)80053-8.

[34] E. G. Rippie, M. D. Faiman, and M. K. Pramoda, "Segregation kinetics of particulate solids systems IV. Effect of particle shape on energy requirements," *J. Pharm. Sci.*, vol. 56, no. 11, pp. 1523–1525, 1967, doi: 10.1002/jps.2600561133.

[35] K. Ahmad and I. J. Smalley, "Observation of particle segregation in vibrated granular systems," *Powder Technol.*, vol. 8, no. 1–2, pp. 69–75, 1973, doi: 10.1016/0032-5910(73)80064-6.

[36] M. H. Cooke, D. J. Stephens, and J. Bridgwater, "Powder mixing - a literature survey," *Powder Technol.*, vol. 15, no. 1, pp. 1–20, 1976, doi: 10.1016/0032-5910(76)80025-3.

[37] A. Rosato, K. J. Strandburg, F. Prinz, and R. H. Swendsen, "Why the Brazil nuts are on top: Size segregation of particulate matter by shaking," *Phys. Rev. Lett.*, vol. 58, no. 10, pp.

1038–1040, 1987, doi: 10.1103/PhysRevLett.58.1038.

[38]   R. M. Iverson, "The physics of debris flows," *Rev. Geophys.*, vol. 35, no. 3, pp. 245–296, Aug. 1997, doi: 10.1029/97RG00426.

[39]   J. Saxton, P. Fralick, U. Panu, and K. Wallace, "Density Segregation of Minerals During High-Velocity Transport Over a Rough Bed: Implications for the Formation of Placers," *Econ. Geol.*, vol. 103, no. 8, pp. 1657–1664, Dec. 2008, doi: 10.2113/gsecongeo.103.8.1657.

[40]   N. K. Mitani, H. G. Matuttis, and T. Kadono, "Density and size segregation in deposits of pyroclastic flow," *Geophys. Res. Lett.*, vol. 31, no. 15, pp. 2–5, 2004, doi: 10.1029/2004GL020117.

[41]   F. J. Muzzio, T. Shinbrot, and B. J. Glasser, "Powder technology in the pharmaceutical industry: The need to catch up fast," *Powder Technol.*, vol. 124, no. 1–2, pp. 1–7, 2002, doi: 10.1016/S0032-5910(01)00482-X.

[42]   A. Santomaso, M. Olivi, and P. Canu, "Mechanisms of mixing of granular materials in drum mixers under rolling regime," *Chem. Eng. Sci.*, vol. 59, no. 16, pp. 3269–3280, 2004, doi: 10.1016/j.ces.2004.04.026.

[43]   S. B. Savage and C. K. K. Lun, "Particle size segregation in inclined chute flow of dry cohesionless granular solids," *J. Fluid Mech.*, vol. 189, pp. 311–335, Apr. 1988, doi: 10.1017/S002211208800103X.

[44]   D. V. Khakhar, J. J. McCarthy, and J. M. Ottino, "Radial segregation of granular mixtures in rotating cylinders," *Phys. Fluids*, vol. 9, no. 12, pp. 3600–3614, Dec. 1997, doi: 10.1063/1.869498.

[45]   A. Tripathi and D. V. Khakhar, "Density difference-driven segregation in a dense granular flow," *J. Fluid Mech.*, vol. 717, pp. 643–669, Feb. 2013, doi: 10.1017/jfm.2012.603.

[46]   N. Jain, J. M. Ottino, and R. M. Lueptow, "Regimes of segregation and mixing in combined size and density granular systems: an experimental study," *Granul. Matter*, vol. 7, no. 2–3, pp. 69–81, Jul. 2005, doi: 10.1007/s10035-005-0198-x.

[47]   C. C. Liao, S. S. Hsiau, and H. C. Nien, "Density-driven spontaneous streak segregation patterns in a thin rotating drum," *Phys. Rev. E*, vol. 89, no. 6, p. 062204, Jun. 2014, doi: 10.1103/PhysRevE.89.062204.

[48]   C. C. Liao, S. S. Hsiau, and H. C. Nien, "Effects of density ratio, rotation speed, and fill

level on density-induced granular streak segregation in a rotating drum," *Powder Technol.*, vol. 284, pp. 514–520, Nov. 2015, doi: 10.1016/j.powtec.2015.07.030.

[49]   D. R. Tunuguntla, O. Bokhove, and A. R. Thornton, "A mixture theory for size and density segregation in shallow granular free-surface flows," *J. Fluid Mech.*, vol. 749, pp. 99–112, Jun. 2014, doi: 10.1017/jfm.2014.223.

[50]   R. J. Atkin and R. E. Craine, "Continuum Theories of Mixtures: Basic Theory and Historical Development," *Q. J. Mech. Appl. Math.*, vol. 29, no. 2, pp. 209–244, 1976, doi: 10.1093/qjmam/29.2.209.

[51]   J. M. N. T. Gray and C. Ancey, "Multi-component particle-size segregation in shallow granular avalanches," *J. Fluid Mech.*, vol. 678, pp. 535–588, Jul. 2011, doi: 10.1017/jfm.2011.138.

[52]   Y. Fan, C. P. Schlick, P. B. Umbanhowar, J. M. Ottino, and R. M. Lueptow, "Modelling size segregation of granular materials: the roles of segregation, advection and diffusion," *J. Fluid Mech.*, vol. 741, pp. 252–279, Feb. 2014, doi: 10.1017/jfm.2013.680.

[53]   M. Larcher and J. T. Jenkins, "Segregation and mixture profiles in dense, inclined flows of two types of spheres," *Phys. Fluids*, vol. 25, no. 11, p. 113301, Nov. 2013, doi: 10.1063/1.4830115.

[54]   M. Larcher and J. T. Jenkins, "The evolution of segregation in dense inclined flows of binary mixtures of spheres," *J. Fluid Mech.*, vol. 782, pp. 405–429, 2015, doi: 10.1017/jfm.2015.549.

[55]   M. Larcher and J. T. Jenkins, "The influence of granular segregation on gravity-driven particle-fluid flows," *Adv. Water Resour.*, vol. 129, pp. 365–372, Jul. 2019, doi: 10.1016/j.advwatres.2017.07.025.

[56]   Clyde Orr, "Particulate Technology.pdf," in *Particulate Technology*, New York: Macmillan, 1966, pp. 124–178.

[57]   R. . Faddick, "Shiploading Coarse - Coal Slurries," *Hydrotransport*, vol. 8, p. 1982, 1982.

[58]   P. A. Shamlou, "Hydraulic transport of particulate solids," in *Handling of Bulk Solids*, Elsevier, 1988, pp. 130–155.

[59]   T. Tavangar, H. Tofighian, and A. Tarokh, "Investigation of the horizontal motion of particle-laden jets," *Computation*, vol. 8, no. 2, pp. 1–13, 2020, doi: 10.3390/COMPUTATION8020023.

[60] R. L. Whitmore, "The sedimentation of suspensions of spheres," *Br. J. Appl. Phys.*, vol. 6, no. 7, pp. 239–245, 1955, doi: 10.1088/0508-3443/6/7/304.

[61] R. H. Weiland and R. R. McPherson, "Accelerated Settling by Addition of Buoyant Particles," *Ind. Eng. Chem. Fundam.*, vol. 18, no. 1, pp. 45–49, Feb. 1979, doi: 10.1021/i160069a011.

[62] R. H. Weiland, Y. P. Fessas, and B. V Ramarao, "On instabilities arising during sedimentation of two-component mixtures of solids," *J. Fluid Mech.*, vol. 142, pp. 383–389, 1984, doi: DOI: 10.1017/S0022112084001154.

[63] R. H. Davis and A. Acrivos, "Sedimentation of Noncolloidal Particles at Low Reynolds Numbers," *Annu. Rev. Fluid Mech.*, vol. 17, no. 1, pp. 91–118, Jan. 1985, doi: 10.1146/annurev.fl.17.010185.000515.

[64] A. Tripathi and A. Acrivos, "Viscous resuspension in a bidensity suspension," *Int. J. Multiph. flow*, vol. 25, no. 1, pp. 1–14, 1999, doi: 10.1016/S0301-9322(98)00036-6.

[65] S. Lee, A. Mavromoustaki, G. Urdaneta, K. Huang, and A. L. Bertozzi, "Experimental investigation of bidensity slurries on an incline," *Granul. Matter*, vol. 16, no. 2, pp. 269–274, 2014, doi: 10.1007/s10035-013-0480-2.

[66] S. Lee, J. Wong, and A. L. Bertozzi, "Equilibrium Theory of Bidensity Particle-Laden Flows on an Incline BT - Mathematical Modelling and Numerical Simulation of Oil Pollution Problems," M. Ehrhardt, Ed. Cham: Springer International Publishing, 2015, pp. 85–97.

[67] I. Grewal, "Mineral Processing Introduction," 2012. http://met-solvelabs.com/library/articles/mineral-processing-introduction/.

[68] H. E. Huppert, "Flow and instability of a viscous current down a slope," *Nature*, vol. 300, no. 5891, pp. 427–429, Dec. 1982, doi: 10.1038/300427a0.

[69] N. Silvi and E. B. Dussan V, "The rewetting of an inclined solid surface by a liquid," *Phys. Fluids*, vol. 28, no. 1, pp. 5–7, Jan. 1985, doi: 10.1063/1.865410.

[70] S. M. Troian, E. Herbolzheimer, S. A. Safran, and J. F. Joanny, "Fingering Instabilities of Driven Spreading Films," *Europhys. Lett.*, vol. 10, no. 1, pp. 25–30, 1989, doi: 10.1209/0295-5075/10/1/005.

[71] J. M. Jerrett and J. R. de Bruyn, "Fingering instability of a gravitationally driven contact line," *Phys. Fluids A Fluid Dyn.*, vol. 4, no. 2, pp. 234–242, Feb. 1992, doi:

10.1063/1.858351.

[72] L. Kondic and A. L. Bertozzi, "Nonlinear dynamics and transient growth of driven contact lines," *Phys. Fluids*, vol. 11, no. 11, pp. 3560–3562, Oct. 1999, doi: 10.1063/1.870213.

[73] L. Kondic, "Instabilities in Gravity Driven Flow of Thin Fluid Films," *Soc. Ind. Appl. Math.*, vol. 45, pp. 95–115, Mar. 2003, doi: 10.1137/S003614450240135.

[74] Y. Nohguchi, K. Hutter, and S. B. Savage, "Similarity solutions for granular avalanches of finite mass with variable bed friction," *Contin. Mech. Thermodyn.*, vol. 1, no. 4, pp. 239–265, 1989, doi: 10.1007/BF01125776.

[75] S. B. Savage and K. Hutter, "The motion of a finite mass of granular material down a rough incline," *J. Fluid Mech.*, vol. 199, pp. 177–215, 1989, doi: DOI: 10.1017/S0022112089000340.

[76] O. Pouliquen, J. Delour, and S. B. Savage, "Fingering in granular flows," *Nature*, vol. 386, no. 6627, pp. 816–817, 1997, doi: 10.1038/386816a0.

[77] B. P. Cook, "Theory for particle settling and shear-induced migration in thin-film liquid flow," *Phys. Rev. E*, vol. 78, no. 4, p. 045303, Oct. 2008, doi: 10.1103/PhysRevE.78.045303.

[78] J. Zhou, B. Dupuy, A. L. Bertozzi, and A. E. Hosoi, "Theory for Shock Dynamics in Particle-Laden Thin Films," *Phys. Rev. Lett.*, vol. 94, no. 11, p. 117803, Mar. 2005, doi: 10.1103/PhysRevLett.94.117803.

[79] B. P. Cook, A. L. Bertozzi, and A. E. Hosoi, "Shock Solutions for Particle-Laden Thin Films," *SIAM J. Appl. Math.*, vol. 68, no. 3, pp. 760–783, Feb. 2007, [Online]. Available: http://www.jstor.org/stable/40233745.

[80] T. Ward, C. Wey, R. Glidden, A. E. Hosoi, and A. L. Bertozzi, "Experimental study of gravitation effects in the flow of a particle-laden thin film on an inclined plane," *Phys. Fluids*, vol. 21, no. 8, p. 083305, Aug. 2009, doi: 10.1063/1.3208076.

[81] J. F. Richardson and W. N. Zaki, "The sedimentation of a suspension of uniform spheres under conditions of viscous flow," *Chem. Eng. Sci.*, vol. 3, no. 2, pp. 65–73, 1954, doi: https://doi.org/10.1016/0009-2509(54)85015-9.

[82] G. K. Batchelor, "Sedimentation in a dilute dispersion of spheres," *J. Fluid Mech.*, vol. 52, no. 2, pp. 245–268, 1972, doi: DOI: 10.1017/S0022112072001399.

[83] E. Barnea and J. Mizrahi, "A generalized approach to the fluid dynamics of particulate

systems: Part 1. General correlation for fluidization and sedimentation in solid multiparticle systems," *Chem. Eng. J.*, vol. 5, no. 2, pp. 171–189, 1973, doi: https://doi.org/10.1016/0300-9467(73)80008-5.

[84]   R. Buscall, J. W. Goodwin, R. H. Ottewill, and T. F. Tadros, "The settling of particles through Newtonian and non-Newtonian media," *J. Colloid Interface Sci.*, vol. 85, no. 1, pp. 78–86, Jan. 1982, doi: 10.1016/0021-9797(82)90237-5.

[85]   P. Snabre and P. Mills, "Settling and fluidization of non Brownian hard spheres in a viscous liquid," *Eur. Phys. J. E*, vol. 1, no. 2, pp. 105–114, 2000, doi: 10.1007/PL00014590.

[86]   M. S. Kirkgöz and M. Ardiçlioğlu, "Velocity Profiles of Developing and Developed Open Channel Flow," *J. Hydraul. Eng.*, vol. 123, no. 12, pp. 1099–1105, Dec. 1997, doi: 10.1061/(asce)0733-9429(1997)123:12(1099).

[87]   C. S. Campbell, "Rapid Granular Flows," *Annu. Rev. Fluid Mech.*, vol. 22, no. 1, pp. 57–90, Jan. 1990, doi: 10.1146/annurev.fl.22.010190.000421.

Appendices

Appendix A Calculation for Flow Developing Zone

The calculations for the flow developing zone (L) based on the equations of Kirkgöz and Ardiçlioğlu [86] are as follows:

$$\frac{L}{D_{CF}} = 76 - 0.0001\,\frac{Re}{F}$$

$$L = D_{CF} \times \left(76 - 0.0001\frac{Re}{F}\right)$$

$$L = 0.7 \times 10^{-2} \times (76 - 0.0001 \times \frac{8.42 \times 10^3}{5.161}) = 0.531m \sim 20.91in$$

To solve this function, the Reynolds number of the flow needs to be analyzed:

$$Re = \frac{\rho_{sl}VD_{CF}}{\mu_{sl}}$$

A.1 Reynolds number calculation

The Reynolds number of the slurry at 24 L/min can be calculated as

$$Re = \frac{\rho_{sl}VD_{CF}}{\mu_{sl}} = \frac{1194.15 \times 1.4 \times 0.7 \times 10^{-2}}{1.39 \times 10^{-3}} = 8420$$

The flow at 24 L/min is in turbulent regime.

The Reynolds number of the slurry at 23 L/min can be calculated as

$$Re = \frac{\rho_{sl}VD_{CF}}{\mu_{sl}} = \frac{1194.15 \times 1.34 \times 0.7 \times 10^{-2}}{1.39 \times 10^{-3}} = 8058$$

The flow at 23 L/min is in turbulent regime.

The Reynolds number of the slurry at 22 L/min can be calculated as

$$Re = \frac{\rho_{sl}VD_{CF}}{\mu_{sl}} = \frac{1194.15 \times 1.29 \times 0.7 \times 10^{-2}}{1.39 \times 10^{-3}} = 7758$$

The flow at 22 L/min is in turbulent regime.

The Reynolds number of the slurry at 8 L/min can be calculated as

$$Re = \frac{\rho_{sl}VD_{CF}}{\mu_{sl}} = \frac{1194.15 \times 0.47 \times 0.7 \times 10^{-2}}{1.39 \times 10^{-3}} = 2826$$

The flow at 8 L/min is in transitional regime.

A.2   Slurry Density

Density of the slurry (ρ_{sl}) is calculated as:

$$\rho_{solids} = 0.25 \times 0.95 \times \rho_{silica} + 0.25 \times 0.05 \times \rho_{iron}$$

$$\rho_{solids} = 0.25 \times 0.95 \times 2600 \frac{kg}{m^3} + 0.25 \times 0.05 \times 7800 \frac{kg}{m^3}$$

$$\rho_{solids} = 2860 \frac{kg}{m^3}$$

$$\rho_{sl} = \frac{100}{\dfrac{25}{\rho_{solids}} + \dfrac{100 - 25}{\rho_{water}}}$$

$$\rho_{sl} = \frac{100}{\dfrac{25}{2860} + \dfrac{100 - 25}{1000}} = 1194.15 \frac{kg}{m^3}$$

A.3   Fluid Velocity

Maximum expected fluid volume: $24 \frac{L}{min}$

Maximum expected fluid velocity (V): $\dfrac{\text{Maximum expected fluid volume}}{\text{Time} \times \text{Area of thin channel entrance opening}}$

$$V = \frac{24 \times 10^{-3} \times 4}{60 \times \pi \times 0.01905^2} = 1.40 \frac{m}{sec}$$

where the diameter of the thin channel entrance opening is 0.75in (0.01905m)

Maximum expected fluid volume: $23 \frac{L}{min}$

Maximum expected fluid velocity (V): $\dfrac{\text{Maximum expected fluid volume}}{\text{Time} \times \text{Area of thin channel entrance opening}}$

$$V = \frac{23 \times 10^{-3} \times 4}{60 \times \pi \times 0.01905^2} = 1.34 \frac{m}{sec}$$

Maximum expected fluid volume: $22 \frac{L}{min}$

Maximum expected fluid velocity (V): $\dfrac{\text{Maximum expected fluid volume}}{\text{Time} \times \text{Area of thin channel entrance opening}}$

$$V = \frac{22 \times 10^{-3} \times 4}{60 \times \pi \times 0.01905^2} = 1.29 \frac{m}{sec}$$

Maximum expected fluid volume: $8 \frac{L}{min}$

Maximum expected fluid velocity (V): $\frac{\text{Maximum expected fluid volume}}{\text{Time} \times \text{Area of thin channel entrance opening}}$

$$V = \frac{8 \times 10^{-3} \times 4}{60 \times \pi \times 0.01905^2} = 0.47 \frac{m}{sec}$$

A.4   Characteristic Distance of the Fluid

The characteristic distance of the fluid (D_{CF}) is measured to be: $0.7 \text{cm} = 0.7 \times 10^{-2} \text{m}$

A.5   Slurry Viscosity

The viscosity of the slurry can be calculated as follows:

$$C_V = C_W \times \left(\frac{\rho_{sl}}{\rho_s}\right)$$

$$C_V = 25 \times \left(\frac{1194.15}{2860}\right) = 10.44 \%$$

C_V is the amount of solid in the mixture in terms of volume.

Volume fraction $\Phi \rightarrow \Phi = 10.44/100 = 0.1044$

The slurry viscosity (μ_{sl}) can be calculated as:

$$\mu_{sl} = \mu_{water} \times (1 + 2.5 \times \Phi + 10.05 \times \Phi^2 + 0.00273 e^{16.6 \times \Phi})$$

$$\mu_{sl} = 1 \times (1 + 2.5 \times 0.1044 + 10.05 \times 0.1044^2 + 0.00273 e^{16.6 \times 0.1044})$$

$$\mu_{sl} = 1.39 \text{ cP}$$

A.6   Froude Number Calculation

Froude number calculation for fluid velocity of 24 L/min

$$F = \frac{V}{\sqrt{g D_{CF}}}$$

$$F = \frac{1.40}{\sqrt{9.81 \times 0.7 \times 10^{-2}}} = 5.16$$

The flow is supercritical as the Froude number is larger than 1.

Froude number calculation for fluid velocity of 23 L/min

$$F = \frac{V}{\sqrt{gD_{CF}}}$$

$$F = \frac{1.34}{\sqrt{9.81 \times 0.7 \times 10^{-2}}} = 5.11$$

The flow is supercritical as the Froude number is larger than 1.

Froude number calculation for fluid velocity of 22 L/min

$$F = \frac{V}{\sqrt{gD_{CF}}}$$

$$F = \frac{1.29}{\sqrt{9.81 \times 0.7 \times 10^{-2}}} = 4.92$$

The flow is supercritical as the Froude number is larger than 1.

Froude number calculation for fluid velocity of 8 L/min

$$F = \frac{V}{\sqrt{gD_{CF}}}$$

$$F = \frac{0.47}{\sqrt{9.81 \times 0.7 \times 10^{-2}}} = 1.79$$

The flow is supercritical as the Froude number is larger than 1.

Appendix B Detailed DOE for Experiments

B.1   DOE for Experimental Setup 1

Cases	Experimental Setup	Riffle Designs	Flowrate (L/min)	Inclination Angle (γ)
1		1	24	15
2		1	24	12
3		1	24	9
4		1	23	15
5		1	23	12
6		1	23	9
7		1	22	15
8		1	22	12
9		1	22	9
10		1.1	24	15
11		1.1	24	12
12		1.1	24	9
13		1.1	23	15
14		1.1	23	12
15		1.1	23	9
16	Setup1	1.1	22	15
17		1.1	22	12
18		1.1	22	9
19		1.2	24	15
20		1.2	24	12
21		1.2	24	9
22		1.2	23	15
23		1.2	23	12
24		1.2	23	9
25		1.2	22	15
26		1.2	22	12
27		1.2	22	9
28		2	24	15
29		2	24	12
30		2	24	9
31		2	23	15
32		2	23	12

33		2	23	9
34		2	22	15
35		2	22	12
36		2	22	9
37		3	24	15
38		3	24	12
39		3	24	9
40		3	23	15
41		3	23	12
42		3	23	9
43		3	22	15
44		3	22	12
45		3	22	9
46		4	24	15
47		4	24	12
48		4	24	9
49		4	23	15
50		4	23	12
51		4	23	9
52		4	22	15
53		4	22	12
54		4	22	9
55		5	24	15
56		5	24	12
57		5	24	9
58		5	23	15
59		5	23	12
60		5	23	9
61		5	22	15
62		5	22	12
63		5	22	9
64		6	24	15
65		6	24	12
66		6	24	9
67		6	23	15
68		6	23	12
69		6	23	9
70		6	22	15

71		6	22	12
72		6	22	9
73		7	24	15
74		7	24	12
75		7	24	9
76		7	23	15
77		7	23	12
78		7	23	9
79		7	22	15
80		7	22	12
81		7	22	9

B.2 DOE for Experimental Setup 2

Cases	Experimental Setup	Flowrate (L/min)	Riffle Designs	Inclination Angle (γ)
1			1	15
2			1	12
3			1.1	15
4			1.1	12
5			1.2	15
6			1.2	12
7			2	15
8			2	12
9	Setup 2	8	3	15
10			3	12
11			4	15
12			4	12
13			5	15
14			5	12
15			6	15
16			6	12
17			7	15
18			7	12

Appendix C Riffle Design Dimensions

Riffle Design V1 — 38.10, 22.86

Riffle Design V1.1 — 39.64, 21.70

Riffle Design V1.2 — 39.64, 21.70

Riffle Design V2 — 29.50, 70°, 43.18, 18.80

Riffle Design V3 — 20.07, 120°, 20.07, 12.70, 21.34

Riffle Design V4 — 31.75, 34.39, 23.80

Riffle Design V5 — 38.10, 72.46°, R2.54, 20.41, 22.10

Riffle Design V6 — 38.10, 70.58°, R2.54, 26.78, 19.81

Riffle Design V7 — 35.18, 4.80, 22.86

TITLE: Riffle Designs

All measurements in mm

SIZE C DWG. NO. 1 REV 1

SCALE: 1:1 WEIGHT: SHEET 1 OF 1

Appendix D Data from Repeated Trials for System Validation of Experimental Setup 1

D.1   System Validation for Heavy Retention in Each Riffle Across Riffle Designs

V1 24L/min	R1	R2	R3
	21.01	38.21	40.77
	56.85	27.85	15.30
	40.32	38.77	20.92
	38.63	39.00	22.37
	30.40	38.13	31.47
Std.dev	13.2833641	4.78817163	10.0196487

V1 23L/min	R1	R2	R3
	40.32	39.52	20.16
	39.24	39.75	21.01
	30.75	39.31	29.93
	28.87	36.08	35.05
Std.dev	5.82402209	1.73173588	7.19352476

V1 22L/min	R1	R2	R3
	46.43	33.25	20.32
	32.04	40.40	27.56
	28.40	44.72	26.88
	33.66	42.07	24.27
Std.dev	7.8463988	4.90678611	3.28239992

V1.1 24L/min	R1	R2	R3
	41.55	35.89	22.56
	34.66	38.50	26.84
	30.30	39.74	29.95
	33.57	30.36	36.07
Std.dev	4.73085596	4.16592469	5.68529842

V1.1 23L/min	R1	R2	R3
	28.48	38.13	33.39
	30.00	41.32	28.68
	29.50	37.50	33.00
	29.37	40.52	30.11
Std.dev	0.63109393	1.84062425	2.27532647

V1.1 22L/min	R1	R2	R3
	34.01	43.03	22.97
	24.48	45.36	30.16
	37.90	40.63	21.48
	28.14	41.99	29.87
Std.dev	5.97761357	1.99767796	4.54141967

V1.2 24L/min	R1	R2	R3
	41.00	39.83	19.17
	49.27	32.03	18.70
	44.41	39.79	15.80
	42.63	42.31	15.06
Std.dev	3.57996501	4.46452171	2.05366539

V1.2 23L/min	R1	R2	R3
	27.15	33.57	39.28
	38.82	40.99	20.19
	27.93	36.00	36.06
	32.16	39.22	28.62
Std.dev	5.34607905	3.30682917	8.5013418

V1.2 22L/min	R1	R2	R3
	30.15	35.01	34.83
	48.65	29.69	21.66
	30.85	39.03	30.12
	30.71	45.28	24.02
Std.dev	9.04296216	6.57577656	5.96440582

V2 24L/min	R1	R2	R3
	47.55	34.19	18.26
	44.31	36.77	18.92
	55.32	26.64	18.04
	51.05	27.89	21.05
Std.dev	4.72707897	4.88482008	1.37507555

V2 23L/min	R1	R2	R3
	54.14	33.04	12.81
	41.35	40.85	17.80
	52.44	32.70	14.87
	54.64	26.80	18.56
Std.dev	6.26679699	5.7618201	2.65998048

V2 22L/min	R1	R2	R3
	45.00	39.96	15.03
	37.46	40.54	22.00
	49.75	34.94	15.31
	46.38	35.75	17.87
Std.dev	5.18996904	2.86166757	3.22732713

V3 24L/min	R1	R2	R3
	38.74	37.48	23.79
	36.95	39.49	23.56
	52.00	30.43	17.57
	55.75	26.55	17.70
Std.dev	9.41105419	6.04033608	3.48816813

V3 23L/min	R1	R2	R3
	41.94	37.98	20.08
	35.61	36.00	28.39
	46.25	33.87	19.88
	51.59	29.30	19.11
Std.dev	6.76326734	3.72553351	4.37084372

V3 22L/min	R1	R2	R3
	42.66	37.41	19.93
	40.60	38.45	20.95
	51.53	32.03	16.44
	56.85	26.71	16.44
Std.dev	7.61544656	5.41354796	2.34726548

D.2   Validation of Overall Recovery

15 deg, 24L/min, Setup 1					
V1	V1.1	V1.2	V2	V3	
71.35	65.54	61.28	58.82	53.81	
75.34	64.63	55.20	54.40	53.34	
62.96	68.09	67.93	59.33	53.89	
68.97	49.82	62.65	56.55	56.50	
62.09					Average Standard deviation
Standard deviation	5.61844907	8.2641273	5.2321092	2.26578169	1.43072243	4.562237938
Mean	68.14	62.02	61.77	57.28	54.39	
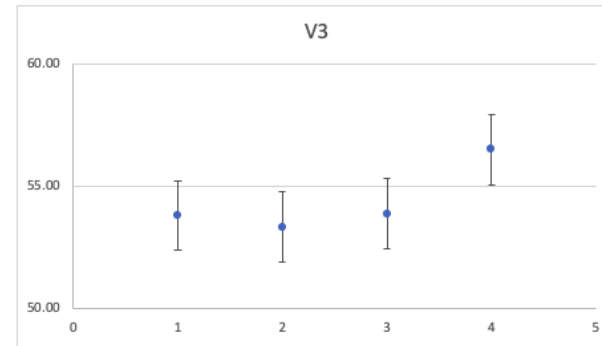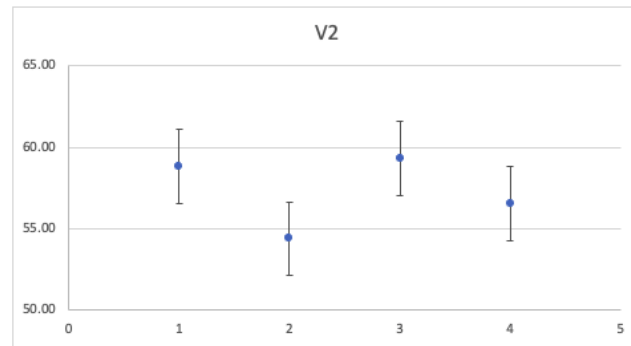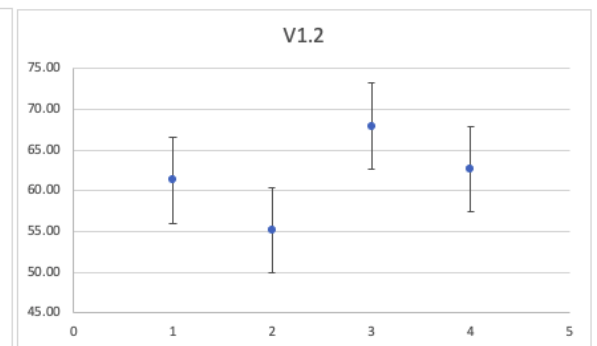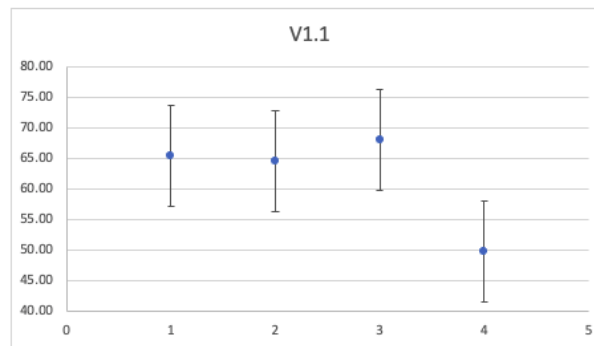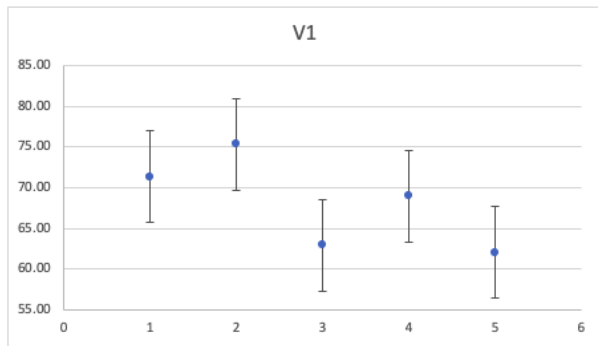
15 deg, 23L/min, Setup 1				
V1	V1.1	V1.2	V2	V3
67.04	66.36	60.50	71.89	60.09
71.78	68.12	57.41	64.92	63.77
68.54	64.91	58.62	62.67	60.41
66.55	62.70	59.70	62.58	58.58

	V1	V1.1	V1.2	V2	V3	Average Standard deviation
Standard deviation	2.35953605	2.29222601	1.34227709	4.38666413	2.18897807	2.513936272
Mean	68.48	65.52	59.06	65.51	60.71	

93
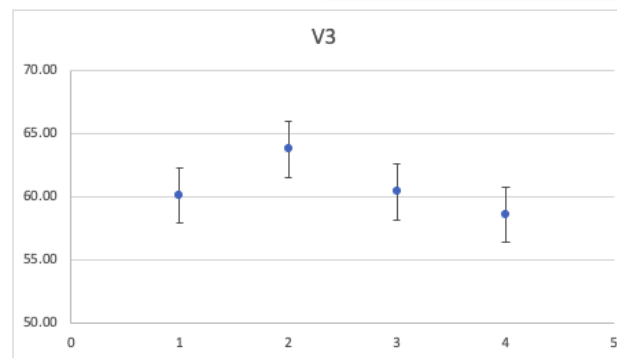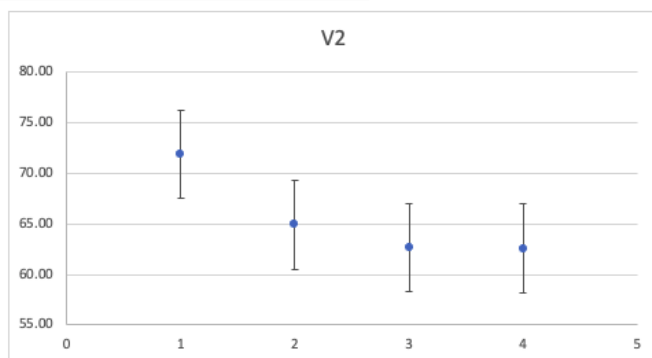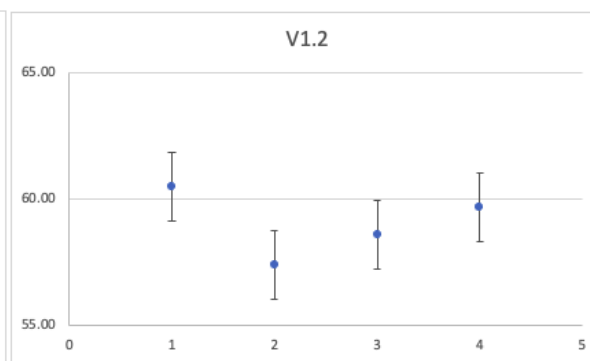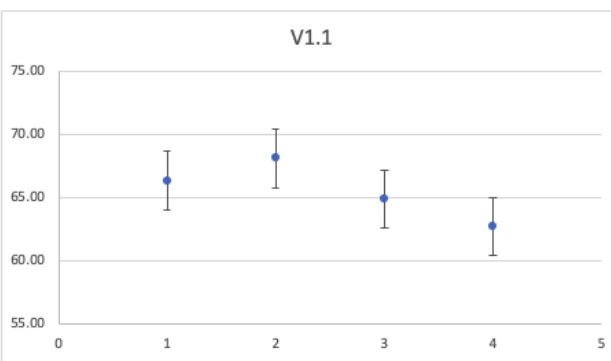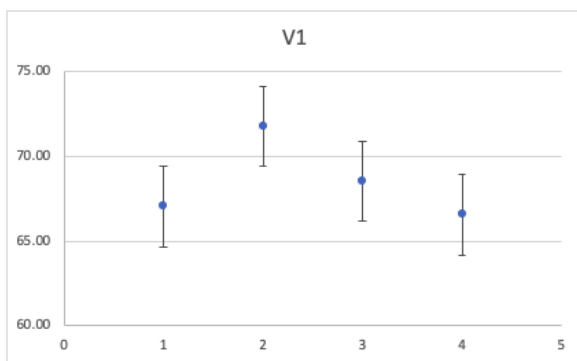
15 deg, 22L/min, Setup 1				
V1	V1.1	V1.2	V2	V3
71.55	70.92	65.48	69.06	64.04
72.13	65.30	59.39	62.20	58.00
71.08	72.83	61.05	67.72	65.66
71.20	65.07	62.56	65.92	62.93

Average Standard deviation

	V1	V1.1	V1.2	V2	V3	
Standard deviation	0.4696652	3.94299664	2.5858549	2.97216976	3.29717892	2.653573084
Mean	71.49	68.53	62.12	66.23	62.66	

V1

V1.1

V1.2

V2

V3
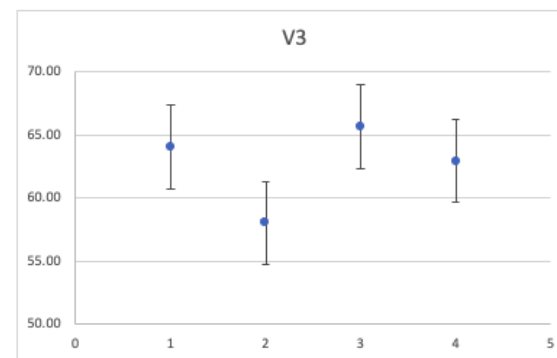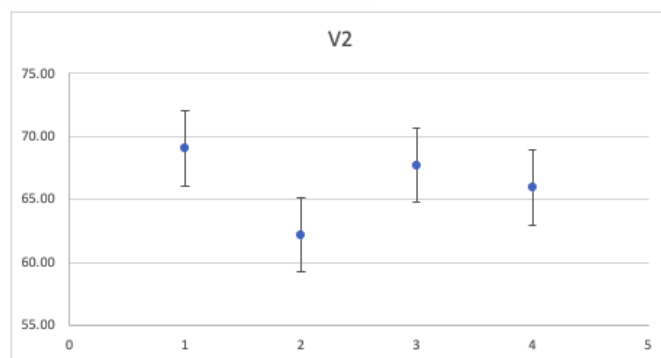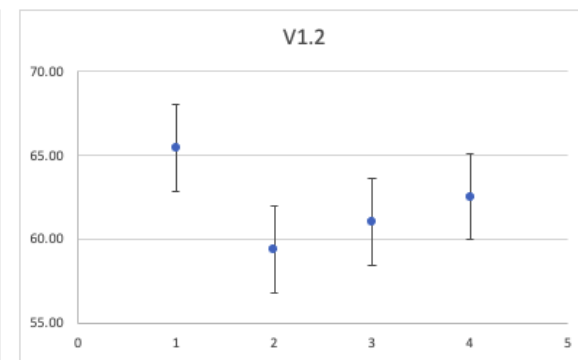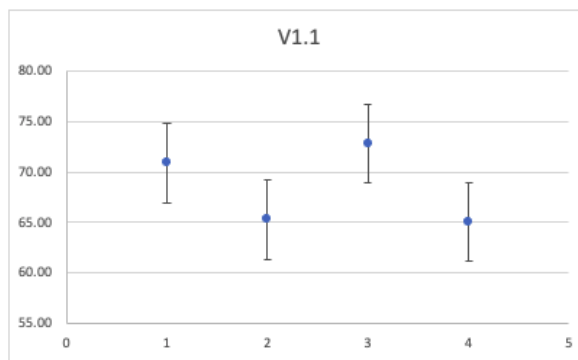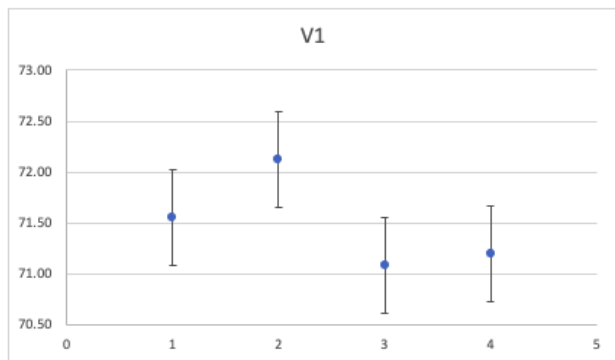
Appendix E Data from Repeated Trials for System Validation of Experimental Setup 2

15 deg, 8 L/min, Setup 2			
V1	V1.2		
92.804428	85.76		
93.4	92.34		
90.5996759	89.05		
			Average Standard deviation
Standard deviation	1.47520922	3.289325646	2.382267435
Mean	92.27	89.05	

V1

V1.2
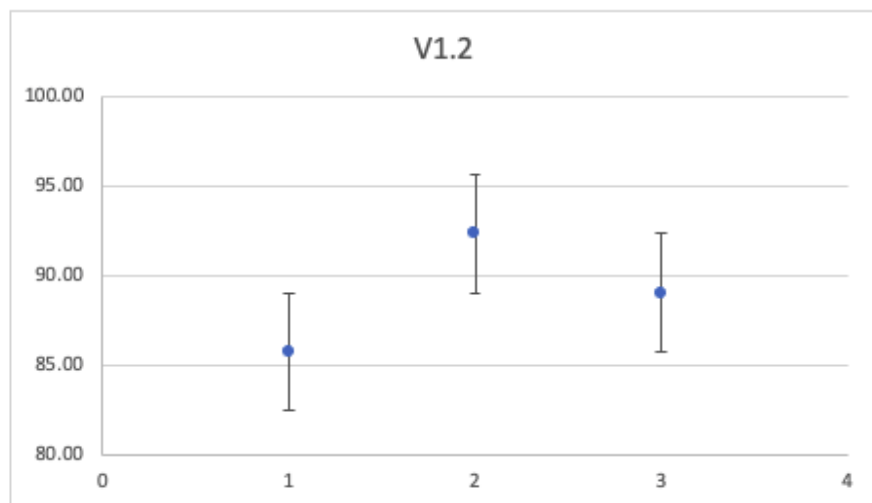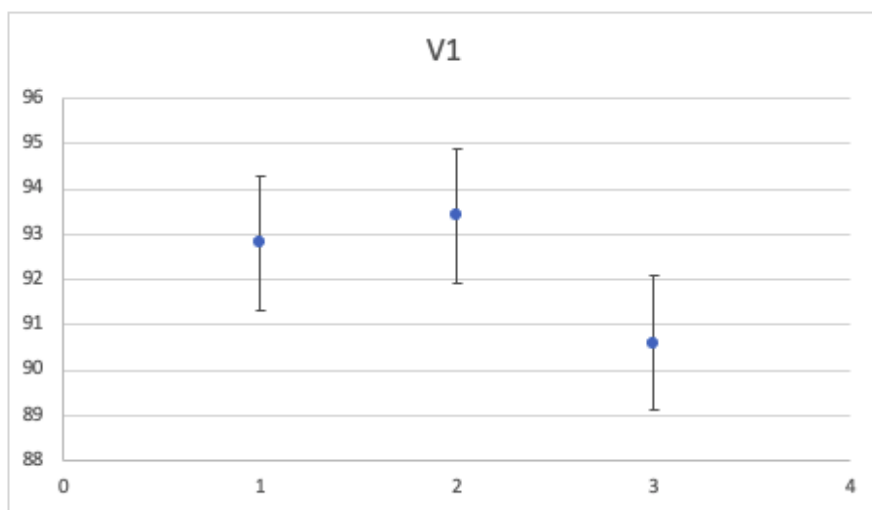
Appendix F Heavy Recovery Across All Riffle Designs